Protein-protein interactions in oligomers studied by solid-state NMR in biomembranes

Zur Erlangung des akademischen Grades eines

DOKTORS DER NATURWISSENSCHAFTEN

(Dr. rer. nat.)

der KIT-Fakultät für Chemie und Biowissenschaften
des Karlsruher Instituts für Technologie (KIT)

genehmigte

DISSERTATION

von
Master-Chemiker Xiaojun Xu
aus
Anhui Provinz in China (中国安徽省)

Dekan: Prof. Dr. Peter Roesky

Referent: Prof. Dr. Anne S. Ulrich

Korreferent: Prof. Wolfgang Wenzel

Tag der mündlichen Prüfung: 22.07.2016

Declaration

The present dissertation was written in the period from Juli.2013 to Jun.2016 in the Institute of Organic Chemistry, Department of Biochemistry of the Karlsruhe Institute of Technology (KIT) under the guidance of Prof. Anne S. Ulrich. I herewith declare that I have authored this submitted thesis independently, and have not used other than the listed resources. Any sentences or ideas including tables, graphs etc. quoted literally are clearly marked.

Acknowledgements

Firstly, I would like to thank my supervisor Prof. Dr. Anne S. Ulrich for her interesting project topic and continuous support during my Ph.D study. Her motivation and immense knowledge inspired and guided me all through the research and writing of this thesis.

I would particularly like to single out my direct mentor Dr. Stephan L. Grage. I want to thank him for his valuable guidance and excellent cooperation. He supported me greatly and was always willing to help me. I could not have imagined having a better mentor for my Ph.D study.

My sincere thank goes to Dr. Parvesh Wadhwani, who gave me great suggestions during the peptide synthesis, identification and purification and provided me tripeptides for REDOR tests. I also thank Andrea Eisele and Kerstin Scheubeck to guide me the work in the laboratory.

I thank Sergii Afonin and Anton Tkachenko for the support of the novel ^{19}F-label CF_3-Thr analogue, and Prof. G. Haufe for his novel ^{19}F-Gln analogue label.

I thank Prof. Wolfgang Wenzel and Prerna Sudera for the cooperation in developing Gō-model of E5 dimer.

In particular, I would like to thank Markus Schmitt for his technical support on the problem solving and maintenance of the NMR spectrometer equipment and Johannes W. Peter for his kindness support on troubleshooting in electronics.

Finally, I want to thank Dr. Benjamin Zimpfer for the cooperation in the TisB part, and Dr. Tamta Turtzeladze, Dr. Birgid Lange, Gabriele Buth for the help with formalities.

List of Abbreviations

AN	Acetonitril
AMPs	Antimicrobial Peptides
CSA	Chemical shifts anisotropy
CPMG	Carr-Purcell-Meiboom-Gill
CODEX	Centerband-Only DEtection of Exchange
CF_3-Thr analogue	*cis*-1-(Fmoc-amino)-3-hydroxylbenzol- (trifluoromethyl)-cyclobutanecarboxyl acid
CF_3-Phg	CF_3-phenylglycine
Com. pulse	Composite pulse
$CHCl_3$	Chloroform
CP	Cross-Polarisation
CD	Circular dichroism
DIC	N,N'-Diisopropylcarbodiimid
DMPC	1,2-dimyristoyl-sn-glycero-3-phosphocholine
DMF	Dimethylformamid
DIPEA	Diisopropylethylamin
DErPC	1,2-dierucoyl-sn-glycero-3-phosphocholine
DNP	Dinitrophenol
EDT	1,2-Ethandithiol
EPR	Electron paramagnetic resonance
equiv.	equivalent
4F-Phg	4F-phenylglycine
^{19}F-Gln analogue	2-amino-4-fluorohex-5-enoic acid
Fmoc	Fluorenylmethoxycarbonyl
FRET	Fluorescence Resonance Energy Transfer
FTIR	Fourier-Transform Infrared spectroscopy
GAL	^{15}N-glycine-^{13}CO-alanine-leucine
HBTU	O-(^{1}H-benzotriazol-1-yl)N,N,N',N'-Tetramethyl-uronium hexafluorophosphate
HOBt	1-Hydroxybenzotriazol
HCl	Hydrochloric acid
HPLC	High-Performance Liquid Chromatography

His	Histidin
IP	IsoPropanol
LC-MS	Liquid Chromatography-Mass Spectroscopy
MeOH	Methanol
Met	Methionin
Me_2S	DimethylSulfid
NMR	Nuclear Magnetic Resonance
NMP	N-Methyl-2-Pyrolidon
NAG	N-acetyl-$^{13}C_\alpha$/^{15}N-glycine
O-Met	Oxidized Methionin
-OBn	-O-benzyl ether protecting group
PDGFR:	Platelet-Derived Growth Factor Receptor protein
PDGFβR:	β-subunit of Platelet-Derived Growth Factor Receptor protein
PGLa	Peptid from Glycine to Leucinamid
PyBOP	Benzotriazol-1-yl-oxytripyrrolidinophosphoniumhexafluorophosphat
POPC	1-palmitoyl-2-oleoyl-sn-glycero-3-3-phosphocholin
P:L	Peptide to Lipid ratio in mol
REDOR	Rotational-Echo DOuble-Resonance
sel-REDOR	carbonyl-^{13}C filtered REDOR
REAPDOR	Rotational-Echo Adiabatic-Passage Double-Resonance
R^2	Rotational Resonance
rf	radio frequency
RP-HPLC	Reversed Phase-HPLC
SPPS	Solid Phase Peptide Synthesis
SUV	Small Unilamellar Vesicle
SFAM	Simultaneous Frequency and Amplitude Modulation
TFA	Trifluoroacetic Acid
TA-system	Toxin / Antitoxin system
TIS	Triisopropylsilan
TA	Thioanisol
TisB	Toxicity-induced by SOS B
TEDOR	Transferred-Echo DOouble-Resonance
U-glycine	Uniformly ^{13}C, ^{15}N-labeled glycine
U-Asp	Uniformly ^{13}C, ^{15}N-labeled asparagine

U-Gln	Uniformly ^{13}C, ^{15}N-labeled glutamine
U-Phe	Uniformly ^{13}C, ^{15}N-labeled phenylanaline
GUV	Giant Unilamellar Vesicle
MLV	Multilamellar Vesicle
NMR	Nuclear Magnetic Resonance
rmsd	root mean square deviation
S / N	Signal to Noise ratio
SDS-PAGE	Sodium Dodecyl Sulfate PolyAcrylamide Gel Electrophoresis
SPPS	Solid Phase Peptide Synthsis
FID	Free Induction Decay

Table of contents

Summary

Distance measurements are central to structural biology, as they can reveal specific details of protein-protein interactions. Solid-state NMR is a versatile tool to determine selective distances on the scale of Å within and between proteins in a membrane environment. There are various approaches to measure such distances employing solid-state NMR, based on either distance-dependent dipolar couplings (e.g., CPMG, REDOR) or spin diffusion (e.g., CODEX). In this study, these three typical approaches (CPMG, REDOR and CODEX) were applied on the systems of TisB, E5, and E5/PDGFβR and compared in their performance.

^{19}F-labels are an advantageous alternative to conventional labels (^{2}H, ^{15}N, ^{13}C), as ^{19}F possesses a higher gyromagnetic ratio and no natural abundance. Thus ^{19}F-labeling is most attractive for distance measurements, in particular if they are challenged by a high molecular mobility, such as in fluid-phase membranes. Therefore, the capability of monoF- and CF_3-groups to gain long-range distances was evaluated and applied to the well-studied antimicrobial peptide PGLa. The CPMG experiment was used on oriented samples to measure weak dipolar couplings, and even in the presence of high molecular mobility, an internuclear distance of 11 Å could be determined. The monoF-label proved to resolve weak ^{19}F-^{19}F dipolar couplings better, whereas the CF_3-label resulted in more complex spectra due to the interaction of 6 spins.

The stress-response peptide TisB is supposed to dimerize with four salt bridges and one hydrogen bond to form a proton channel. The four salt bridges (Asp-Lys) were labeled with ^{13}C and ^{15}N, and REDOR experiments were carried out to gain the ^{13}C-^{15}N intermolecular distances. No dipolar coupling could be detected, indicating a long internuclear distance over 5 Å. However, CPMG experiments were performed with ^{19}F-reporters positioned in the hydrogen bond (postulated between Gln19 - Gln19) and revealed a dipolar coupling indicating a distance lower than 10 Å. This way, direct evidence for the formation of TisB dimers was provided for the first time by solid-state NMR.

The viral oncogenic peptide E5 dimerization was studied with CPMG and CODEX utilizing five single ^{19}F-labeled E5 analogues, labeled in positions 6, 7, 9, 17, 28. From CPMG, no resolved dipolar spectra could be obtained, however, by analyzing the line broadening, the existence of dipolar coupling could be confirmed. On the other hand, using CODEX, more detailed information on intermolecular distances could be determined. Positions 6, 17, 28 showed inter-residue contacts and are probably located on the dimer interface, whereas

position 9 indicated an additional contact between neighboring dimers. Although frozen samples were required for the CODEX approach, it shows a good agreement with the results of the CPMG experiments. Based on these experimental results, a Go-model of the E5 dimer was developed.

The interaction of E5 and PDGFβR proteins within the membrane was studied by REDOR experiments, again ^{19}F-labels were introduced to extend the limit of the distance range. Throughout all the measurements, only a weak dipolar coupling was obtained between ^{13}C-^{19}F, indicating a long intermolecular distance between 8 Å - 11 Å. This interaction was also confirmed by CODEX experiments using a sample of an E5/PDGFβR mixture.

This study evaluated three distance approaches. The CPMG experiment was found to be capable of revealing long-range internuclear distances even in fluid membranes, however, was only applicable to well-defined dimers or spin pairs with a uniform distance. The REDOR experiment, which addresses heteronuclear dipolar couplings, has been used successfully to probe contacts between different peptides, but also, with an appropriate heteronuclear labeling and selective pulse sequence scheme, to study homo-oligomers. Finally, the CODEX allowed to detect the oligomeric states and inter-helical distances in cases, where the CPMG experiment was limited by molecular mobility and the presence of monomers. Altogether, this thesis contributes a basis for future distance measurements in biomembranes.

Zusammenfassung

Abstandsmessungen stellen ein Kernelement strukturbiologischer Untersuchungen dar, da sie zur Entschlüsselung bestimmter Prozesse bei Protein-Protein-Interaktionen beitragen können. Die Festkörper-NMR ist ein vielseitig einsetzbares Werkzeug, welches herangezogen werden kann, um selective Abstände innerhalb von Proteinen in einer Membranumgebung im Angström-Maßstab zu ermitteln. Es gibt eine Vielzahlt von Methoden und Experimente zur Abstandsmessung mittels Festkörper-NMR, die entweder auf abstandsabhängigen dipolaren Kopplungen (z.B. CPMG, REDOR) oder auf Spindiffusion (z.B. CODEX) beruhen. In dieser Arbeit wurden CPMG, REDOR und CODEX-Experimente zur Untersuchung der Systeme TisB, E5 und E5/PDGFβR durchgeführt, und miteinander vergleichen.

Eine Markierung mit ^{19}F bietet eine sehr geeignete Alternative zu den gängigen Markierungen (^{2}H, ^{15}N, ^{13}C) bietet, da ^{19}F ein größeres gyromagnetisches Verhältnis besitzt und in der Natur in Peptiden nicht vorkommt. Deswegen ist ^{19}F ideal für for Abstandmessungen, die durch molekulare Mobilität beispielweise in Membranen in der fluiden Phase eingeschränkt sind. Das Potential, weitreichende Abstände mit monoF- und CF_3-Gruppen zu ermitteln, wurde anhand des gut charakterisierten antimikrobiellen Peptids PLGa getestet. CPMG-Experimente wurden an orientierten Proben und in fluider Membran durchgeführt. Es zeigte sich, dass monoF-Label schwache ^{19}F-^{19}F dipolare Kopplungen besser auflösen kann, wohingegen CF_3-Markierungen aufgrund ihres Multi-Spin Systems, bestehend aus 6 Spins, in ein komplexeres Spektrum resultierten.

Das Peptid TisB ist Teil der SOS-Antwort in E.coli. Es wird angenommen, dass TisB mittels vier Salzbrücken und einer Wasserstoffbrücke dimerisiert und so einen Protonenkanal ausbildet. Die vier Salzbrücken (Asp-Lys) wurden ^{13}C- und ^{15}N-markiert hergestellt und mittels REDOR-Experimenten untersucht, um die intermolekularen ^{13}C-^{15}N Abstände zu ermitteln. Dabei wurde allerdings keine Dephasierung innerhalb der limitierenden Dephasierungs-Zeit erhalten, was für einen langen intermolekularen Abstand größer als 5 Å spricht. Zudem wurden CPMG-Experimente mit ^{19}F-Markierungen in der Wasserstoffbindungen (bestand aus Gln19 – Gln19) durchgeführt, welche einen Maximalabstand von 10 Å aufzeigten. Damit konnte zum ersten mal mit Festkörper-NMR ein direkter Hinweis für eine TisB-Dimer erhalten werden.

Das Dimerisierungsverhalten des viralen Onkoproteins E5 wurde mittels CPMG- und CODEX-Experimenten untersucht. Dazu wurden fünf einfach mit ^{19}F in den Positionen 6, 7, 9,

17 und 28 markierte E5 Analoga herangezogen. Durch CPMG-Experimente konnten keine aufgelösten dipolaren Spektren erhalten werden, jedoch konnte durch die Analyse der Linienverbreiterung das Auftreten dipolarer Kopplungen bestätigt werden. CODEX-Experimente ermöglichen es nicht nur, Aussagen über den Dimerisierungs-Zustand zu treffen, sondern liefern auch präzise Abstände. Hierbei zeigten die Positionen 6, 17 und 28 interhelikale Kontakte untereinander und liegen wahrscheinlich entlang des Dimerinterfaces. Die Position 9 zeigte ebenfalls einen zusätzlichen Kontakt zu benachbarten Dimeren. Obwohl CODEX-Messungen mit gefrorenen Proben durchgeführt wurden, zeigten sie große Übereinstimmung mit den Ergebnissen aus CPMG-Experimenten. Schließlich konnte ein Go-Modell von E5-Dimeren entwickelt auf der Basis dieser experimentellen Daten werden.

Die Interaktion von E5 und PDGFβR innerhalb der Membran wurde mittels REDOR-Experimenten untersucht. Dazu wurden ^{19}F-Markierungen eingefügt, um den Abstandsbereich zu erweitern. Bei allen durchgeführten Messungen wurde nur eine geringe Dephasierung zwischen ^{13}C-^{19}F beobachtet, was für einen langen intermolekularen Abstand zwischen 8 Å - 11 Å spricht. Diese interaktion wurde auch bestimmt by CODEX-Experimenten mit einer E5/PDGFβR-Gemisch Probe.

In dieser Arbeit wurden drei Mothoden zur Abstandmessung mittels Festkörper-NMR verglichen. Das CPMG Experiment war in der Lage, langreichweitige Abstände in fluiden Membranen zu messen, war jedoch nicht anwendbar für ungleichmäßig dimerisierte Systeme. Das REDOR Experiment, mit dem sich heteronukleare dipolare Kopplungen bestimmen lassen, wurde erfolgreich zur Bestimmung von Kontakten zwischen verschiedenen Peptiden verwendet, konnte aber auch, mit geeigneten Markierungen und selektiven Pulssequenzen, zur Charakterisierung von Homo-Dimeren eingesetzt werden. Mit dem CODEX-Experiment konnten die Oligomerenzahl und interhelikale Abstände bestimmt werden in den Systemen, in denen CPMG durch molekulare Beweglichkeit und die Gegenwart von Monomeren limitiert war. Insgesamt konnte diese Arbeit eine Grundlage für Abstandsmessungen mittels Festkörper-NMR in Biomembranen beitragen.

1. Introduction

1.1 Biomembranes

The cell membrane is a biological membrane composed primarily of phospholipid bilayers and proteins. The biomembranes serve as a semi-permeable boundary to regulate the transport of essential cellular nutrition, and at the same time to separate and protect the cell from the outside. They also provide a microenvironment to perform a range of tasks related to cell signaling and metabolic activities. For these functions the membrane-associated proteins play a crucial role.

According to the 'fluid mosaic' model of the cell membrane structure firstly presented by Singer and Nicolson [1], as shown in Fig.1.1, the biomembrane could be described as a dynamic viscous solvent consisting of phospholipid molecules that are self-assembled into bilayers in aqueous environment due to their amphiphilic properties. This arrangement results in an oriented two-layered sheet with the polar lipid headgroups in contact with water molecules and the non-polar tails pointing into the middle, and membrane proteins are 'mosaicly' distributed in the fluid lipid matrix and more or less laterally diffused.

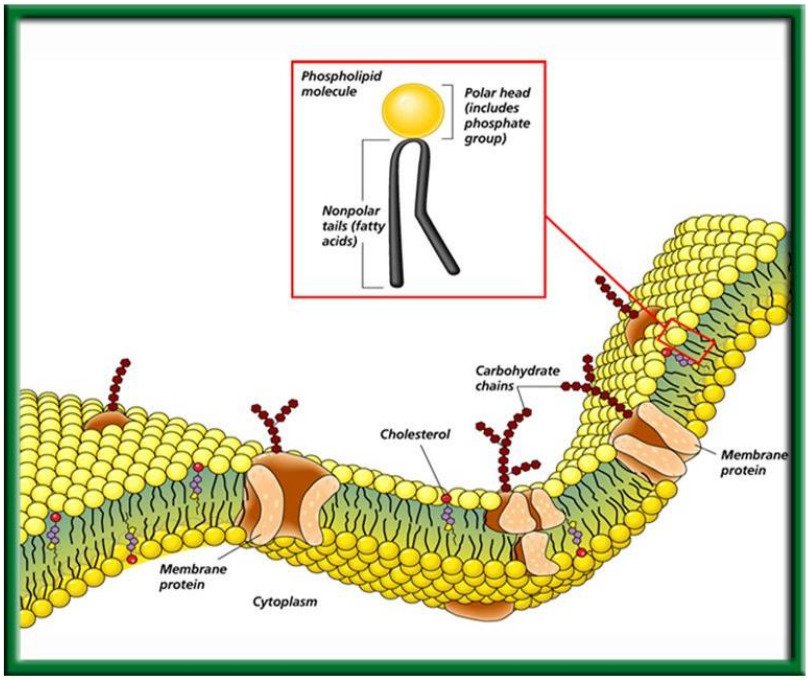

Fig. 1.1 Fluid mosaic model of the biomembrane structure according to Singer and Nicolson [1], modified from a public image.

As shown in Fig. 1.2A, the structure of phospholipids is in common consisted of two fatty acid chains and one phosphate head (phosphate group + R) attached to a glycerol backbone, whereas the chemical nature of their head groups and fatty acyl chains varies in species. According to structure of the head groups (R), as shown in Fig. 1.2B, the main membrane phospholipids are phosphatidyl serine (PS), phosphatidyl ethanolamine (PE), phosphatidyl choline (PC), phosphatidyl glycerol (PG), phosphatidylinositol (PI).

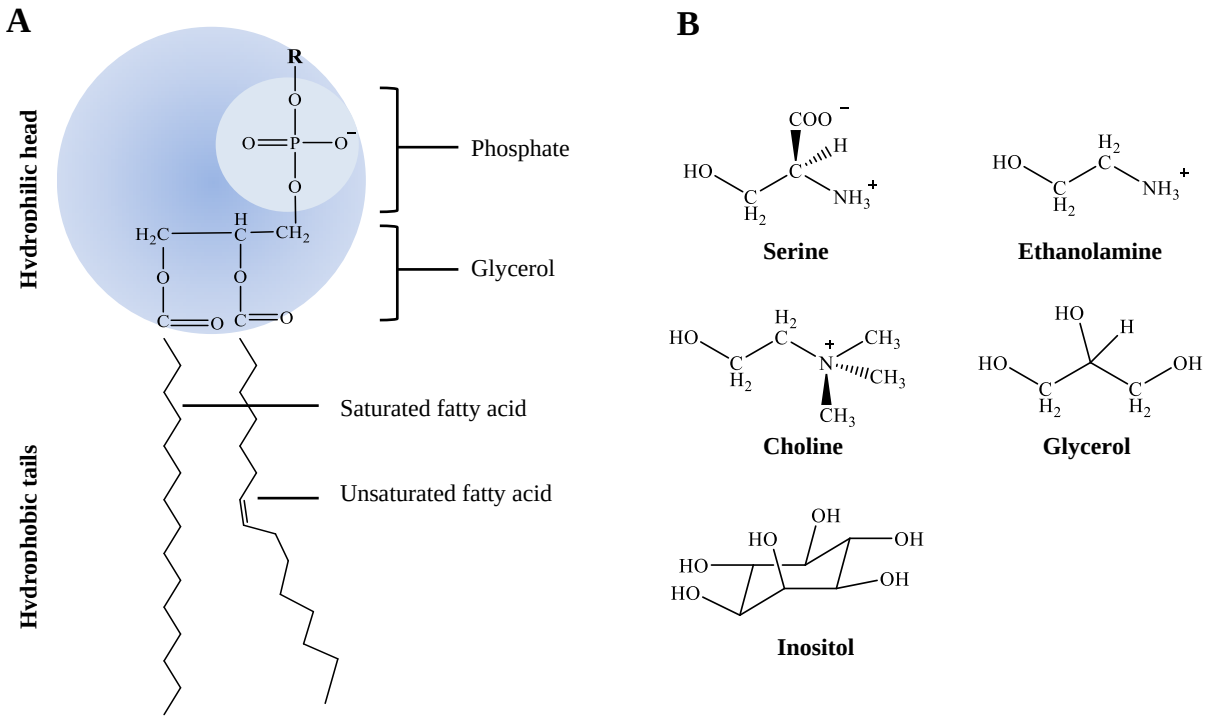

Fig. 1.2 Illustration of membrane phospholipids. (A) Structural shames of phospholipids [2]; (B) The phosphate head can be modified with simple organic molecules, they are serine, ethanolamine, choline, glycerol, inositol, which are attached to the phosphatidic acid by an ester bond.

1.2 Membrane-associated proteins

As illustrated in Fig. 1.1, membrane-associated proteins are either integrally anchored in the membrane or peripherally situated on the surface of it [3, 4]. Integral membrane proteins are permanently embedded in membranes, and can only be separated from the biomembranes by detergents or denaturing agents. They possess different topologies (as shown in Fig. 1.3A) and related to many cellular processes, e.g., serve as transport channels, or work for cell-cell communications and cell signaling with extra or intracellular domains [5, 6], such as Insulin receptor [7] or Glycophorin [8]. Peripheral membrane proteins are reversibly attached to the surface of the membrane (as shown in Fig. 1.3B) and act as a carrier partner in transport by integral proteins [4], such as cytochrome c [9]. Membrane active proteins do not only

participate in different biological processes, but also interact with almost half of drugs, such as ion channels and G-protein coupled receptors [10]. Thus, membrane proteins present an important target in structural biology. Until now, 1108 unique membrane proteins of known structures are recorded [11].

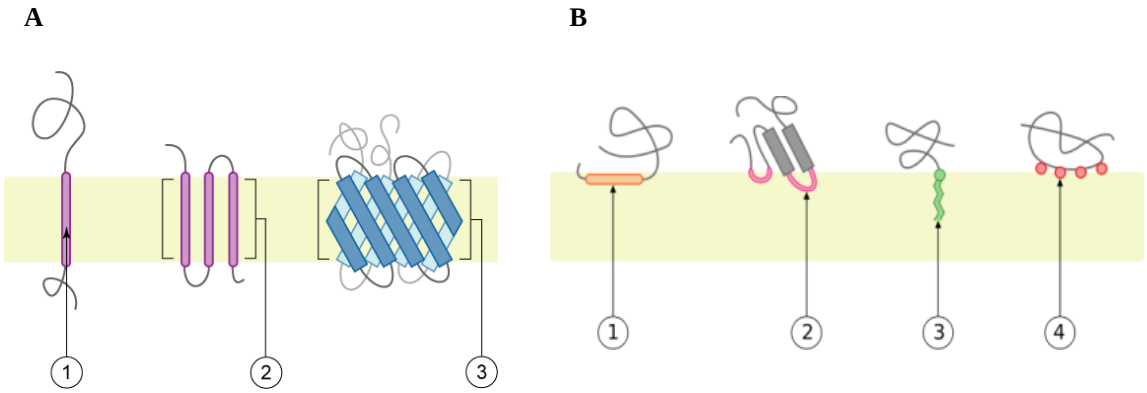

Fig. 1.3 Schematic illustration of integral (A) and peripheral (B) membrane proteins [12]. (A) (1) Protein with a single α-helix transmembrane chain; (2) Helix bundle protein with more α-helix transmembrane chains; (3) Beta barrel protein with more β-sheet transmembrane segments. (B) Peripheral membrane proteins are bound to membranes due to (1) amphipathic effect, (2) hydrophobic loop, (3) covalently interaction with membrane lipids or (4) electrostatic interactions with membrane lipids.

1.3 Oligomerization in biomembranes

The membrane proteins do not act isolated. To carry out their functions, the proteins often interact with nucleic acids, small molecules and other proteins (homo-/hetero-oligomerization). It is reported that over 35 % of membrane proteins are oligomers and that oligomerization plays crucial role in the regulations of ion channels, membrane receptors and transcription factors [13, 14]. Examples include: nicotinic acetylcholine receptor, which allows Na^+ ions pass through when binds to acetylcholine [15]; antimicrobial peptides (AMP), such as PGLa, Magnainin that dimerize within membrane to form pores which leads to mechanical damages and this way kill bacteria [16]; G protein-coupled receptor could activate inside signal cascades after binding ligands outside the cell [17]. Understanding the oligomerization may hence provide opportunities to control their functions or some related diseases. Oligomerization is involved in various mechanisms and recent studies suggest that hydrophobic packing, electrostatic interaction or covalent linking (e.g., disulfides) initiate protein interactions within the biomembra nes [18, 19][20]. However, only little of membrane protein oligomer structure is known in detail and recorded in the protein data bank due to experimental and technical limitation [21].

1.4 Membrane peptide oligomers studied

1.4.1 Antimicrobial peptide PGLa

A large variety of pathogens can use human bodies as hosts, e.g., bacteria, viruses, fungi. Conventional antimicrobial drugs used against life threatening infections are mostly small but complex molecules. Many drugs interfere in the synthesis processes of bacterial essential substances, e.g., proteins, nucleic acids, resulting in response by the bacteria by chromosomal changes. It should be noted that such resistances are becoming a serious problem for modern medicine. Tremendous effort has been invested in the improvement of antimicrobial activity of drugs and to decrease the bacteria resistance. However, novel antibiotics are still required, since bacteria have been able to overcome each new synthesized drug [22]. Recently, it is proposed to utilize antimicrobial peptides (AMPs) as potential new antibiotic drugs, which are small peptides that kill bacteria by permeabilizing their membranes. Compared with conventional antibiotics, it would be probably more difficult for bacteria to develop resistance against AMPs [23-25]. The antimicrobial peptide PGLa is one of them, which is a distant member of the magainin family with a broad-spectrum antimicrobial activity. PGLa was originally isolated from the skin of the African clawed frog *Xenopus laevis* [26-28]. The 21-aa peptide PGLa

5 19
G M A S K A G A I A G K I A K V A L K A L

contains four positively charged residues (blue) and forms an amphipathic α-helix upon binding to the membrane [29]. PGLa has been broadly studied in terms of its structure and biological functions. Previous studies demonstrated that PGLa can align parallel to the oriented membrane, with the hydrophilic residues binding onto lipid head groups and the hydrophobic sites pointing to the membrane interior, named surface-bound ‘S-state’ (Fig. 1.4A, B, left of C). Increasing the peptide concentration, the peptide can tilt with C-terminus into the membrane as ‘T-state’ by self-assembly as a dimer (Fig. 1.4C middle), or it can insert into the membrane in a nearly standing ‘I-state’ (Fig. 1.4C right) [30, 31], which is facilitated by the synergy with magainin 2. [32-35]. The PGLa peptide orientation also shows dependence on temperature, where it was found to adopt an S-state above 45 ℃ and a T-state with reduced temperature and even an I-state below 25 ℃ [36]. The antimicrobial mechanism

has been suggested to be pore-formation to permeabilize the microbial membranes [25, 37-41]. The most common models of the pores are ‘toroidal’- and ‘barrel-stave’-models [40].

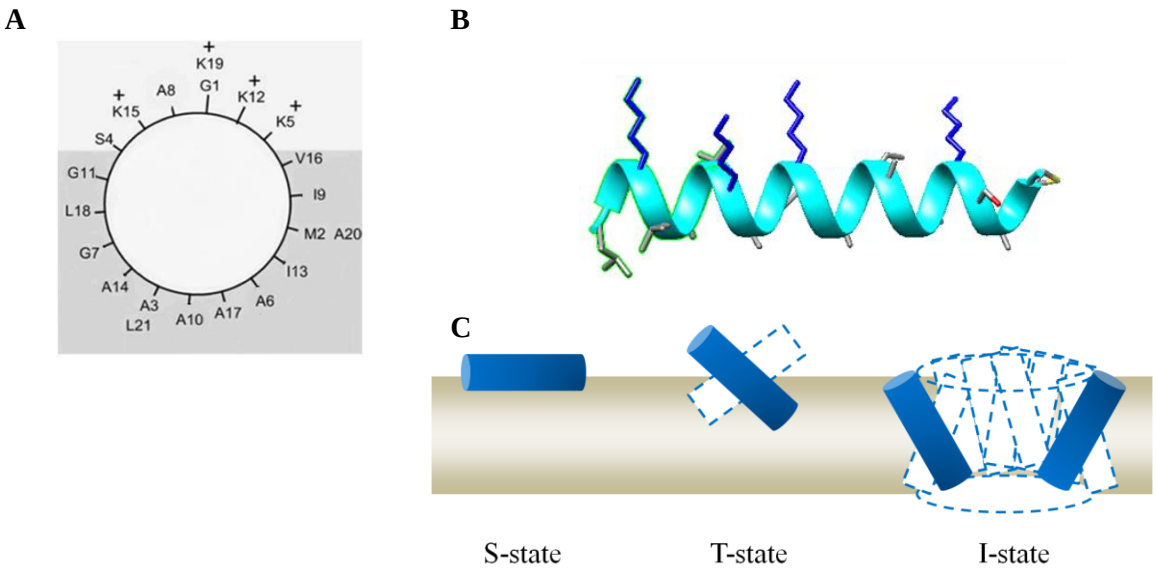

Fig. 1.4 Illustration of the alignment of PGLa with respect to the oriented membrane. (A) Helical wheel representation of the amphiphilic PGLa peptide in the membrane (brown box) in the ‘S-state’. The positions labeled with ‘+‘ indicate the charged lysines (modified from [33]). (B) Standard α-helical model of PGLa in the ‘S-state’. The charged lysine side chains are shown in dark blue. (C) Three states of PGLa observed in a DMPC membrane.

1.4.2 Stress-response peptide TisB

A growing problem for modern medicine is to deal with diseases induced by drug resistant bacteria. Thus AMPs as antibiotics are now developed, which can penetrate the membrane of bacteria and lead to cell lysis. However, even with the use of AMPs, the formation of the bacterial resistance can also be triggered [42]. It is therefore crucial to understand firstly how the antibiotic resistance is generated and then to develop new drugs overcoming the resistance. So-called ‘persister’ cells were firstly found by J.W. Bigger in 1944, which were survived by treatment with antibiotic penicillin [43]. These persistent cells are in a dormant state and show no or very slow growth in the presence of antibiotics. Meanwhile they can produce chronic bacterial biofilms, which are tolerant to antibiotics and induce chronic infections [44-46]. Unfortunately, the mechanism of persister cell formation is not fully understood. The most probably explanation is the activation of a toxin / antitoxin (TA) systems due to higher expression of the chromosomal TA genes [46, 47].

TA-systems are ubiquitous in chromosomes and plasmids from bacteria and archaea [48]. They consist of at least two closely related genes, which encode one stable protein (toxin) and one instable antitoxin protein. The toxin usually inhibits cellular processes and this way regulates the biological activity, whereas the antitoxin inactivates the toxin by binding TA complexes [49-51]. The transcription of TA genes is regulated by the SOS response, which is released by DNA damages by, e.g., antibiotics [48, 52, 53]. Until now, more than 33 TA-systems have been found in *E. Coli*, of which TisB / istR1 was linked with the persister cells formation [54-56]. The 29-aa peptide TisB

```
    5                   19        26
M N L V D I A I L I L K L I V A A L Q L L D A V L K Y L K
```

contains three cationic (dark blue), two anionic (red), as well as two polar (light blue) residues. The so-called stress-response peptide TisB is expressed by DNA damage under stress in *E.coli*, and forms an amphiphilic α-helix upon binding to the membrane, as shown in Fig. 1.5. These charged amino acids lining up along the helix facilitate the TisB dimerization, because the charges of the second TisB helix can be compensated when they are aligned as an antiparallel dimer. This neutral dimer spans the membrane, and can provide a proton conductive strip formed by the row of charged residues [47, 48, 57]. This can decrease the proton gradient across the membrane and leads to ATP depletion and essentially shuts down the cellular energy production. Unlike the pore-formation by PGLa, TisB does not induce cell death but leads to dormancy. As shown in colors in Fig. 1.5C, four salt bridges are supposed to be formed, and the central Gln19 interact with each other by a hydrogen bond [57].

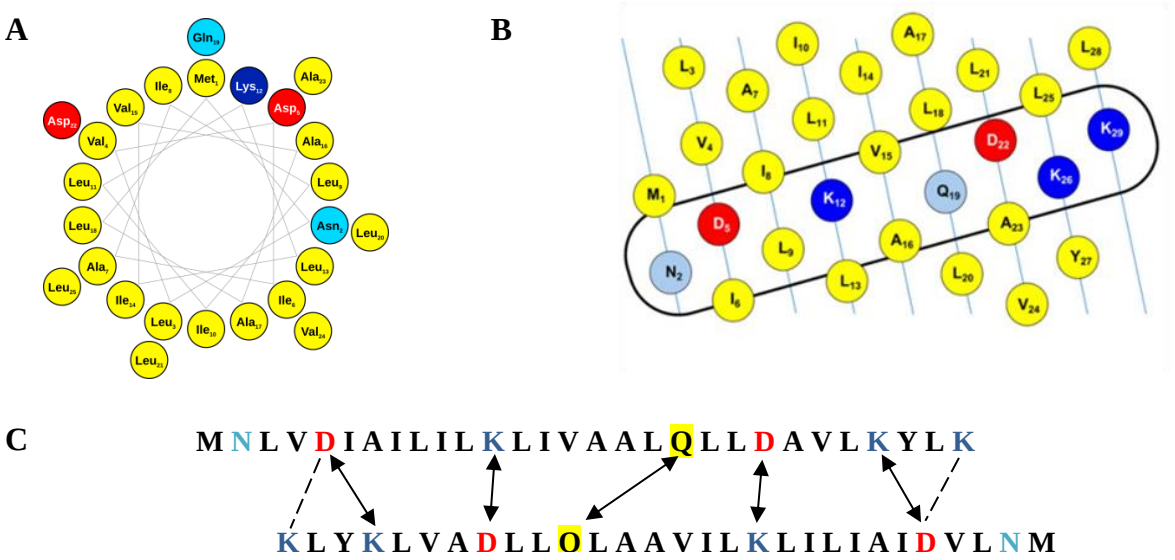

Fig. 1.5 (A) The peptide TisB illustrated in helical wheel; (B) The 29-amino acids sequence consists of three cationic (blue), two anionic (red) and two polar (light blue) residues along the sequence [57]; (C) The antiparallel TisB dimer. Cationic residues are colored in blue and polar residues in light blue, anionic residues in red, central hydrogen-binding Gln19 in yellow.

1.4.3 Oncogenic peptide E5 and membrane receptor protein PDGFβR

Viruses can infect all forms of live, from humans to bacteria. They always consist of genetic DNA or RNA and a surrounded protein coat. They parasite in host cells and transform the host cells by integrating their genome into the cellular DNA. Viruses can also encode proteins mimicking the membrane protein receptor or command the cellular signaling in a ligand-free manner, such as bovine papillomavirus (BPV) [58-61]. The BPV encodes a small protein E5

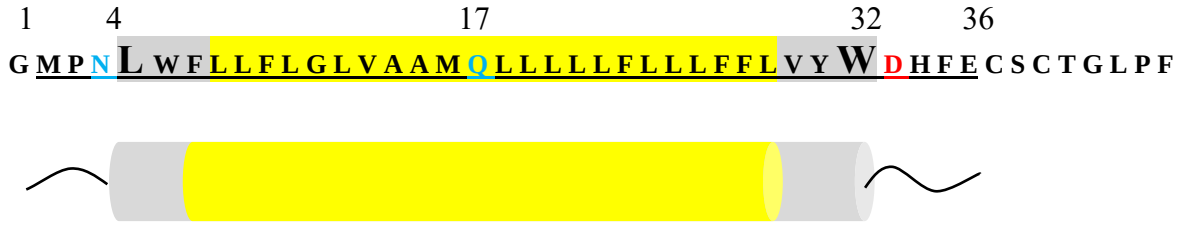

which can induce the fibroblast transformation on its own by activating the platelet-derived growth factor beta receptor (PDGFβR) [62-66]. The oncogenic protein E5 is the smallest oncoprotein known and possesses a highly hydrophobic composition, which facilitates transmembrane-spanning [67], and it is always located in plasma and Golgi membranes [68]. The 44-amino acids sequence has only one charged residue, Asp33 (in red), two polar residues (light blue) and a hydrophobic helical region from Leu4 to Trp32 (grey), in which the putative transmembrane segment is highlighted in yellow. Investigations indicated that the E5 protein located in membranes as α-helix and self-associates into dimers even without the Cys^{37}-Ser^{38}-Cys^{39} motif at C-terminus, which is known to form disulfide bands to stabilize the dimerization [69]. Thus, the truncated sequence from Met1 to Glu36 was investigated in this study.

The E5 protein encoded by bovine papillomavirus can self-dimerize in the transformed cell, and then binds to the transmembrane (TM) segment of the membrane PDGFβ-receptor protein with high affinity, inducing the receptor dimerization to elicit response of signal cascade in a ligand-independent manner [58, 70-72]. The platelet-derived growth factor receptor (PDGFR) protein is located in the cell membrane and is involved in multiple cellular processes, such as cell growth and development, or cellular differentiation [73-76]. Its two subunits α and β can

be activated by homo- or heterodimerization in a ligand-binding manner [73, 77-79]. The transmembrane segment of PDGFβR

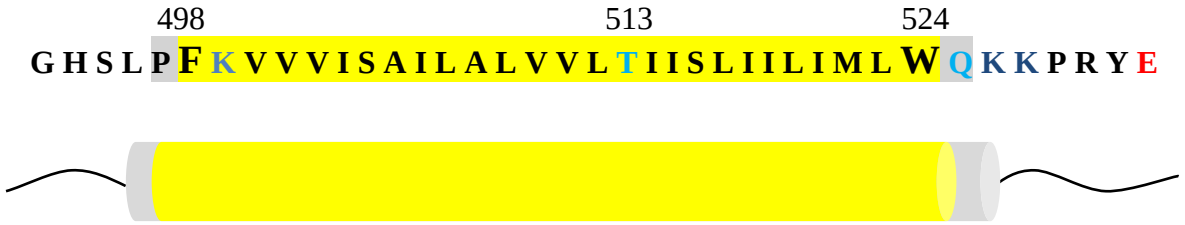

consisting of 39 amino acids from Gly493 to Glu531 was the focus in this study. The highly hydrophobic part from Pro497 to Gln525 (grey) forms α-helix with a long transmembrane segment from Phe498 to Trp524 highlighted in yellow, which consists of one cationic (dark blue) in the N-terminus and one polar residue (light blue) in the middle. The structure of this transmembrane segment in detergent micelles has been determined recently by solution-state NMR [80]. The results show a left-handed dimer with crossing angle of ~ 20°, as shown in Fig. 1.6B. The amino acids involved in the dimer interface are Ile 515, 518, 519, and Leu 509, 512, 520, 523, and Val 500, 501, 502, 511.

T. Surti [58] illustrated in 1998 firstly a structural model of E5 dimers arising from hydrophobic-packing of the leucine residues. Five amino acids were proposed to lie along the dimer interface, they are Leu24, Leu21, Gln17, Ala14 and Leu10 (Fig. 1.5A). This model is still in use nowadays, however, the detailed structural information and the driving forces of dimerization are still lacking. After the E5 dimers are formed, they can bind to PDGFβR and force the dimerization or conformational change of PDGFβR without ligand. The E5 / PDGFβR complexes are supposed to be stabilized by two interactions between them (Fig. 1.6C). One is the electrostatic interaction between the cationic residue Asp33 of E5 and the anionic Lys499 of PDGFβR; the other one is the hydrogen bound linking the middle Gln17 of E5 and Thr513 of PDGFβR, where the Gln17 also plays an important role in the E5 homodimerization [70, 71, 81, 82].

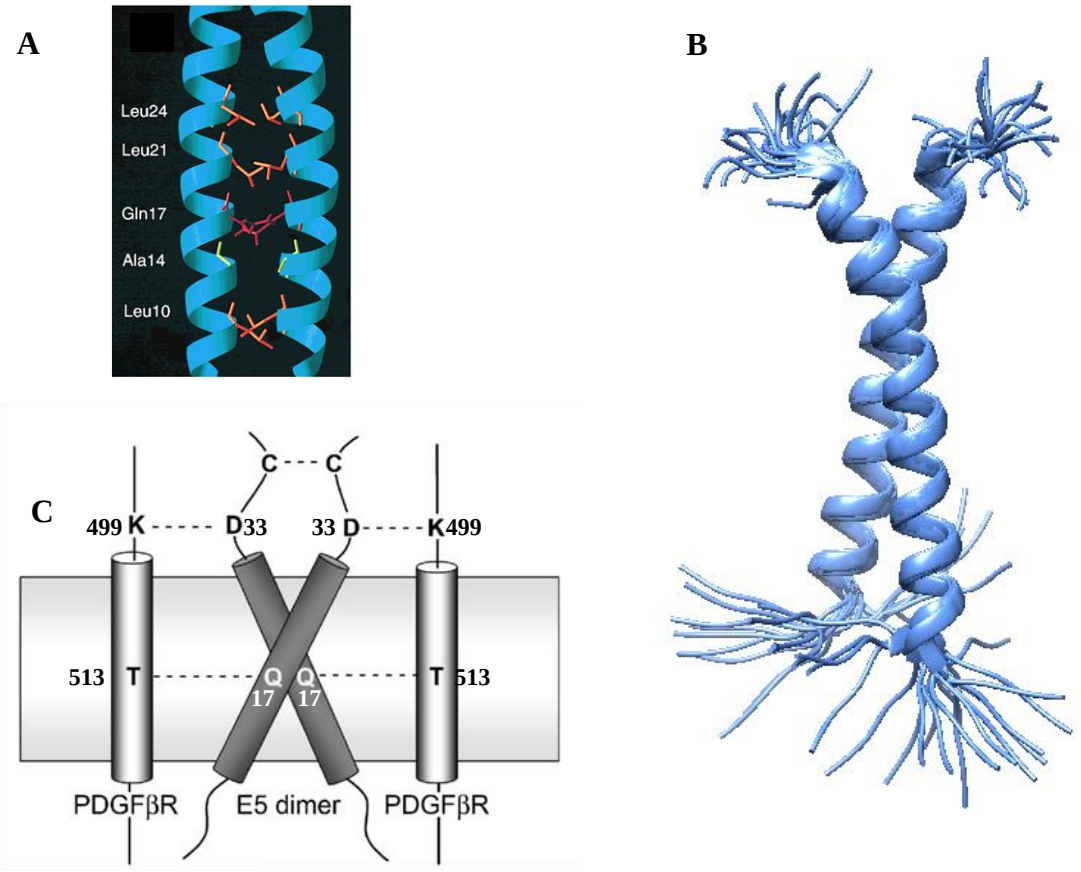

Fig. 1.6 (A) Structural model of E5 dimer postulated by T. Surti [58]; (B) Illustration of PDGFβR-TM dimer with disordered N and C termini (PDB ID: 2L6W); (C) Schematic illustration of E5 / PDGFβR interactions [71]. Electrostatic interactions between Thr531 - Gln17 and Lys499 - Asp33 stabilize the dimer formation.

1.5 Study of oligomers in biomembranes

The protein weight can be revealed using sodium dodecyl sulfate polyacrylamide gel electrophoresis (SDS-PAGE) [83], and molecular structures can be solved by X-ray crystallography in crystal state [84] and solution-state nuclear magnetic resonance (NMR) spectroscopy [85]. Focused on special functions of membrane proteins, such as protein-ligand binding, it is essential to synthesize part of them (e.g., transmembrane segment) wild type or with incorporated florescence or isotope markers. Such markers can be tracked using florescence spectroscopy or solid-state NMR to help understanding the mechanism of the interactions occurring in membranes [86, 87]. Among all the analytical methods, solid-state NMR, which is mainly applied in this study, represents a versatile instrument for the analysis of the structure and dynamic behavior of membrane-active peptides in all kinds of environments such as fluid, soft and solid. Furthermore, solid-state NMR takes advantage of a wealth of different methods emerging with recent technical progress [88].

2. Theoretical background

NMR applications for distance measurements in biomembranes

2.1 Model membranes

To study membrane-associated proteins in the laboratory, a wide variety of simple model membrane systems has been developed, as biological membranes are so complex and vary enormously in composition. To assess membrane protein structure, it is acquired to simplify the membrane system reserving only the essential lipid bilayer structure and those physical properties of the bilayer are important for the activity and structure of the studied membrane proteins. The three most common model membrane systems are liposomes, micelles and oriented lipid bilayers on solid supports (Fig. 2.1). The size, geometry and composition of the membranes can be tailored precisely using natural or synthetic pure lipids [89, 90]:

(A) Micelles are composed of a monolayer in mostly spherical morphology, resulting from aggregation of detergents, which consist of a polar head and only one nonpolar tail.

(B) Liposomes are vesicles composed of lipid bilayers. According to the vesicle morphology and size (diameter), four main types of liposomes are distinguished as follows: small unilamellar vesicles (SUV, <50nm), large unilamellar vesicles (LUV, 100-500nm), giant unilamellar vesicles (GUV, 5-100μm) and multilamellar vesicles (MLV).

(C-D) Oriented lipid bilayers can be obtained with solid supports (glass plates in our case). They are comprised of a stack of glass plates in between which peptides of interest (green) are embedded in thousands of bilayer membranes.

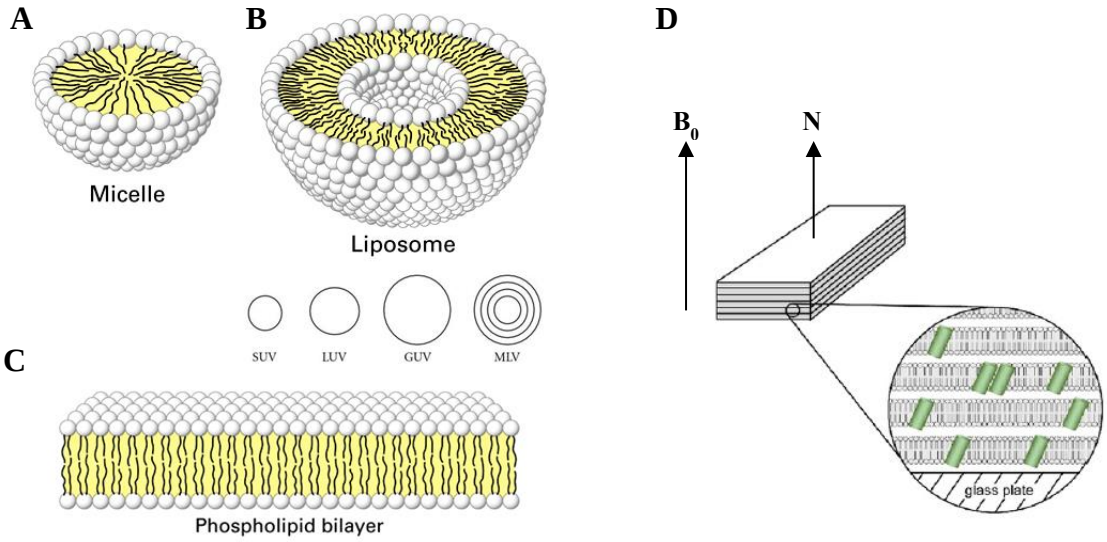

Fig. 2.1 Model membrane systems for studying membrane-associated proteins (modified from [91][92]). (A) Micelle. (B) Liposome, four different liposomes are distinguished according to the vesicle morphology and size, namely SUV, LUV, GUV, MLV. (C) Phospholipid bilayer. (D) Macroscopically oriented lipid bilayers sample on glass plates as solid supports. N: the membrane normal; B_0: the static magnetic field.

2.2 Application of ^{19}F-NMR on membrane-active peptides

Conventional isotopes relevant for studies of biological macromolecules are ^{13}C, ^{15}N, ^{31}P, which possess a spin of I = 1/2, and ^{2}H with spin of I = 1, as summarized in Table 2.1. In contrast to these conventional labels, the ^{19}F nucleus with spin of I = 1/2 rarely occurs in biological molecules, and this lack of natural abundance makes ^{19}F-NMR free of background. Furthermore, ^{19}F possesses the highest gyromagnetic ratio γ after ^{1}H, thus theoretically allows to gain a 1000-fold sensitivity compared to ^{15}N, as the signal-to-noise ratio (S/N) scales with $|\gamma|^{5/2}$ [93]. Practically this factor is reduced to ~100 because of efficient cross-polarization (CP) from ^{1}H [94], that means, ^{19}F-labeled peptide needs only minutes to hours to be observed, whereas the same amount of ^{15}N-labeled sample takes days to achieve the same S/N ratio. With such high γ, ^{19}F is also beneficial for addressing long-range internolecular distances. For instance, from a dipolar splitting of 100Hz (see Table 2.1), a maximum distance of 11.7 Å is accessible for a ^{19}F spin pair, while it is only 4.8 Å for ^{13}C nuclei.

Table 2.1 Properties of biologically relevant isotopes.

Isotope	^{1}H	^{2}H	^{13}C	^{15}N	^{19}F	^{31}P
Gyromagnetic ratio, $\gamma/2\pi$ (MHz/T)	42.58	6.53	10.70	−4.31	40.03	17.23
Sensitivity (%)						
$\sim I(I+1)\ \gamma^3$	100	0.96	1.59	0.10	83.3	6.63
$\sim I(I+1)\ \gamma^{5/2}$	100	2.46	3.17	0.33	85.8	10.4
Natural abundance (%)	99.985	0.015	1.1	3.7	100	100
Typical CSA (ppm)	20	20	100	200	100	100
Accessible distances (Å) from resolved dipolar splittings						
10 Hz	26.2	7.5	10.4	5.7	25.2	14.3
30 Hz	18.2	5.2	7.2	4.0	17.5	9.9
100 Hz	12.2	3.5	4.8	2.6	11.7	6.7

^{19}F-NMR relies on selectively ^{19}F-labeled molecules to yield local backbone conformation, orientational constraints, and dynamics of peptides in lipid membranes. The CF_3- or ^{19}F-reporter group is required to be rigidly attached to the peptide backbone in a well-defined geometry and without compromising the structural and biological function of the peptides. Until now a series of conformationally restricted ^{19}F-labeled amino acids were designed [95-100], as shown in Fig. 2.2. To maintain the natural peptide structure and function to maximum extent, the replacing ^{19}F-labels should have similar side chains, polar or nonpolar, aliphatic or aromatic as the substituted residue. Besides, the labels with ^{19}F distant from its amino and

carboxylic functional groups are preferred, as the strong electron-withdrawing character of the fluorine-reporters may cause local structural changes.

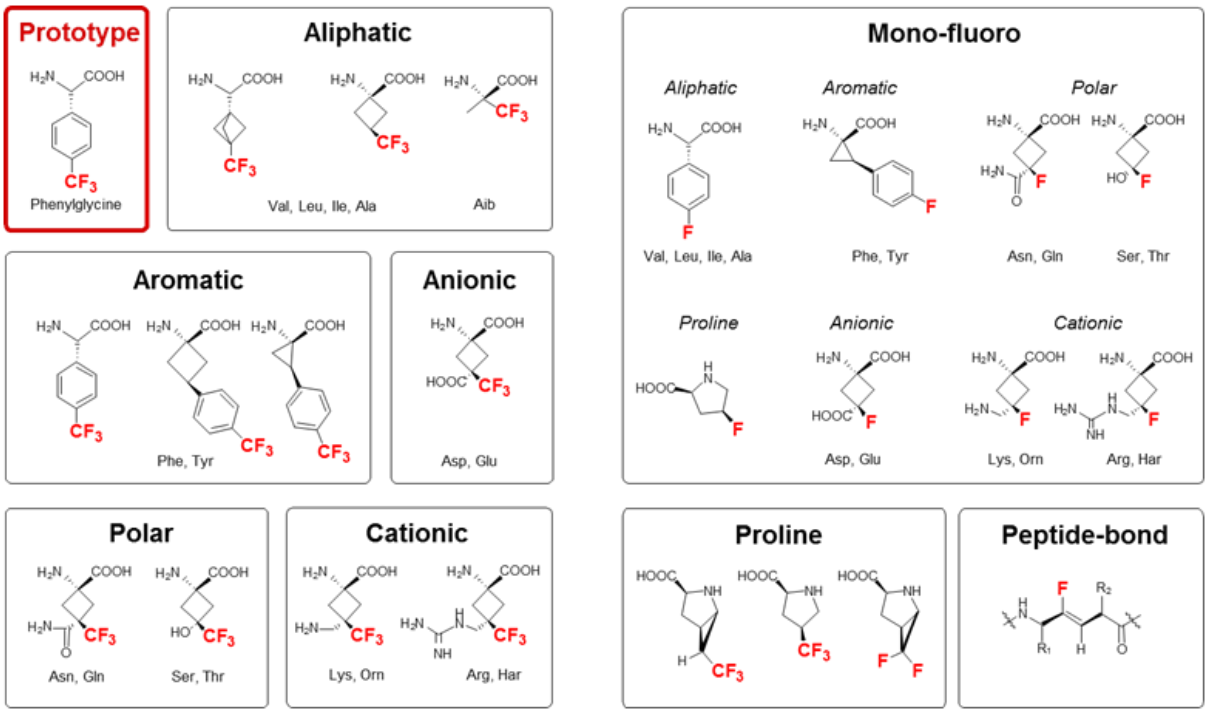

Fig. 2.2 ^{19}F-lalled amino acids designed by the Prof. Ulrich's group [101].

2.3 Solid-state NMR orientation dependence

2.3.1 ^{15}N-NMR for qualitative determination of helix orientation

The mostly used approach to study membrane-associated peptides is solid-state ^{15}N NMR. When the peptide forms an α-helix upon binding to the membrane, the σ_{33}-element of the CSA lies almost along the ^{15}N-H bound and more or less parallel to the helix-axis (Fig. 2.3A). Thus, via the ^{15}N-chemical shift the peptide orientation within the macroscopically oriented lipid bilayers becomes assessable. The line width of ^{15}N can also yield the information on the mobility of the peptide, i.e., a sharp line indicates that the peptide undergoes fast rotation, whereas a broad line means that it is quite rigid. Note that, from one single ^{15}N-chemical shift, the precise peptide orientation cannot be determined. However, different alignment can be distinguished by the ^{15}N-NMR qualitatively. Nonetheless, the precise tilt angle of the peptide could be determined by more ^{15}N-labels with PISEMA experiments [88]. The analysis of the peptide orientation is shown in the Fig. 2.3B-C, the chemical shift at 200 ppm denotes membrane-spanning alignment, and the value around 90 ppm means that the peptide does not

insert into the membrane but lies on the membrane surface. All the other chemical shifts between 90 ~ 200 ppm indicate a tilted orientation of the peptide.

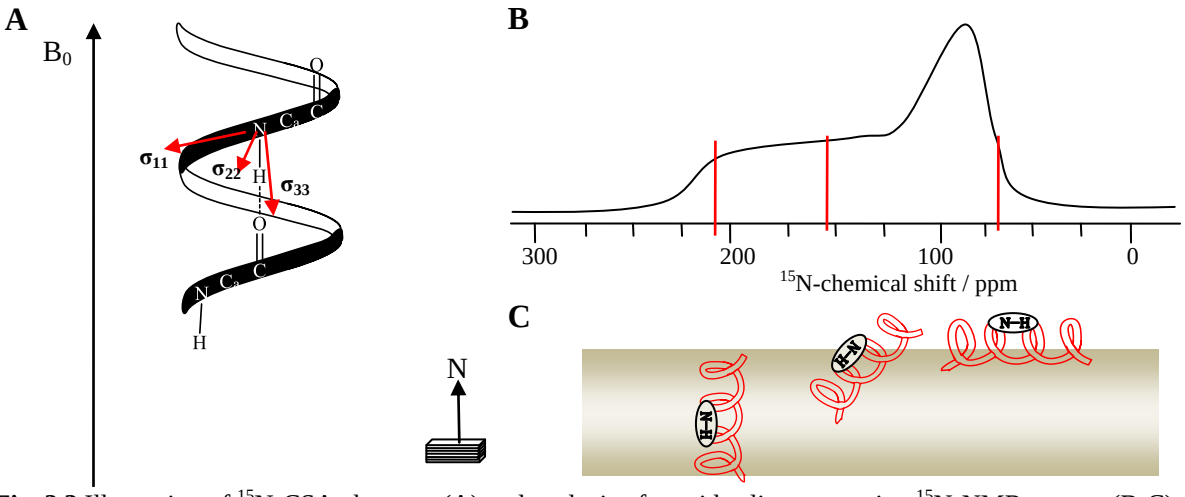

Fig. 2.3 Illustration of ^{15}N-CSA elements (A) and analysis of peptide alignment using ^{15}N-NMR spectra (B-C).

2.3.2 Chemical shift anisotropy

Chemical shifts reflect not only the structure but also the orientation of the molecule with respect to the magnetic field. Taking 4F-Phg as an example, the CSA tensors in the principal axis system (σ^{PAS}) are illustrated in a three-dimensional ellipsoid representation as shown in Fig. 2.4A. In solution NMR, such anisotropic effects are averaged out by the fast molecular motion, leaving only the time-averaged isotropic chemical shift σ_{iso} as an observable. In solid-state NMR, the effect of the CSA is reflected in the NMR spectra. As shown in Fig. 2.4B, from mono-fluoro phenyl-ring groups in a non-oriented sample, a characteristic spectrum termed 'powder pattern' could be obtained, in which, as indicated underneath the powder pattern, all possible orientations are equally presented. When the phenyl-ring is aligned perpendicular to the magnetic field, the phenyl π-system yields to a strong shielding of the ^{19}F nucleus, thus a low chemical shift of -155 ppm (σ_{33}) is observable. In the contrary, the highest chemical shift of -55 ppm (σ_{11}) is obtained if the magnetic field is oriented along the phenyl-ring plane and perpendicular to the C_α-C_β-^{19}F axis. The σ_{22} of -125 ppm lies between them. The isotropic chemical shift $\sigma_{iso} = (\sigma_{11} + \sigma_{22} + \sigma_{33})/3$ is only observable in fully mobile molecules. In solid and oriented samples, only one orientation could be observed, and the chemical shift is given by the zz-component of CSA tensors in laboratory frame. Another two important parameters are the anisotropy parameter δ describing the overall width of the spectrum, defined as $(\sigma_{33} - \sigma_{iso})$, and the asymmetry of the spectrum η, defined as $(\sigma_{22} - \sigma_{11})/\delta$, resulting in $0 \leq \eta \leq 1$. In the case of membrane-associated peptides reconstituted into

macroscopically oriented bilayer samples, once the values of CSA tensors are known, the peptide orientation in the membrane with respect to the magnetic field can be determined.

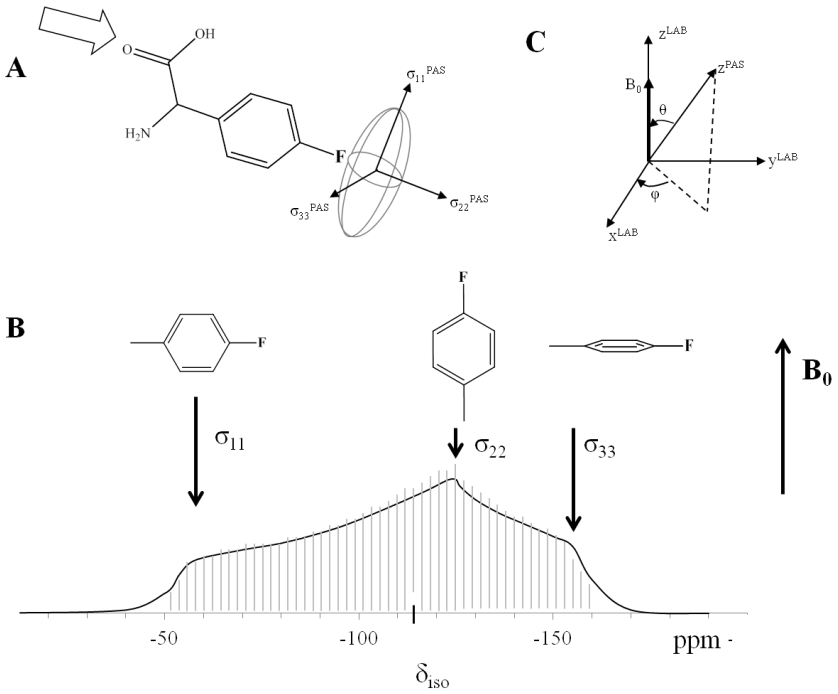

Fig. 2.4 Schematic illustration of chemical shifts anisotropy (CSA) tensors observed on mono fluoro phenylglycine (4F-Phg)

2.3.3 ^{19}F-NMR measuring orientation-dependent dipolar coupling

As shown in Fig. 2.5, the peptide orientation within oriented membranes can be described by three parameters: peptide tilt angle τ, azimuthal rotation angle ρ and order parameter S_{mol}. The usage of CF_3-reporter with dipolar approach makes accurate measurements of peptide orientation (τ, ρ, S_{mol}) robust [31]. The static dipolar coupling between the CF_3-group D can be calculated with known ^{19}F-^{19}F distance to be 32 kHz with the CF_3-axis parallel to the magnetic field B_0 (θ = 0). As the CF_3-goups undergo fast rotation around C-CF_3 axis, which leads to motional averaging of the coupling, the

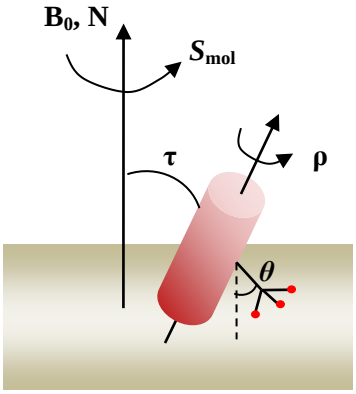

Fig. 2.5 Illustration of peptide orientation (τ, ρ, S_{mol}). S_{mol} denotes peptide motion around membrane normal N. τ is the tilt angle of peptide helix with respect to the magnetic field B_0. ρ describes azimuthal rotation angle around helical axis. θ is the angle between C-CF_3 axis and magnetic field B_0.

observable dipolar coupling is scaled by S_{rot} = -0.5, that is $|D^0_{CF_3}|$= 16 kHz. The time-averaged orientation θ of the CF_3-label can be determined from the orientation dependent dipolar coupling:

$$D_{CF_3} = \left|\frac{3\cos^2\theta - 1}{2}\right| S_{mol} \times D^0_{CF_3} \qquad (2.1)$$

where the order parameter S_{mol} ($0 \leq S_{mol} \leq 1$) describes the averaged peptide mobility.

With CF_3-group labels in more than four positions one by one (Fig. 2.6A), the peptide orientation (τ, ρ, S_{mol}) can be precisely determined by searching the best-fit between the experimental dipolar splittings and simulated values through all possible orientations (0～180 °) (Fig. 2.6B).

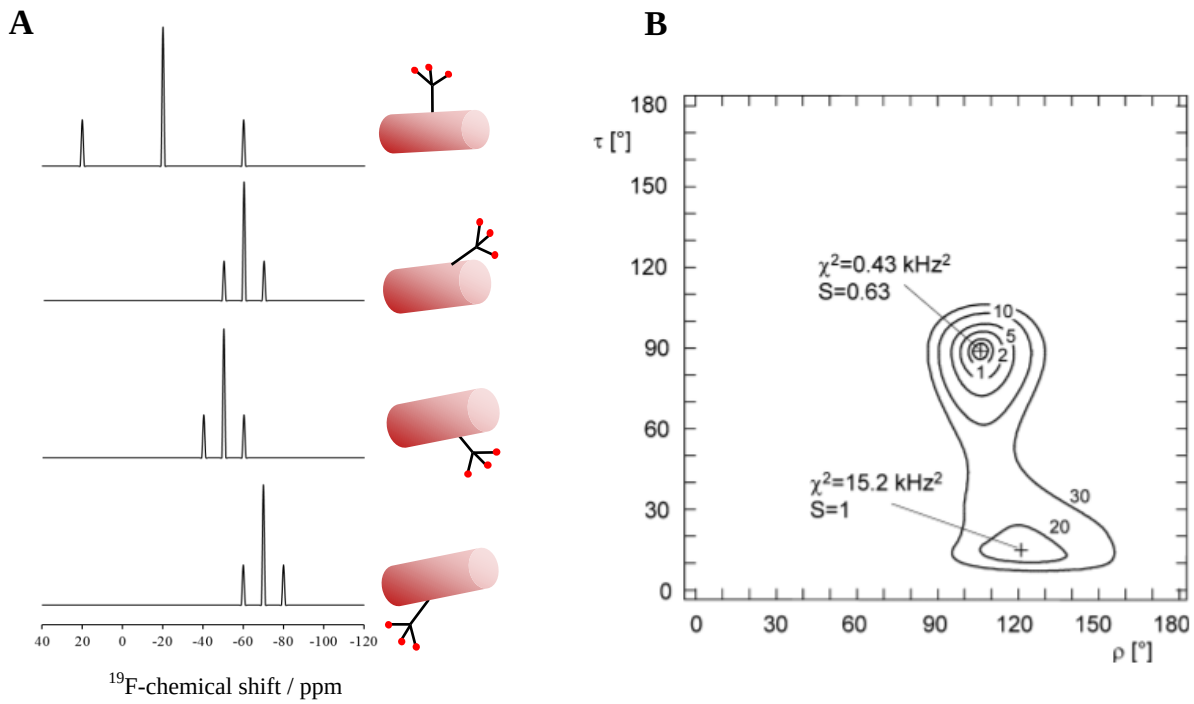

Fig. 2.6 Determination of peptide orientation (τ, ρ, S_{mol}) depending on dipolar approach with CF_3-labels. (A) ^{19}F-NMR spectra of oriented peptide labeled with CF_3-groups in four positions; (B) rmsd plots (modified from [31]), in which the minimum shows the best-fit between the experimental dipolar splittings and simulated values through all possible orientations.

2.4 Solid-state NMR methods for distance measurements

2.4.1 Dipolar interaction

The internuclear dipolar interaction plays a central role in NMR, as many NMR methods based on them. Each spin in a molecule generates a magnetic field around it. Two spins nearby in space experience each other's magnetic field, and the local field generated by external magnetic field B_0 would be slightly changed, an effect named dipole-dipole coupling. This interaction can be utilized for distance measurements or orientation determinations, since the dipolar coupling depends strongly on the distance *r* between the two spins as well as the orientation θ of the spin-spin vectors with respect to the external magnetic field, as shown in Fig. 2.7.

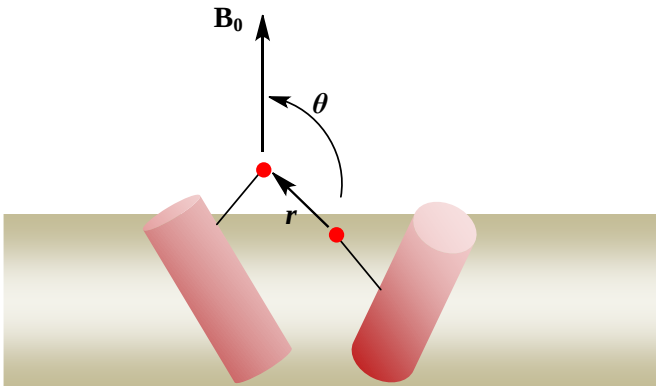

Fig. 2.7 Illustration of spin-spin dipolar coupling using labeled peptides (blue, isotope labels in red) embedded in membranes (gray). The strength of internuclear dipolar coupling is determined by the internuclear distance *r* and the orientation θ of spin-spin vector with respect to the magnetic field B_0.

The general dipolar coupling strength is given by:

$$D = \left| 2 f \hbar \gamma_1 \gamma_2 \frac{\mu_0}{4\pi} \frac{1}{r^3_{12}} \frac{3\langle \cos^2 \theta \rangle - 1}{2} \right| \tag{2.2}$$

with

$\hbar = 1.05459 \times 10^{-34}\, Js$

$\frac{\mu_0}{4\pi} = 10^{-7}\, Hm^{-1}$

for the values of Planck's constant $\hbar$, and magnetic field constant $\frac{\mu_0}{4\pi}$. γ_1 and γ_2 denote the gyromagnetic ratios, the factor f is 1.5 in the case of homonuclear coupling, and for heteronuclear dipolar coupling it is 1. The angular brackets describe a time averaged motion of the label side chain and the entire peptide within the bilayer. For ^{19}F-^{19}F homonulear

dipolar coupling of interest in this study, taking the molecular order parameter S_{mol} into account, we will get:

$$D = 319441Hz \times \frac{1}{(r/A^{\circ})^3}\left|\frac{3\cos^2\theta - 1}{2}\right| \times S_{mol} \qquad (2.3)$$

2.4.2 NMR approaches applied for distance measurements

NMR distance approaches are based on homo- or heteronuclear spin pairs selectively substituted. (a) For distances between homonuclear spins, the ^{19}F nucleus was always utilized in terms of sensitivity. CPMG experiments have been utilized to measure intramolecular ^{19}F-^{19}F distances as long as 6 Å in gramicidin S [102] and 11 Å in PGLa [103] within fluid membranes. Similarly, with a single 4F-Phe, CODEX experiments determined a nearest interhelical distance of M2 protein (M2TMP) to be 7.9-9.5 Å, and moreover, revealed the oligomer state as tetramers in membranes [104]. (b) For distances between heteronuclear spins, REDOR experiments have been broadly used for characterizing a wild range of materials. For instance,^{13}C-^{15}N REDOR determined a distance of 3.43 Å within simple tripeptide crystal [105]. And a long range ^{31}P-^{19}F distances in the range of 12-16 Å was measured in an enzyme-substrate complex [106] and 13-14 Å in the DNA phosphodiester backbone [107].

2.4.2.1 CPMG

The CPMG (Carr-Purcell-Meiboom-Gill) experiment named after its inventors was previously used for determination of relaxation times [108], but was also adapted to measure homonuclear diplolar couplings (^{19}F-^{19}F in this study) and internulcear distances [102, 103, 109, 110]. It consists of a train of thousands 180 ° pulses with a interpulse delay (2τ), after a first 90 ° radiation pulse, as shown in Fig. 2.8A. The composite pulses of 90 °- 180 °$_{90^\circ}$- 90 °(P) with a xy8 phase cycling were introduced to suppress errors arising from imperfections of 180 ° pulses and from infinite pulses. Between every two successive pulses, about 16 points were sampled and averaged. After thousands of echos, all the interactions such as chemical shifts anisotropy, heteronulcear dipolar couplings, field inhomogenities are all averaged out, leaving only homonuclear dipolar couplings, no ^{1}H-decoupling is needed. The echos were sampled, and recorded with a dwell time (dw) as a function of acquisition time t (Fig. 2.8B). After Fourier-transformation dipolar spectra with pure homonuclear dipolar coupling could be

obtained, as shown in Fig. 2.8C. The typical dipolar spectrum is doublet-like, reflecting the X-X dipolar coupling of a 2-spin system (in this work X = ^{19}F).

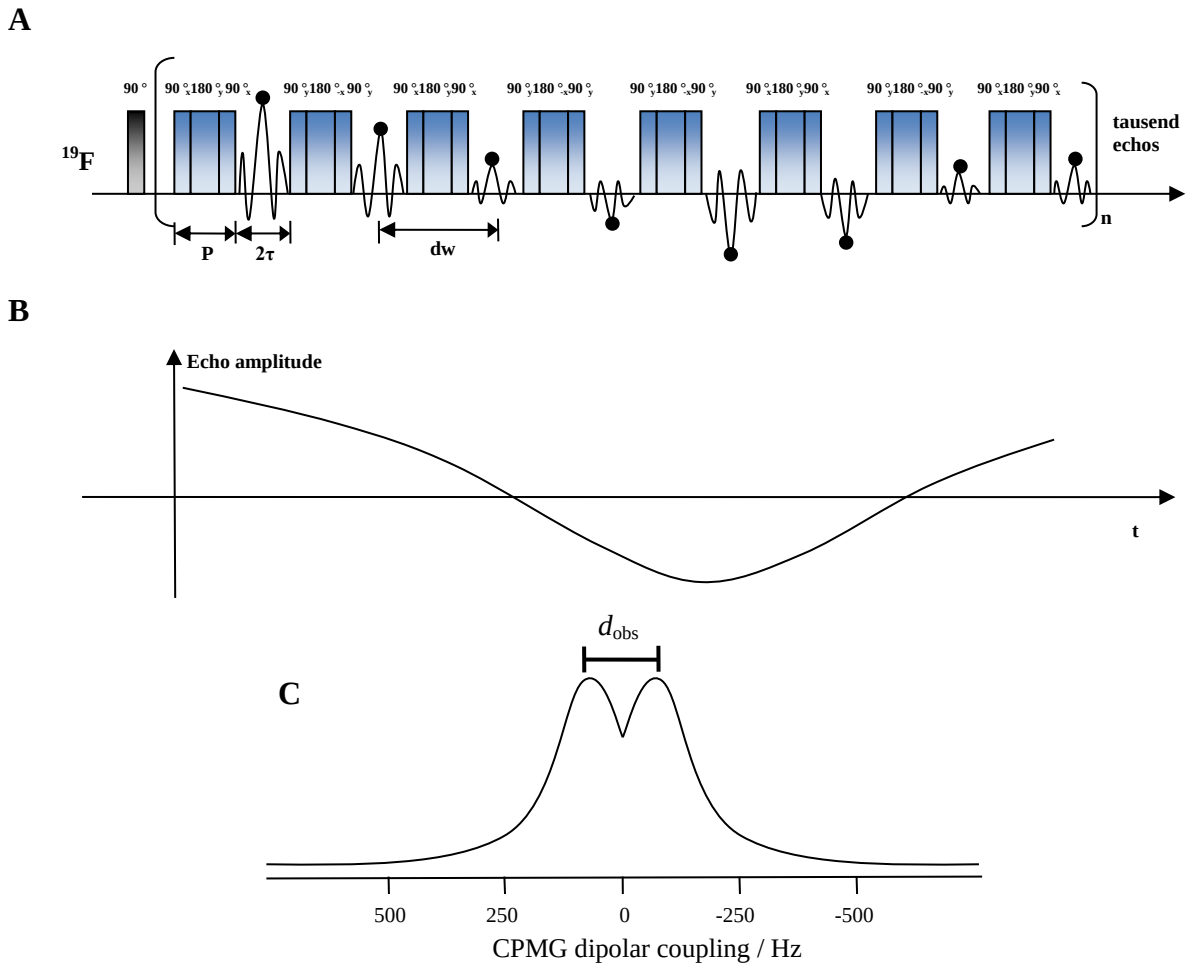

Fig. 2.8 Schematic illustration of CPMG experiments. (A) CPMG multipulse sequqnce on ^{19}F-chanel; (B) Echo points sampled and averaged between two successive pulses as a function of time t; (C) A pure dipolar spectrum could be obtained after Fourier-transformation of B.

2.4.2.2 CODEX

The CODEX (Centerband-Only DEtection of Exchange) experiment based on MAS (magic-angle spinning) technology was introduced for determination of the peptide oligomer numbers in aggregates [104, 111, 112]. In the present study, we applied this method not only for counting oligomer numbers, but also addressing precise intermolecular distances with the aid of sensitive fluorine solid-state NMR. As shown in Fig. 2.9A, the CODEX sequence contains a pair of rotor-synchronized 180 °-pulse trains spaced by T_m termed mixing time (T_r : one rotor period), which is integer number of T_r. The π-pulse trains recouple the CSA interactions. After the second 90 ° pulse, the magnetization flips back to z-direction and during the T_m,

dephases only by spin diffusion between chemically equivalent but orientationally inequivalent ^{19}F-spins. After the second π-pulse train and before acquisition a short time T_z of $2T_r$ is added. For each desired T_m, two spectra (S_0 and S) are acquired with interchanged T_m and T_z, and the dephasing could be obtained via the reduced intensities of the spectra (Fig. 2.9B). With a series of T_m, the CODEX curves can be determined with S / S_0 as a function of T_m as shown in Fig. 2.9C. If an oligomer of m monomers exists, the curves decay to an equilibrium value of 1/m, and a slow or fast decay indicates a long or short intermolecular distance.

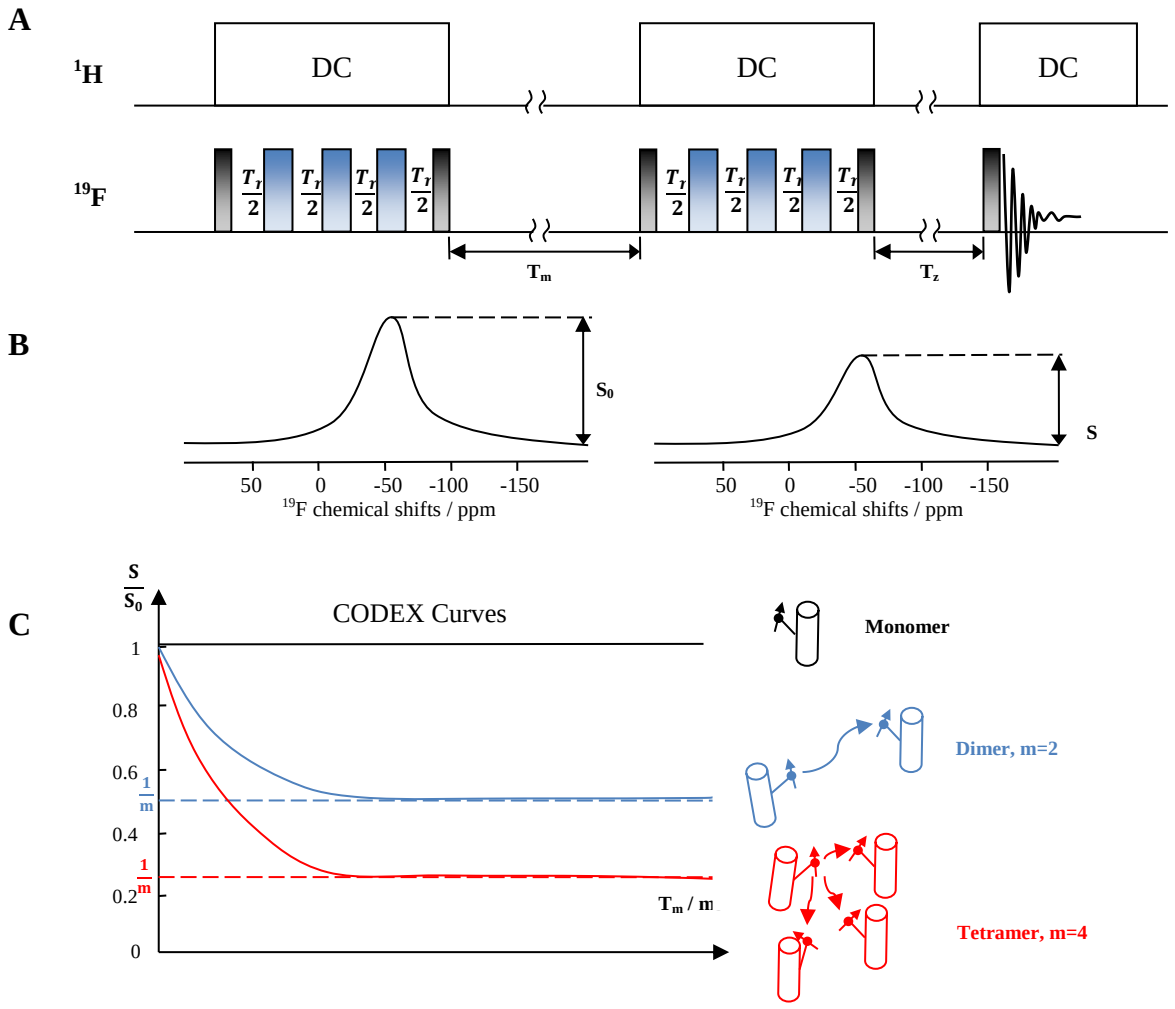

Fig. 2.9 Schematic illustration of CODEX experiments. (A) CODEX multipulse sequqnce, 'DC' means ^{1}H-decoupling; (B) For each T_m, two spectra are obtained with exchange of T_m and T_z; (C) CODEX curves plotted as a function of T_m, for a monomer (black), dimer (blue) and tetramer (red).

2.4.2.3 REDOR

The REDOR (Rotational-Echo DOuble-Resonance) experiment allows to determine heteronulcear dipolar couplings, such as ^{15}N-^{13}C [107, 113-121]. In the present work, we took ^{15}N as the 'observed' nucleus, and ^{13}C as the 'dephased' nucleus, as the ^{13}C of interest is the carbonyl-^{13}C (-^{13}C=O) and lines resulted are always broad and obscured by the nature abundance signals of lipids. As shown in Fig. 2.10A, the rotor-synchronized 180 °-pulses on the ^{13}C-chanel results in dephasing of ^{15}N magnetization transversed from ^{1}H by corss-polarization (CP). The obtained ^{15}N spectrum is termed S, and a reference spectrum S_0 is acquired without ^{13}C-pulses. The extent of the dephasing determined by the ^{15}N-^{13}C dipolar coupling can be obtained by the reduced intensity of spectrum S compared to S_0 (Fig. 2.10B). With a series of dephasing times, REDOR curves can be plotted with $\Delta S / S_0$ as y-axis and dephasing time NT_r as x-axis (Fig. 2.10C). By comparing the experimental data and simulated REDOR curves, the best-fitted value of intermolecular distance r could be found.

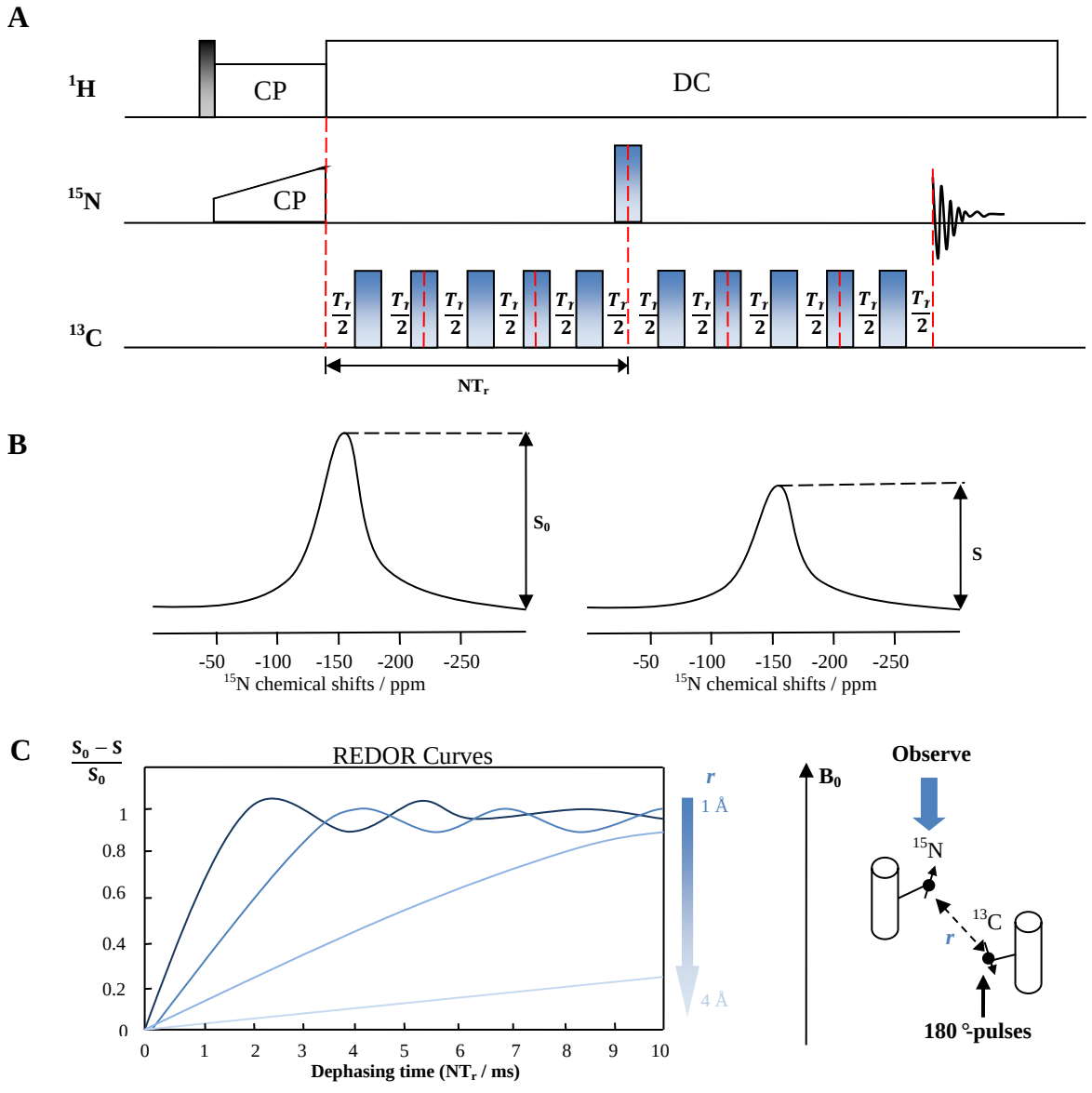

Fig. 2.10 Schematic illustration of REDOR experiments. (A) REDOR multipulse sequqnce, 'DC' is for ^{1}H-decoupling and 'CP' for cross polarisation; (B) With each desired dephasing time NT_r, one dephasing spectrum S and one reference spectrum S_0 are obtained by turning on and off the dephasing chanal (^{13}C); (C) REDOR curves plotted as a function of dephasing time, the interspin distances can be revealed by comparing the experimental data and simulated curves.

3. **Aims of this study**

The prominent interaction of proteins within membranes is dimerization or higher-order oligomerization. Understanding the mechanism of protein interactions within the membranes is of large pharmaceutical importance. However, the study of structural details of these molecular complexes in membranes is always challenged by the intrinsic mobility of the membranes.

The aim of this study therefore was to evaluate and develop methods based on solid-state NMR, which allow the detection of distance-dependent dipolar couplings to determine inter-atomic distances precisely and to measure the oligomer number through 'spin counting'. The usage of highly sensitive ^{19}F-NMR labels was envisaged to extend the sensitivity and distance range. The following distance measurements were to be applied in this study and their performance in membrane systems was to be evaluated:

- Carr Purcell Meiboom Gill (CPMG) experiments on oriented bilayer samples to measure homonulcear ^{19}F-^{19}F dipolar couplings and determine intermolecular distances inparticular in the presence of the high mobility of lipid bilayers in the fluid phase
- Rotational Echo DOuble Resonance (REDOR) experiments to measure dipolar couplings between heteronuclear spin pairs with a wide range of choices (in this study, ^{13}C-^{15}N and ^{13}C-^{19}F) and the distances between them
- Centerband Only Detection of EXchange (CODEX) experiments to count the number of ^{19}F-labels in oligomers, this way determine the oligomer number and also the distances inbetween the oligomer components

To understand the structural principles of such oligomerization processes in membranes, the self-association of the following systems were studied (Fig. 3.1):

- Antimicrobial peptide PGLa: it is postulated to self-dimerize in bacterial membranes and further oligomerize to form pores and kill bacteria by membrane lysis, and this dimerization is facilitated by synergy with Magainin-2;
- Stress-response peptide TisB: it is thought to dimerize to form a proton channel. When exposed to external stress (e.g., antibiotics), bacteria can activate toxins such as the

peptide TisB, which can decrease the proton gradient across the membrane and this way induce dormancy.

- Oncogenetic peptide E5 and PDGFβR protein: E5 is postulated to form dimers in membranes and drive two PGDFβ-receptor protein molecules close in contact to elicit a response of the signal cascade, which would otherwise only happen upon ligand binding.

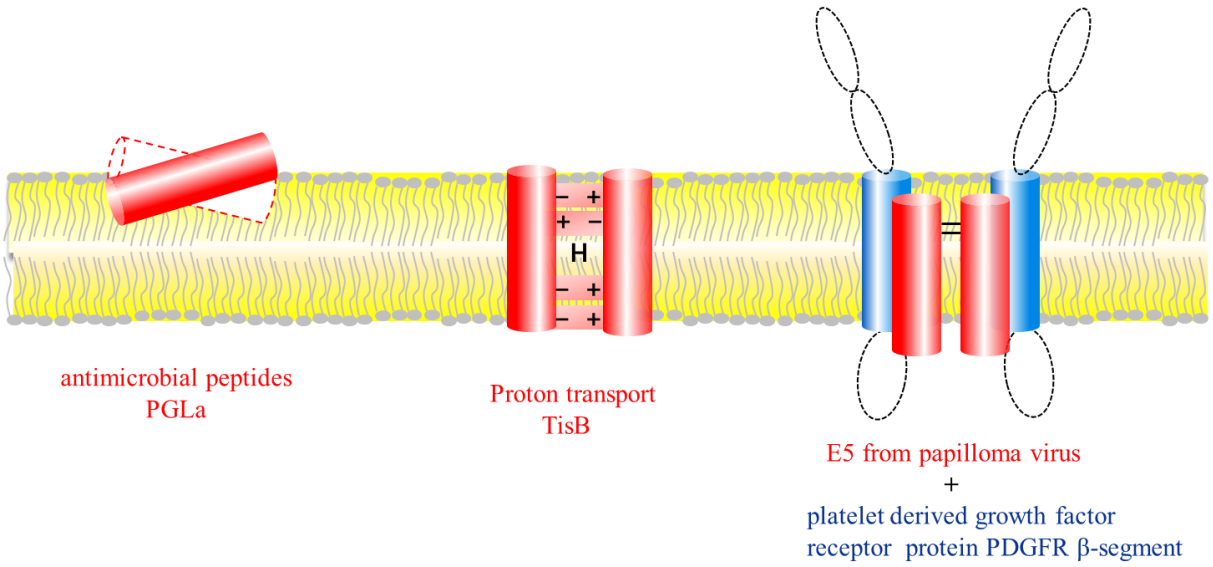

Fig. 3.1 Schematic illustration of dimerisations of antimicrobal peptide PGLa, stress response peptide TisB and oncogenetic peptide E5 with PDGFβR.

Intermolecular distances were to be determined within membranes with the aid of oriented lipid bilayers, maintaining the membrane mobility, or using frozen samples if required by the chosen technique. Structural models of the membrane protein / peptide oligomerization shall be established to understand the intermolecular interactions of membrane-active peptides and receptor proteins. Subsequently, the strengths and weaknesses of the distance approaches for different peptide / protein systems were to be evaluated.

4. Materials and methods

4.1 Amino acids with NMR-labels

All the labels used in this study are summarized in the following Tab. 4.1.1. ^{19}F-labels were used for the CPMG and CODEX measurements, and ^{15}N- and ^{13}C-labels were employed in the REDOR experiments.

Tab. 4.1.1 All the NMR-labels used in this study. ^{13}C- and ^{15}N-labels are marked with '*'.

Name	Structure	Source
L-4-fluoro-phenylglycine (**4F-Phg**) $C_8H_8FNO_2$ 169 g/mol	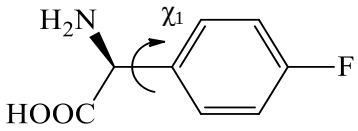	The pure *L*-4F-Phg was bought from Acivate Scientific GmbH (Prien, Germany) and Fmoc-protected with Fmoc-Cl [122] for peptide synthesis.
D/*L*-4-trifluoromethyl-phenylglycine (**CF_3-Phg**) $C_9H_8F_3NO_2$ 219 g/mol	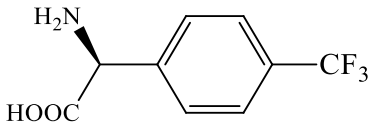	A racemic mixture of *D*/*L*-CF_3-Phg was purchased from ABCR GmbH (Karlsruhe, Germany) and Fmoc-protected [122] for peptide synthesis.
L-2-amino-4-fluorohex-5-enoic acid (**^{19}F-Gln analogue**) $C_6H_9FNO_2$ 146 g/mol	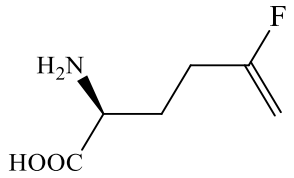	The pure *L*-^{19}F-Gln analogue was purchased from Prof. Günter Haufe [123] and Fmoc-protected [122].
cis-1-(Fmoc-amino)-3-hydroxylbenzol-(trifluoromethyl)-cyclobutanecarboxyl acid (**CF_3-Thr analogue**) $C_{28}H_{23}F_3NO_5$ 510 g/mol	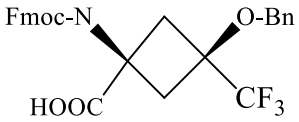	The Fmoc-protected CF_3-Thr analogue was provided by Sergii Afonin [96].
L-aspartic acid-$^{13}C_4$, ^{15}N (**U-Asp**) $C_4H_7NO_4$ 138 g/mol	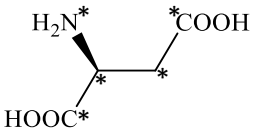	The pure Fmoc-protected uniformly ^{13}C, ^{15}N-labeled Asp was purchased from Cortecnet, Voisins Bretionex, France.

L-lysin-$^{15}N_2$ (**$^{15}N_2$- Lys**) $C_6H_{14}N_2O_2$ 148 g/mol	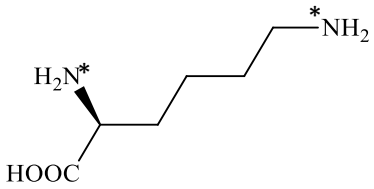	The pure Fmoc-protected uniformly ^{15}N-labeled Asp was purchased from Cortecnet, Voisins Bretionex (France).
L-glutamine-$^{13}C_4$, ^{15}N (**U-Gln**) $C_5H_{10}N_2O_3$ 152 g/mol	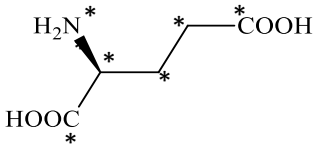	The pure Fmoc-protected uniformly ^{13}C, ^{15}N-labeled Gln was purchased from Iris Biothech GmbH (Germany).

4.2 Solid-phase peptide synthesis

Theoretical background

All the peptides were synthesized according to the solid-phase peptide synthesis (SPPS) pioneered by Nobel Prize carrier Robert B. Merrifield [124]. As shown in Fig. 4.1, the first amino acid is immobilized on a solid (resin beads) by a peptide linker and further amino acids are coupled one by one with the aid of coupling reagents. The resins are retained with growing peptide chain throughout the peptide synthesis until cleavaged by TFA, while all the other liquids incl. by-products are washed away. The peptide synthesis proceeds from C- to N-terminus; the N-terminal amine of all the amino acids is protected by Fmoc-group, which is then removed to free the N-amine for the coupling of the next Fmoc-protected amino acid.

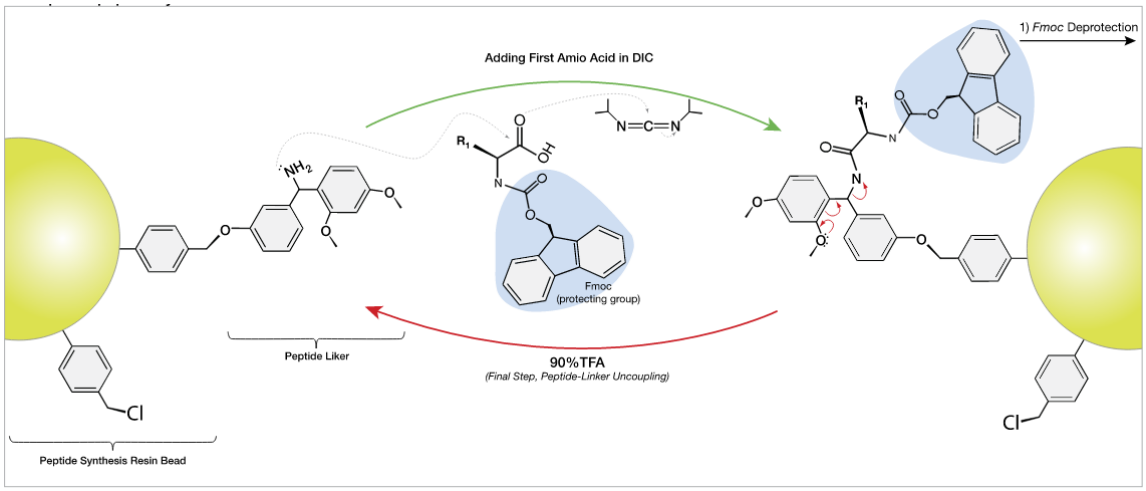

Fig. 4.1 Solid-phase peptide synthesis with Fmoc-strategy. The resin shown is rink amide resin.

Automated synthesis

The peptide synthesis was carried out on a peptide automated synthesizer or microwave synthesizer (CEM) using standard solid phase Fmoc protocol [125] with activator HBTU / HOBt in presence of DIPEA as base. Suitable resin was chosen and soaked in DMF for 1 h before the synthesis. Each Fmoc-protected amino acid was individually dissolved in DMF with the concentration that calculated for a 100 μmol synthesis and then placed in the synthesizer for continuous reactions with the repeated cycles of:

Deprotection of Fmoc → wash → coupling ×2 → wash

For the coupling of each amino acid, 2.5 h (each coupling for 1 h, deprotection for 30 min) were acquired at room temperature for automate synthesizer and 13 min (each coupling for 5 h, deprotection for 3min) at 75 ℃ for CEM. The wash solvent used for CEM was NMP.

Manual synthesis

The labels were manually coupled. Since ^{19}F-labels easily racemized, the coupling reactions of not only the labels themselves but also after the label up to the N-termini were performed manually with 2 h for the label and 1 h × 2 after the label, followed by deprotection for 30 min.

Protection by Fmoc-group

Some amino acids such as ^{19}F-labels should be protected by an Fmoc-group before usage in peptide synthesis. The Fmoc-protecting was achieved with following reagents[122]:

1.0 equiv. amino acid
1.1 equiv. Fmoc-Cl
2.5 equiv. 10% Na_2CO_3 in H_2O

Deprotection of Fmoc-group

The deprotection was carried out with 2 mL 20% piperidine in DMF for 30 min, resulting in a peptide-resin salt.

Test cleavage (‘harsh’)

The test cleavage was performed before and after the labeling with small amount of the resin using the harsh cocktail (92.5 % TFA, 2.5 % H_2O, 5 % TIS, in volume) for one hour at room temperature. Then the coupling efficiency was be checked by MS-LC.

Final cleavage ('mild')

The final cleavage of the peptide from the resin was performed using a 'mild' cocktail (77.5 % TFA, 5 % TA, 5 % H_2O, 5 % EDT, 5 % TIS, 5 % Phenol, in volume) for 1 h at room temperature.

Reductive cleavage

To reduce the oxidized Met and prevent further oxidations [126], the final cleavage should not use the usual mild cleavage but a reductive cleavage. The reductive cleavage cocktail (5 mL) composed as follows. After solvent 2 was completely dissolved, poured into solvent 1, where white flocky precipitate appeared, which after a while turned red / brown. Then I waited until the solvent mixture was clean and clear, gave it to the peptide-resin mixture and left the cleavage interaction in an ice-bath for 1 hour.

Solvent 1		**Solvent 2**	
TFA	4.125 mL	NH_4I	250 mg
EDT	125 µL	H_2O	250 µL
TA	250 µL		
Me_2S	250 µL		
TIS	500 µL		
Phenyl	375 µL		

Crude peptide preparation

After the final cleavage, the resin was then removed by filtration and the filtrate was concentrated under a nitrogen or argon stream. Then the product was precipitated with cool diethyl ether, dissolved in a mixture of AN / water (1:1) and frozen in the refrigerator at -80 ℃ overnight and then lyophilized to white floccules, which is ready for HPLC purification.

4.3 Peptide synthesis, purification and identification

PGLa

The coupling reagents used were: 4 equiv. amino acid; 4 equiv. HOBt; 3.9 equiv. HBTU; 8 equiv. DIPEA. Rink amide MBHA resin (100 - 200 mesh) was chosen to carry the growing

peptide. The syntheses from the C-terminus to the labeling positions were performed on automate synthesizer. The couplings after (incl.) the label 4F-Phg or CF_3-Phg were done manually with combined coupling reagents of HOBt / DIC (2 : 5) to avoid racemization. A racemic mixture of CF_3-Phg was used, since the racemisation of this label cannot be avoided during synthesis anyway. All the other single labeled peptides mentioned in this study were synthesised and purified using the same approach, after then measured using the same experimental equipment and conditions. One problem during the synthesis should be noticed that the coupling efficiency of the label CF_3-Phg was unusually low (only about 10%), probably due to steric hindrance of the bulky side chain of the label. To solve the problem, white sand was added (1:1 in weight) to the resin to dilute the growing peptides to let the bulky CF_3-Phg get in touch with the interaction spots.

The crude peptide was gained by mild cleavage and purified with the help of RP-HPLC with standard gradient of 10-90 % B (solvent A: 90 % H_2O, 10 % AN, 5 mM HCl; solvent B: 10 % H_2O, 90 % AN, 5 mM HCl) over 32 min at 35 ℃. The peptide was dissolved in AN / H_2O (1 : 1) to be highly concentrated solvent (5 mg / mL). The semi-preparative column C18 was used with flow rate of 0.35 mL / min, and for every run 1 mL peptide solution was injected. Per HPLC and LC-MS, we found that, all the double-labeled PGLa analogues were racemized, but fortunately, the racemizers could be separated. After HPLC, all the fractions collected were frozen and lyophilized to be pure white powder.

The *LL*-form PGLa 6-10 and 6-13 labeled with 4F-Phg were identified by comparing the chemical shifts with *L*-single-labeled analogues using liquid-state NMR. Those labeled with CF_3-Phg were discriminated by the chemical shifts and intra-CF_3 dipolar couplings in oriented samples with the aid of solid-state NMR.

TisB

The labeled TisB analogues were synthesized and purified by Dr. Benjamin Zimpfer in our group [127]. The peptide synthesis was performed on CEM. As resin the Fmoc-Lys (Boc)-Wang Resin (0.66 mmol / mg, 0.70 mml /mg, 0.34 mmol / mg) was employed. The amino acids were solved in NMP for 0.57 mol / L and coupled in two steps. Firstly, the coupling reagents used were: 5 equiv. amino acid; 5 equiv. HOBt; 3.9 equiv. HBTU; 10 equiv. DIPEA.

For the second coupling step the HBTU was replaced with PyBOP. Each reaction took 5 min at 75 ℃. For position 11, another 30 min at room temperature was needed for the coupling

reaction. The synthesis with ^{19}F-labels and after the label up to the N-terminus was performed with the same coupling reagents but manually instead of on CEM.

The crude peptide was gained by reductive cleavage and purified by RP-HPLC with standard method of 0-58 % B (solvent A: 90 % AN, 10 % H_2O, 5 mM HCl; solvent B: MeOH) over 16 min at 35 ℃. The peptide was dissolved in A / B (1 : 1) to be highly concentrated (5 mg / mL). The semi-preparative column C4 was used with a flow rate of 7 mL / min.

E5

The E5 peptides were synthesized on CEM from the C-terminus up to the labeling position. After the label position (incl. label) up to the N-terminus the peptides were synthesized manually. The coupling reagents used on CEM synthesizer were: 2 equiv. amino acid; 2 equiv. HOBt·H_2O; 1.9 equiv. HBTU; 5 equiv. DIPEA.

Fmoc-Glu (otBu)-wang resin *LL* (M = 0.29 mmol / g) was used. The synthesis on CEM was performed at 75°C with every coupling for only 5 min and deprotection of Fmoc-deprotection for 3 min, except for His, which is prone to recemize and where the temperature was reduced to 50 °C. The wash solvent used for CEM was NMP. The manual synthesis was done with HOBt / DIC (1:1) at room temperature. The crude peptides were gained with mild cleavage.

The gradient used was 20-50 % B (solvent A: 10 % H_2O, 90 % AN, 5 mM HCl; solvent B: MeOH) over 20 min at 35 ℃ with flow rate of 7 mL / min. The crude peptide was divided into 5mg portions, each portion was dissolved individually in 200 µl AN / MeOH (1 : 1) before injection. The semi-preparative column C4 was applied. After the HPLC purification, the purity of the peptides was checked by liquid-state ^{19}F-NMR in MeOH. Trifluoroacetate (TFA) counterions resulting from HPLC were removed by solving the peptide in 5 M HCl and freeze-drying, until the TFA peaks disappeared in the NMR spectra. After all, we got pure *L*-^{19}F-E5 analogues (purity > 95 %).

PDGFβR

The peptides PDGFβR were synthesized on the peptide synthesizer, and the coupling reagents used were: 2 equiv. amino acid; 2 equiv. HOBt·H_2O; 1.9 equiv. HBTU; 5 equiv. DIPEA. Fmoc-Glu (otBu)-wang resin *LL* (M = 0.29 mmol / g) was used. Manual labeling of ^{15}N, ^{13}C was performed with the same coupling reagents as the synthesizer, and the labeling of ^{19}F was with HOBt / DIC (1 : 2). Although CEM is especially efficient for long-sequence peptide

synthesis, it was not successful to gain PDGFβR, probably because PDGFβR protein is very sensitive to break up or oxidize (O-Met). The final cleavage was done by reductive cleavage.

One another problem which happened during the synthesis was that, the -OBn protecting group could not be 100 % removed after the cleavage, and it was difficult to deal with it further without destroying the peptide PDGFβR. Fortunately, the fraction with failed removal of the protection group was barely seen after HPLC and lyophilisation.

The gradient used was 30-70 % B (solvent A: 95 % H_2O, 5 % AN / IP, 5 mM HCl; solvent B: 95 % AN / IP, 5 % H_2O, 5 mM HCl) over 5 min and then 70-100 % B over 11 min at 35 ℃ with flow rate of 6 mL / min. The crude peptide was divided into 3mg portions, each portion was dissolved individually in 200 µl A / B (1 : 4) before injection. The semi-preparative column C18 was applied. After the HPLC purification, the purity of peptides was checked by liquid-state ^{19}F-NMR in MeOH. The rest TFA counterions resulting from HPLC were removed by solving the peptide in 5 M HCl and freeze-drying, until the TFA peaks disappeared in the NMR spectra. After all, we got pure PDGFβR analogues (purity > 95 %).

4.4 Sample preparation

PGLa

To prepare oriented samples, 0.3 mg peptide was co-dissolved with DMPC (1,2-dimyristoyl-sn-glycero-3-phosphocholine) in methanol with a peptide to lipid ratio of either 1 / 150 (S-state) or 1 / 50 (T-state), and the solution was spread onto thin glass plates (12 × 7.5 × 0.06 mm^3), on each glass plate 30 µl drops containing max. 1mg materials were deposited. After complete evaporation, the plates were stacked, hydrated for 24h at 48 ℃ in a humid atmosphere (96% r.h.) over a saturated K_2SO_4 solution and then immediately wrapped in parafilm and plastic foil. The quality of the membrane alignments was monitored by ^{31}P NMR to be over 95%, as shown in following Fig. 4.2.

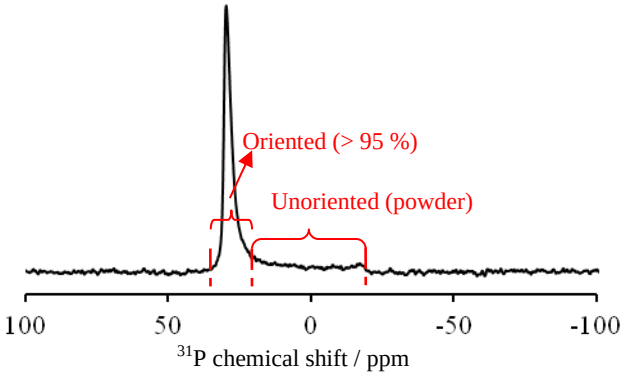

Fig. 4.2 ^{31}P-NMR spectrum of macroscopically oriented sample.

TisB

For CPMG experiments, the fluorinated TisB was embedded in POPC bilayer at a peptide to lipid ratio of 1 : 50 (peptide = 1mg) to prepare oriented samples as previously described (see section 4.4 PGLa). The peptides were once neutralized by dialysis to remove H^+ ions, which could hamper the charge-zipper formation and thus destroy the dimerization. 10 mg peptide was co-dissolved with POPC (1-Palmitoyl-2-oleoyl-sn-glycero-3-3-phosphocholin) with a peptide to lipid ratio of 1 / 50 in MeOH / H_2O (1 : 1), and the solution was put in a ion-exchange membrane bag for dialysis of one week. Then the solution was taken out in a 10 mL tube and frozen at -80 ℃ over night and then lyophilized for 2 days. For REDOR experiments, the TisB / POPC powder mixture (peptide ≈ 5 mg) was filled in a 4 mm rotor and then distilled water (mixture / water = 1 : 1 in weight) was dropped into it to dissolve the powder. After repeated centrifugation and freeze-thaw, the rotor was filled with a white viscous solvent material, where the peptides were homogeneously embedded in POPC liposomes.

E5

For CPMG experiments, oriented samples were made as previously described (section 4.4 PGLa). For CODEX measurements, vesicles filled in 2.5 mm rotor were acquired. Each E5 peptide of 0.5 mg were co-dissolved with ~11 mg DErPC (P / L = 1 : 50) in MeOH and the solvent was then removed under N_2 gas. After that, ~20 µL distilled water was added and with 10 min vortex, white viscose liquids were produced. The liquids were then carefully filled in the rotor. Further 10 min vortex was needed.

E5 and PDGFβR

As described previously in section 4.4 of TisB and of E5, the peptides E5 and PDGFβR (1 : 1 molar, totally ca. 4 mg) were mixed and reconstituted in DErPC with a peptide to lipid ratio of 1 : 50, and filled in a 4 mm rotor for REDOR experiments, Using the same protocol, the samples for CODEX experiment was prepared in a 2.5 mm rotor (total peptide ～1 mg).

4.5 NMR spectroscopy

PGLa (CPMG)

All the measurements in this study were performed on a Bruker Avance 600 MHz spectrometer. The samples were measured at 35 ℃ in the liquid crystalline phase of the lipid membranes and were oriented with the membrane normal parallel (0 °) or perpendicular (90 °) to the magnetic field. ^{1}H-NMR spectra were firstly obtained to indirectly reference the ^{31}P- or ^{19}F-NMR spectra. ^{31}P-NMR spectra were acquired at 243 MHz resonance frequency with a Hahn-echo sequence using an HFX probe equipped with a flat solenoid coil. The one-pulse ^{19}F-spectra were obtained at 565 MHz with one 90° pulse of 2.5μs in length and a π pulse with a delay time of 2μs as well as 15-20 kHz ^{1}H decoupling, using combined HF probe equipped with a goniometer. The dipolar couplings were resolved using a modified CPMG multipulse sequence with a xy8 phase cycling composed of 2048 composite pulses of 90 °-180 °$_{90}$-90° of 10μs in length and time delays of 30 μs without any ^{1}H decoupling. Between two adjacent pulses, 16 data points were sampled, averaged and contributed to the FID. Due to the finite pulses, the measured dipole coupling needed to be corrected by a scaling factor:

$$D_0 = D_{obs} / (1\text{-}1.12d) \qquad (4.1)$$

The duty cycle d can be calculated by P / (P + TD) to be 0.25, where P (10 μs) is the length of the refocusing pulse and TD = 30 μs (see section 3.1). The constant of 1.12 was determined from the observed couplings of a standard substance (FFA) with known coupling in a series of varying duty cycles (see master work of X. Xu) and agrees well with previously reported theoretical value of 9/8 [110]. All the CPMG spectra shown in this study were scaled with this duty factor.

TisB (REDOR and CMPG experiments)

All the experiments were performed on a Bruker Avance 600 MHz spectrometer employing using a 4 mm MAS HXY probe. MAS and cross polarization (CP) were employed. The

recycle delay was set to be 6 ~ 20 s depending on the sample. The contact time was usually 1 ~ 3 ms. The chemical shifts of ^{13}C and ^{15}N were measured with respect to TMS and liquid ammonia using the ^{1}H chemical shift from H_2O to indirectly reference the ^{13}C and ^{15}N spectra. The 90 °pulse lengths used for ^{13}C and ^{15}N were 5 μs and 7 μs, respectively.

For REDOR experiments, ^{1}H was radiated at 600.18 MHz by a 90° pulse of 3.125 μs in length, and the generated magnetisation was transferred to ^{15}N by CP-ramp 100 - 80 %. Two rotor-synchronized π pulse trains of were placed on ^{13}C at 60.8 MHz, each π pulse is 16 μs in length. Before acquisition there is an echo pulse of 10 μs in the middle of ^{15}N observed channel, and for sel-REDOR, the echo pulse is replaced by a selective 180 °-Gaussian pulse, the length is depent on the width of resonance ^{13}C=O. During the REDOR pulse radiation, a ^{1}H-decoupling of 20 kHz was applied, which was increased to 80 kHz for sel-REDOR, and during acquisition it was 80 kHz. The transmitter of ^{15}N was set to near the line of amine-^{15}N, and those of ^{13}C and ^{1}H were set on the lines of ^{13}C=O and $^{1}H_2O$.

The CPMG experiments were performed as previously described (section 4.5 PGLa).

E5 (CPMG and CODEX experiments)

The CPMG experiments were performed as previously described (section 4.5 PGLa).

The CODEX experiments were performed on a Bruker Avance 500 MHz pectrometer (Karlsruhe, Germany), operating at a resonance frequency of 500.16 MHz for ^{1}H, and 470.62 MHz for ^{19}F, using a $^{1}H/^{19}F$-X MAS probe equipped with 2.5mm spinner modules, which allows simultaneous tuning and matching of the ^{1}H and ^{19}F frequencies on one single channel. The experiments were carried out at 223K using Bruker BCU II -80/60 cooler (Bruker Biospin GmbH, Fällanden, Switzerland) and with MAS = 25 kHz. ^{1}H decoupling of 50 kHz and a recycle delay of 3s were used. The pulse sequence applied for ^{19}F CODEX experiments consists of two rotor-synchronized π-pulse trains after the first radiated pulse of 90°, which recouple the chemical shifts anisotropy (CSA) interaction under MAS, as described earlier [104]. The pulse number in the π-pulse train was set to be 6 for measurements of E5 Phe8, Gln17, and 2 for E5 Phe6, Leu7, Phe9, as the later three peptides showed shorter T_1 relaxation time. The other two important parameters are the mixing time T_m between the two recoupling π-pulse trains and the z-filter time t_z before the acquisition. The t_z was added to correct T_1 effects during the mixing time and set to be 80 μs (equal to two rotor periods). On the basis of spin diffusion of ^{19}F - ^{19}F, the magnetization intensity would be reduced during T_m, if

oligomer bundles exist. With each T_m, two experiments S (with desired T_m and shorter T_z) and S_0 (reference measurement with exchanged T_m and T_z) were conducted. Measuring the normalized intensity S / S_0 as a function of T_m composes the CODEX spectrum. Error bars were addressed from the signal-to-noise of the S and S_0 spectra.

E5 and PDGFβR (REDOR and CODEX experiments)

The $^{15}N\{^{13}C\}$REDOR experiments were performed on a Bruker Avance 600 MHz spectrometer with a 4 mm MAS HXY probe, as previously described in section 4.5 TisB. The $^{13}C\{^{19}F\}$REDOR was also performed on the 600 MHz spectrometer with a 4 mm MAS HFX probe. ^{1}H was set to be 5 μs at 6.2 dB, and transferred to ^{13}C by CP with 35 kHz and contact time of 1 ms. ^{19}F was set to be 7 μs at 11 dB. The ^{1}H decoupling used was 50 kHz. $^{15}N\{^{19}F\}$REDOR was performed on a Bruker Avance 500 MHz spectrometer with a 4 mm MAS HFX probe. ^{1}H was 3.125 μs and the transferred ^{15}N was 6 μs with contact time of 0.8 ms. ^{19}F was set to be 7 μs.

The CODEX experiments were performed as previously described in section 4.5 E5.

5. Results and discussion: study of intermolecular dimers in the lipid bilayer

5.1 Distance limits and method development using PGLa

Introduction

NMR is a versatile method for membrane-active peptides studies addressing their structure and dynamic behaviour in a quasi-native lipid membrane environment [102, 128-132]. The two dominant structural parameters which solid-state NMR allows to measure are (i) the alignment of the entire peptide within the membrane, and (ii) inter-molecular distance *r* using a pair of labels, which can reveal an oligomerisation. ^{19}F is a formidable label for such measurements on grounds of its high NMR sensitivity and a lack of background signals [98, 99, 133]. Until now a wealth of ^{19}F-labeled amino acids have been designed [95-97, 99, 134, 135], but only a few of them are suitable as ^{19}F-NMR labels for the envisaged structural investigations, since the CF_3-or F-reporter group is required to be rigidly attached to the peptide backbone in a well-defined geometry and without compromising the structural and biological function of the peptides. Furthermore, the labeled amino acid should be chemically stable throughout the solid-phase peptide synthesis (SPPS) (Fig. 5.1.1) [99, 136].

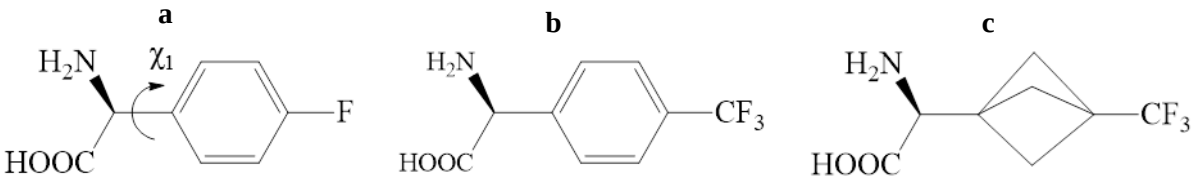

Fig. 5.1.1 Suitable ^{19}F-labeled amino acids for membrane-active peptides studies: (a) *L*-4-fluoro-phenylglycine, 4F-Phg, (b) *L*-4-trifluoromethyl-phenylglycine, CF_3-Phg, (c) 3-trifluoromethyl-bicyclopent-[1.1.1]-1-ylglycine, CF_3-Bpg.

Fig. 5.1.1 shows three prominent ^{19}F-substituted amino acids comprised of phenylglycine (Phg) or bicyclopentylglycine (Bpg) carrying either an ^{19}F- or CF_3-reporter. In 4F-Phg (Fig. 5.1.1a), the uncertainty of the rotation χ_1 of the phenylring around the C_α-C_β bond makes the analysis of the chemical shift anisotropy (CSA) difficult, as it leads to ambiguous orientational interpretations. This torsion also exists in CF_3-Phg and CF_3-Bpg (Fig. 5.1.1b and c), however, fast rotation of the CF_3-group makes all the ^{19}F interactions symmetric along C_α-

C_β bond, and the intra-CF_3 dipolar splitting refers to the segmental orientation, which renders the CF_3-reporter more suited for peptide alignment analyses. One unavoidable drawback of the fluorine-Phg is that it racemizes even under optimised conditions of peptide synthesis. However, the stereoisomers can be separated by reversed-phase high-performance liquid chromatography (RP-HPLC) and distinguished by further analysis with the aid of NMR measurements [103]. If not, the bicyclopentylglycine (Bpg, Fig. 5.1.1c) is a viable alternative [98]. For distance measurements, the 4F-Phg has been previously used to gain an intra-molecular distance of 6 Å in peptide Gramicidin A, using a modified Carr-Purcell-Meiboom-Gill (CPMG) sequence, which was carried out on macroscopically oriented samples without magic angle spinning (MAS) [102]. Also a long-range distance of ~11 Å (80 Hz) between a pair of labels within the peptide PGLa embedded in fluid membranes has been revealed [103]. With the same approach, a weak inter-label coupling of 20 Hz also has been demonstrated with CF_3-Phg incorporated in peptide gramicidin S even in the presence of a more than fourfold stronger intra-CF_3-group coupling [110]. Although the CPMG approach in that work was used to distinguish different epimeric peptides, it opens up a new opportunity for distance measurements from multiple-^{19}F labels. However, such small dipolar splitting obtained in gramicidin S may be a challenge for PGLa, since it is two times larger than gramicidin S, which leads to broader ^{19}F-NMR lines and poorer resolution.

In this study, we chose the antimicrobial peptide PGLa (Tab. 5.1.1), whose structure in oriented lipid membranes is already well-known on the basis of ^{2}H, ^{15}N- and ^{19}F-labeled analogues as a test case for distance measurements [31-33, 98, 137-140]. At first, we compared the use of 4F-Phg and CF_3-Phg to determine the orientation of a peptide. Aim was to evaluate the impact of the rotamer on the orientation determination. To this aim, PGLa was labeled with a single 4F-Phg in position 6, 10, 13 or 14 (Tab. 5.1.1). With the four singly ^{19}F-labeled PGLa analogues, the typical problem of 4F-Phg concerning the impact of the phenylring torsion on the orientation analysis was illustrated by a best-fit analysis. The capability of 4F-Phg and CF_3-Phg for distance measurements was then demonstrated and compared by doubly labeled PGLa substituted in the same positions using the CPMG approach. For this purpose, the labels were placed into PGLa in positions 6 and 13, which are two helical turns apart, to give a rather weak inter-label coupling, and in positions 6 and 10 to provide a comparably strong dipolar coupling [103]. Theoretically, the fast methyl rotation of the CF_3-group could reduce T_2-relaxation and enhance the resolution; it is therefore expected to be more advantageous for gaining weak dipolar cou plings. However, a better performance

of 4F-Phg was obtained. These results may be important for further experiments for studying membrane-associated peptides and proteins.

Tab. 5.1.1 Synthesized ^{19}F-labeled PGLa analogues. Labels are marked in bold and yellow.

Name	**Sequence**	**Molar mass [g/mol]**
L-PGLa 6	GMASK-**4F-Phg**-GAIAGKIAKVALKAL-NH_2	2300
L-PGLa 10	GMASKAGAI-**4F-Phg**-GKIAKVALKAL-NH_2	2300
L-PGLa 13	GMASKAGAIAGK-**4F-Phg**-AKVALKAL-NH_2	2240
L-PGLa 14	GMASKAGAIAGKI-**4F-Phg**-KVALKAL-NH_2	2300
LL-PGLa 6-10	GMASK-**4F-Phg**-GAI-**4F-Phg**-GKIAKVALKAL-NH_2	2380
LL-PGLa 6-13	GMASK-**4F-Phg**-GAIAGK-**4F-Phg**-AKVALKAL-NH_2	2368
LL-PGLa 6-10	GMASK-**CF_3-Phg**-GAI-**CF_3-Phg**-GKIAKVALKAL-NH_2	2480
LL-PGLa 6-13	GMASK-**CF_3-Phg**-GAIAGK-**CF_3-Phg**-AKVALKAL-NH_2	2438

Data analysis

- **Orientation analysis**

Aim was to determine the orientation of the peptide, defined by a set of Euler angles (τ, ρ) relating the laboratory frame (LAB) and a molecule fixed frame (MOL) and the molecular order parameter (S_{mol}). In oriented samples, the measured ^{19}F-NMR frequency depends on the ^{19}F-CSA tensor, and hence on the sidechain orientation, allowing to obtain orientational constraints. The chemical shift resonance frequency can be predicted for a given peptide orientation by transforming the CSA tensor from principal its axis system (PAS) to the laboratory frame (LAB):

$$\sigma = (\sigma^{LAB})_{zz} = (R^{PAS \to LAB} \times \sigma^{PAS} \times (R^{PAS \to LAB})^{-1})_{zz} \tag{5.1}$$

The transformation from PAS to LAB can be achieved in two steps,

$$R^{PAS\rightarrow LAB} = R^{PAS\rightarrow MOL} \times R^{MOL\rightarrow LAB} = R(\alpha,\beta,\gamma) \times R(0°,\tau,\rho) \tag{5.2}$$

where PAS→MOL describes the principle axis system of the CSA tensor of the ^{19}F-label related to the whole peptide molecule, and the symbols α, β, γ denote the Euler angle of the label side chain with respect to the peptide backbone. MOL→LAB illustrates the relationship between the peptide molecule and the laboratory system, in which the external magnetic field B_0 is along the z-axis, and the tilt angle τ and azimuthal rotational angle ρ are used to define the orientation of the peptide in the laboratory frame.

With α = 140°, β = 120°, γ = 65 ° determined by molecular modelling (specific for 4F-Phg residue in a perfect α-helix), we simulated the chemical shift frequencies as a function of τ and ρ, and performed a best-fit analysis with the experimental data using computer programme, which was written by S. Grage. The quality of the fit was determined by the root mean square deviation (rmsd) quantifying the difference between four experimental ^{19}F-NMR frequencies and the respective predicted values. The alignment of the peptide PGLa could be determined by a grid search in the range of 0° ≤ τ < 180° and 0° ≤ ρ < 180 ° to find the best-fit (minimum rmsd) by comparing the experimentally measured chemical shifts of the four 4F-Phg labeled PGLa analogues and the simulated data. Note, that the molecular mobility S_{mol} as well as the label side chain rotation χ and wobble should be taken into consideration. To simplify the calculation, the value of molecular order parameter S_{mol} as 0.75 for T- and 0.66 for S-state of PGLa in oriented membranes were used [31]. The rmsd-plots was drawn as a function of τ and ρ applying values of χ_1 in the range of 0 ∼ 360 ° with four different fluctuation range of ± 0 °, ± 30 °, ± 60 °, and ± 90 °.

- **Distance analysis**

As previously illustrated (section 2.4.1), the general dipolar coupling between two ^{19}F-spins is related to the inter-spin distance *r* and the ^{19}F-^{19}F vector orientation θ with respect to the external magnetic field B_0 (eq. 2.2 and 2.3). In our case of known orientation of PGLa in the S-state (τ = 89°, ρ = 106 °, S_{mol} = 0.66), the inter-nuclear distances could be revealed from experimental values of the dipolar coupling and the calculated orientation θ of the inter-fluorine vector.

In the case of CF_3-labels, the situation is more complex, since there are 6 spins involved. Not only the couplings between the two CF_3-groups (3*d*) but also within the triad (3*D*) are present.

Underneath the triplet-like pattern of the CPMG spectra there are actually many peaks due to interactions between all 6 spins, which though are broadened by mosaic spread due to imperfect molecular alignment, and relaxation. The best-fits of intra-CF_3 couplings *D* were searched in the region -2.5 kHz < *D* < 2.5 kHz by rmsd analysis comparing the simulated and the experimental 1-pulse ^{19}F-spectra, using the computer program written by S. Grage [31]. Then with fixed values of *D*, the weaker *inter*-label couplings were best-fitted in the region -500 Hz < *d* < + 500Hz by comparing simulations and experimental CPMG spectra. Mosaic spread and line broadening were taken into consideration in the simulation.

Results

- **Orientation analysis**

Using four single CF_3-labeled peptide analogues, the orientational constraints (τ, ρ, S_{mol}) of the peptide in membranes have been determined previously with the aid of the anisotropic dipolar coupling within the CF_3-group [31]. In this study, instead of the CF_3-group, a single fluorine reporter of 4F-Phg was introduced into PGLa at position 6, 10, 13, 14, respectively, giving rise to a single peak in the 1-pulse ^{19}F-experiments (Fig. 5.1.2). The PGLa analogues were embedded in oriented membranes at a peptide to lipid ratio of 1 / 150 (Fig. 5.1.2a-d) and of 1 / 50 (Fig. 5.1.2e-h) and the samples were measured with membrane normal parallel to the external magnetic field B_0. In the ^{19}F-spectra of these oriented samples, only the chemical shifts could be obtained, which are orientation-dependent. At first glance, only slight differences could be observed between the four peptide analogues. Take for instance pos. 6, 13 and 14 in the T-state (Fig. 5.1.1e, g, h), their chemical shifts are around 110 ppm and barely distinguishable. In principle, identical chemical shifts of pos. 6 and pos. 13 are expected, since the pitch angle between their residues is only 20 °, nevertheless, also the 100 ° turn between pos. 13 and 14 is not reflected in the spectra.

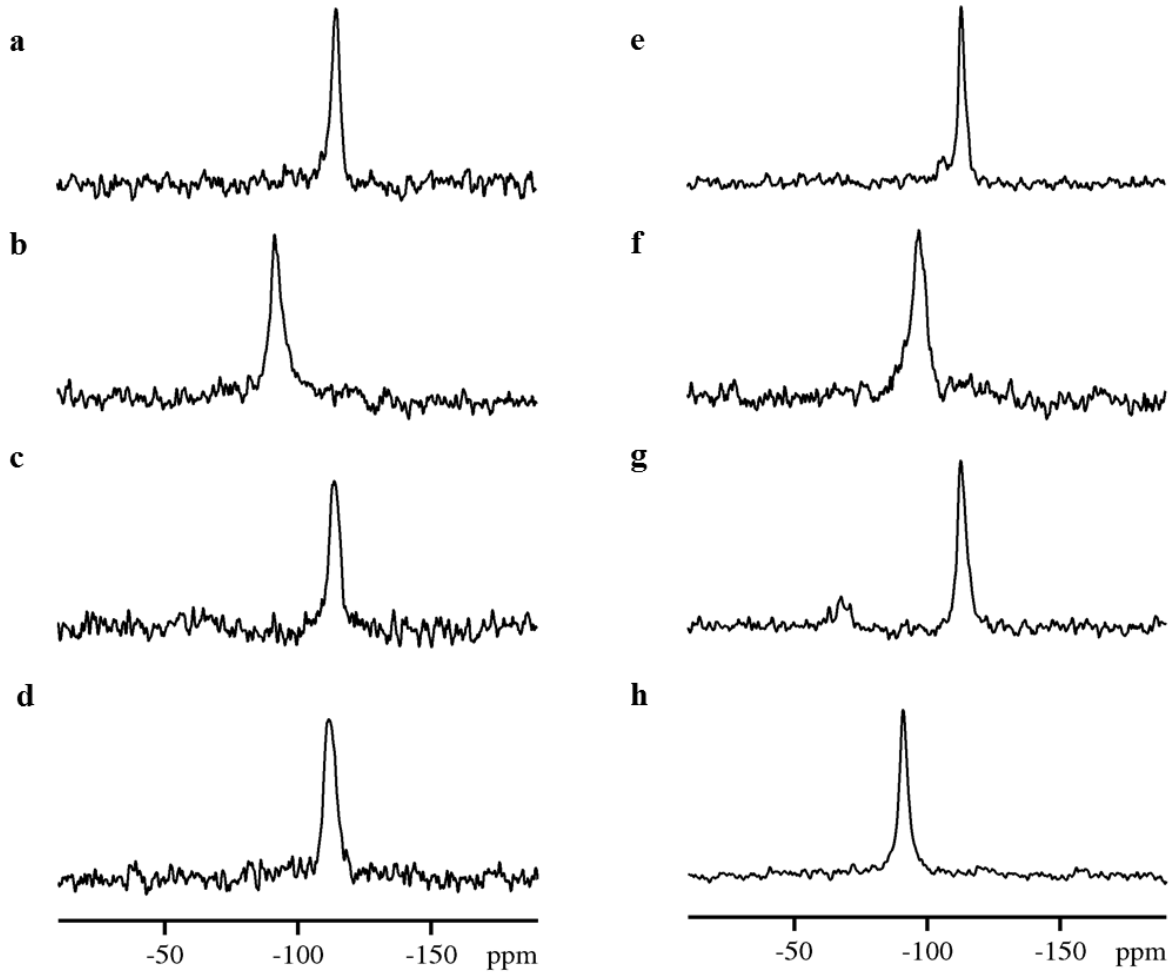

Fig. 5.1.2 1-pulse ^{19}F-experiments of 4F-Phg labeled PGLa at positions 6, 10, 13, 14 embedded in oriented DMPC bilayer membranes with a peptide to lipid ratio of 1 / 150 (a-d) and of 1 / 50 (e-h). All the oriented samples were measured at 35 ℃ with the membrane normal parallel to the magnetic and with 4000 transients.

Note, that not only the helical orientation, but also the phenylring rotation angle χ_1 of the phenylring has an impact on the CSA tensor orientation and hence the observed chemical shift. Therefore, unlike the symmetrically rotating CF_3-group, χ_1 needs to be taken into consideration in the orientation analysis, since the knowledge of the CSA tensor's principal axes frame is vital for the analysis. S. Afonin [132] observed a minimum value of $\chi 1$ for a broad range from 80 ° to 150 ° for an α-helix per 'energy profiles' of 4F-Phg in an ideal poly-Ala peptide, an order parameter S_{phg} describing the oscillation of the 4F-Phg side chain was introduced and was found to strongly affect the best-fit calculation for peptide alignment. Here, we assume that the torsion angle χ_1 of the 4F-Phg are identical for all positions in PGLa. Not only the side chain torsion angle but also a wobble influence the CSA tensor and observed frequency. To compare both the influence of the torsion angle and the wobble, we varied the average angle of χ_1 in the range of 0 ° to 360 ° and the fluctuation angle in following

best-fit calculation. Note that, the rotation angle χ_1 is orientationally equivalent to $\chi_1 + 180°$. Four different side chain oscillation angles ($\pm 0°$, $\pm 30°$, $\pm 60°$, $\pm 90°$) were examined. As illustrated in Fig. 5.1.3, comparing the predicted chemical shifts (colored lines) and our experimental data (black dotted lines), the minimum rmsd were found to be 5 ppm with $\chi_1 \approx 30°$ for S-state, and the fluctuation did not have much impact on the observed chemical shifts (Fig. 5.1.3A). For T-state (Fig. 5.1.3B), the minimum is obtained to be 5 ppm with $\chi_1 \approx 40° \pm 60°$, which is only slightly different from the value in the S-state.

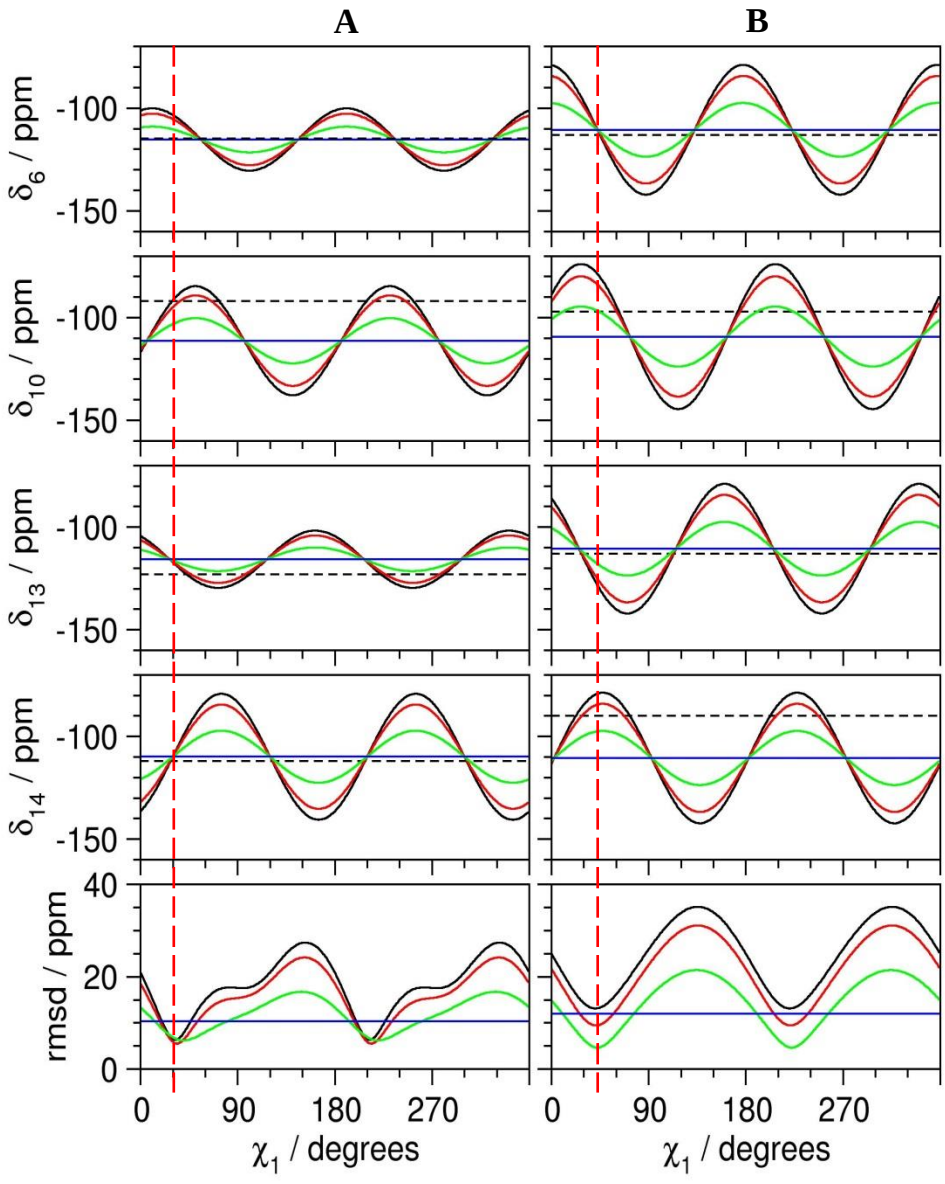

Fig. 5.1.3 Predicted chemical shifts of single 4F-Phg labeled PGLa (A: P / L = 1 / 150, B: P / L = 1 / 50) in four different positions with χ_1 angle in the range of $0 \sim 360°$ ($\chi_1 = 180° + \chi_1$). Four wobble amplitudes were taken into consideration; they are 0 ° (black), 30 ° (red), 60 ° (green), 90 ° (blue). The dotted lines indicate our experimental values.

To evaluate the influence of the rotamer on the orientation analysis, the tilt angle τ and azimuthal angle ρ were searched in the region 0 ° ∼ 180 ° by comparing predicted chemical shifts and experimental data, as shown in Fig. 5.1.4. For PGLa in the S-state (Fig. 5.1.4A), the rmsd values are quite similar for all χ_1 studied, indicating that it is difficult to determine the χ_1 angle. With varied χ_1, the tilt angle τ does not change much, whereas the angle ρ strongly depends on it. Although the best-fit of fluctuation angle could be found by minimum rmsd (Fig. 5.1.4A, black line), the angles τ, ρ do not show a significant dependence on the wobble. For the T-state (Fig. 5.1.4B), there are two rmsd minima with $\chi_1 \approx 20°$ and 130°, but the best fits approaching the experimental data (Fig. 5.1.4B, dotted lines) were found with $\chi_1 \approx 40°$ with a fluctuation of ± 60 °, which shows a good agreement with the results by chemical shifts analysis (Fig. 5.1.3B).

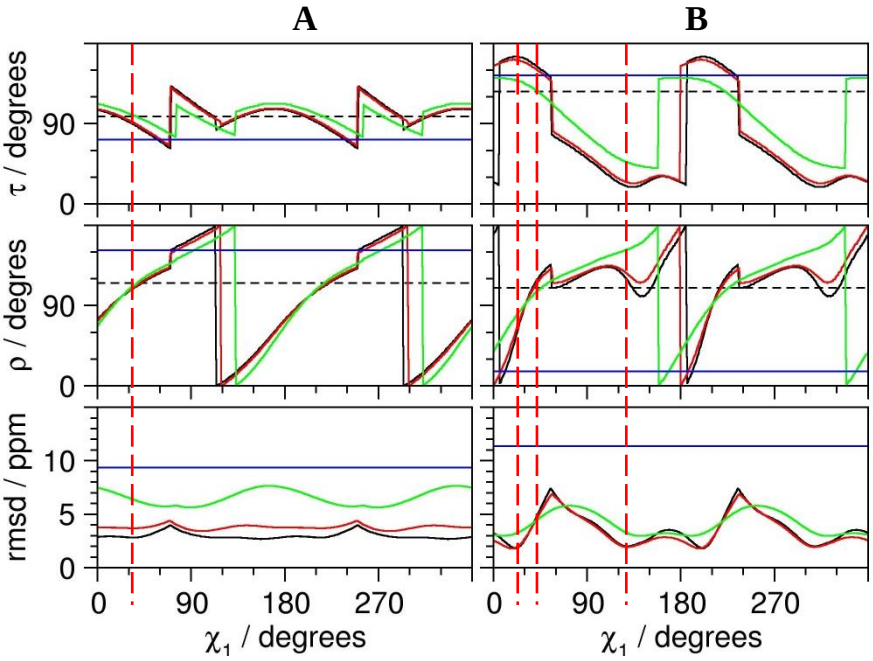

Fig. 5.1.4 The best-fits of τ (helix tilt angle) and ρ (azimuthal rotation angle) and the minimum rmsd were plotted as a function of the phenyl torsion angle χ_1 angle in the range of 0 ∼ 360 ° (χ_1 = 180° + χ_1), and four averaged wobble angles about the equilibrium values of χ_1, they are 0 ° (dark blue), 30 ° (red), 60 ° (green), 90 ° (blue). The values of τ and ρ were searched in the region 0° ≤ τ < 180°, 0° ≤ ρ < 180° comparing the four experimentally measured chemical shifts with the simulated values on the basis of finding the minimum values of rmsd, S_{mol} = 0.75 for PGLa in T-state (A: P / L = 1 / 150) and 0.66 for S-state (B: P / L = 1 / 50) were employed for the calculations. The dotted lines show the expected values of τ and ρ as reported (τ = 119°, ρ = 113 ° for T-state; τ = 91°, ρ = 125° for S-state) [31, 33].

- **CPMG dipolar spectra**

To assess and compare the property of the CF_3- and monoF-reporter as NMR-label in terms of distance measurements, the antimicrobial peptide PGLa was chosen as test molecule and doubly labeled with 4F-Phg or CF_3-Phg in either positions 6 and 10 (PGLa 6-10) or positions 6 and 13 (PGLa 6-13). Under the same conditions, a simple ^{19}F-NMR spectrum and a CPMG spectrum of each labeled peptide were obtained. To reveal the inter-^{19}F-group distances, a modified CMPG sequence composed of a train of 180 ° pulses was employed to extract a spectrum of pure ^{19}F-^{19}F homonuclear dipolar couplings, leaving all the other interactions, such as chemical shift anisotropies, heteronuclear dipolar couplings and field inhomogeneities, averaged out. Technically important, CPMG needs no MAS and ^{1}H-decoupling. Furthermore, as CPMG does not require freezing of the sample, which is usually required for most MAS techniques, CPMG allows to obtain structural parameters in fluid membranes under physical conditions.

As shown in Fig. 5.1.5, the two monofluoro-labels within PGLa 6-10 (Fig. 5.1.5a) and PGLa 6-13 (Fig. 5.1.5b) contribute two peaks in the ^{19}F-NMR spectra. The two peaks from PGLa 6-13 (Fig. 5.1.5b) show nearly the same chemical shifts around -113 ppm and thus overlap, as these two positions are located in the helix exactly two turns apart and their residues differ only 20 ° in orientation. Therefore the right peak at -118 ppm in spectrum (Fig. 5.1.5a) of PGLa 6-10 is referenced to the label of position 6 with a small shift, and the left line at -95 ppm to position 10. Note that, only the ^{19}F-chemical shifts are observable here, and the small splittings expected from the weak inter-^{19}F-label dipolar coupling are obscured by the chemical shift and therefore invisible.

The triads of the CF_3-reporters manifest themselves as triplet around -50 ppm in the simple ^{19}F-spectra (Fig. 5.1.5, c-d), and the splittings indicate the intra-CF_3 group dipolar couplings, depending on the segmental orientations of the labels. Due to the small helical turn of 20 ° between position 6 and 13, they should have nearly the same segmental orientations and thus similar chemical shifts as well as intra-CF_3 group dipolar splittings. As shown in spectrum (Fig. 5.1.5d), superposed triplets with splittings of about 6 kHz are observed for PGLa 6-13. For PGLa 6-10 (Fig. 5.1.5c), the resolved triplet is arising from position 6, whereas position 10 contributes only to the right-most peak, because the dipolar coupling is too small and therefore obscured by linebroadening. These observed dipolar couplings and chemical shifts agree very well with the earlier reported *L*-epimers [31], thus, the doubly labeled PGLa analogues used in this study can be identified as pure *LL*-forms.

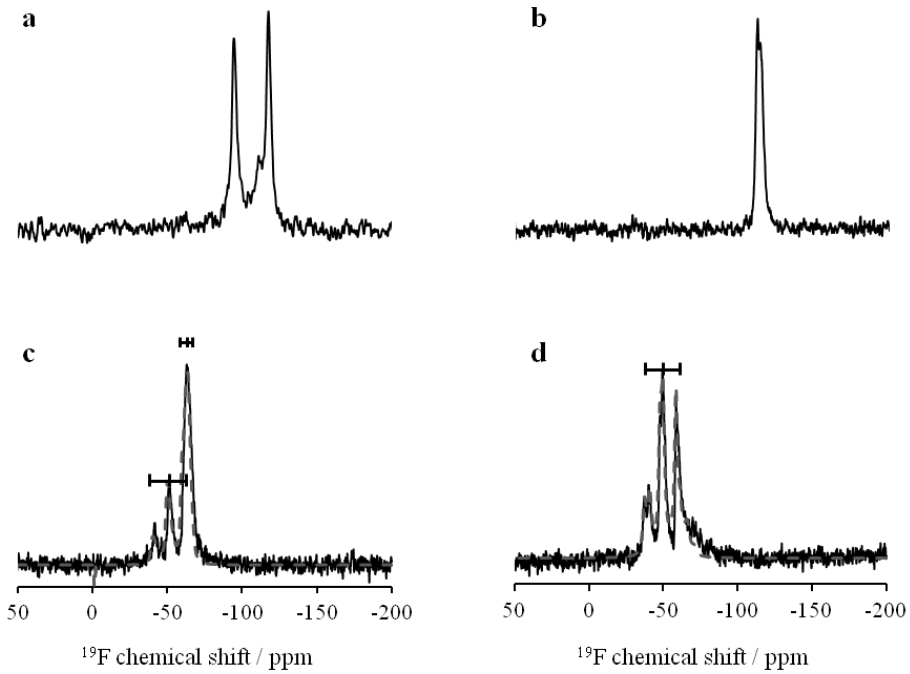

Fig. 5.1.5 1-pulse ^{19}F-NMR spectra of 4F-Phg (a-b) and CF_3-Phg (c-d) labeled PGLa. PGLa were double-labeled in positions 6-10 (a, c) or 6-13 (b, d) and embedded in oriented DMPC lipid bilayers with a peptide to lipid molar ratio of 1 to 150. The spectra were obtained with 4000 scans.

With the aid of the CPMG approach, not only the intra-CF_3 but also the obscured weak inter-label dipolar couplings were addressed, as shown in Fig. 5.1.6. Compared to the monofluoro-reporter, CF_3-group was expected to perform better, as the rapid methyl rotation should lead to shorter T_2, and thus increase the resolution. However, at first glance, the weak inter-label dipolar coupling of both of the 4F-Phg labeled PGLa are resolved (Fig. 5.1.6a-d), whereas with CF_3-Phg the weaker one of PGLa 6-13 is unresolved (Fig. 5.1.6f).

The CPMG spectra of monoF-labeled PGLa exhibit a doublet (Fig. 5.1.6, a-d), from which the pure inter-^{19}F dipolar couplings d_{obs} can be directly read, they are 376 $\pm$17 (c) and 79 $\pm$12 Hz (d) for PGLa 6-10 and PGLa 6-13, respectively. The weak coupling of about 79 Hz indicates a long range distance of ~11 Å, which is unpresidented in distance measurements of biological molecules in a native fluid membrane.

Unlike the doublet from monofluoro-labels, the dipolar spectra of PGLa with CF_3-Phg as labels possess a triplet-like pattern (e and f), originating from the strong intra-CF_3-group couplings D_1 and D_2, which are depended on orientation of the labeled residues. In addition, there is a small splitting across the central peak in the case of PGLa 6-10 (e), which results from the weak dipolar coupling between the two CF_3-labels. However, the dipolar couplings cannot be directly determined from the splittings of the triplet, in fact, the line shape pattern

of a 6-spins system is more complex than its first-glance appearance, to analyse the data, the line broadening and mosaic spread should be taken into consideration to simulate the line shape.

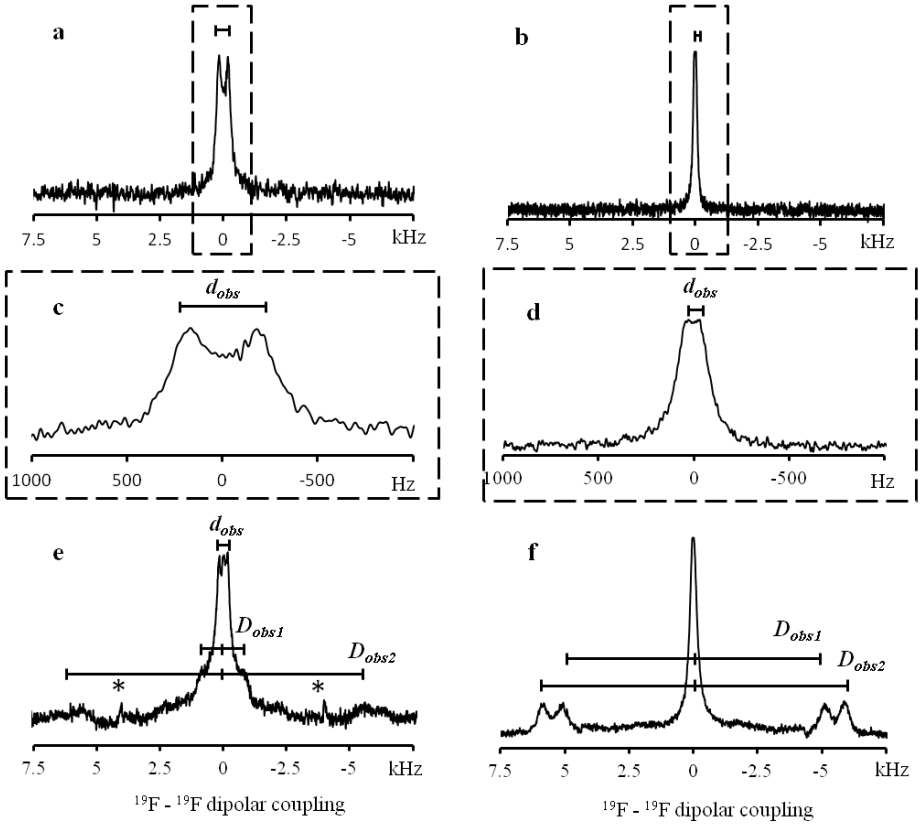

Fig. 5.1.6 CPMG spectra of 4F-Phg (a-d) and CF_3-Phg (e-f) labeled PGLa. PGLa were double-labeled in positions 6-10 (a, c, e) or 6-13 (b, d, f) and embedded in oriented DMPC lipid bilayers with a peptide to lipid molar ratio of 1 to 150. All the spectra shown here were measured at 35 ℃ and with the membrane normal parallel to the magnetic field. 'xy8' phase cycling introduced in CPMG spectra can suppress the errors caused by the imperfection of the π pulses, however, sometimes leads to sidebands (h, marked with '*'). The spectra were obtained with 4000-6000 scans.

Note that the imperfection of the 180 ° pulses leads to a systematic error, resulting to signal losses. Therefore, xy8 cycling was introduced to suppress the errors, which sometimes gave rise to sidebands (Fig. 5.1.6 e, marked with '*'). Fortunately, in this study we can distinguish the peaks of interest from these artefact signals. However, one other problem cannot be avoided, that is the poor resolution even with more scans. As shown in spectrum Fig. 5.1.6e, the signal of coupling D_2 seems to be a triplet with peaks around ± 6 kHz just like that in spectrum (f), but burried in the noise on the down field wing, which makes it difficult to obtain D_1 and d by simultaneous automated fitting. Thus, it was better to fix D_1 and D_2 values

obtained from the experimental 1-pulse ^{19}F-NMR spectrum on the basis of finding the minimum rmsd and vary *d* in the fitting simulation.

Hence, as a first step in the analysis, the intra-CF_3 group dipolar couplings D_1 and D_1 were determined from the 1-pulse ^{19}F-NMR spectra by lineshape fitting. As shown in Fig. 5.1.7, the rmsd plots (Fig. 5.1.7a, e) show two minima with the same rmsd values of 0.00077 for the intra-CF_3 dipolar couplings D_1 and D_2. The minima always occur in pairs but are equivalent, as they lead to identical spectra with interchanged D_1 and D_2. The solution are (D_1, D_2) = (+ 380 Hz, -1920 Hz) for PGLa 6-10 (Fig. 5.1.7a) and (D_1, D_2) = (- 1730 Hz, - 2030 Hz) for PGLa 6-13 (Fig. 5.1.7e), which are marked with '+'. The couplings of *D* show a good agreement with the earlier reported data [31], and the simulations reproduce the experimental 1-pulse ^{19}F-NMR spectra well (as shown in Fig. 5.1.7 b and f, the dashed spectra in grey denote the simulated spectra), With the known values of D_1 and D_2, the inter-CF_3 coupling *d* could be obtained by a grid search comparing simulated and experimental dipolar spectra in the region of -500 Hz ~ +500 Hz, and from the one-dimensional rmsd plot (Fig. 5.1.7c, g), $3d = 120 \times 3 = 360$ Hz for PGLa 6-10 (c) and $3d = 26 \times 3 = 78$ Hz for PGLa 6-13 (g) agree well with the data determined from the 4F-Phg [103]. The dipolar spectra (d, h) were then correctly reproduced with the best fitted D_1, D_2 and *d*, the small coupling *d* for PGLa 6-13 (h) is buried in linebroadening and unresolved (simulated spectra without mosaic spread and lower linebroadening, displaying the underlying dipolar pattern (gray) are shown in gray in Fig. 5.1.7b,f).

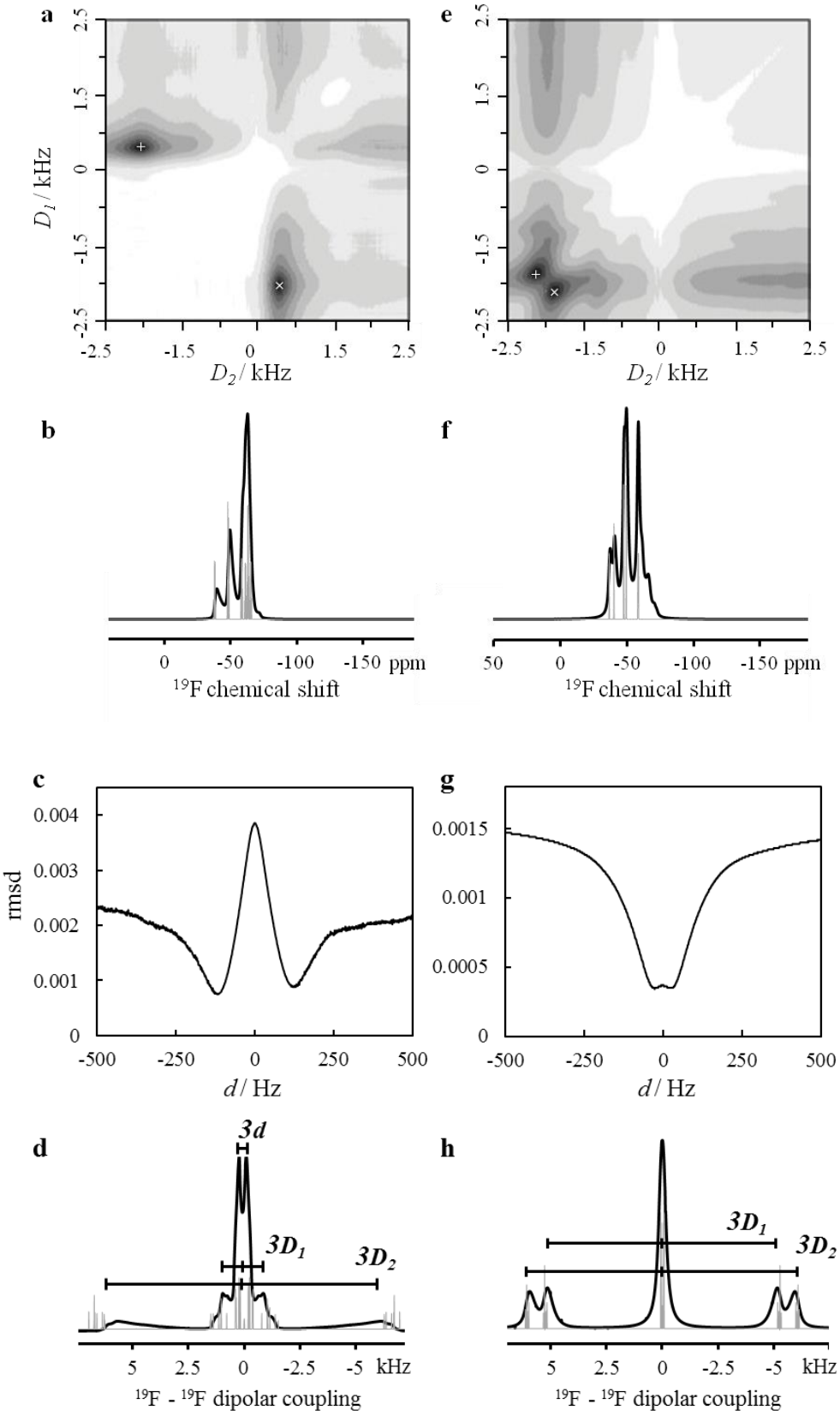

Fig. 5.1.7 The best-fits of the *intra*-CF_3 dipolar couplings D_1, D_2 and the weak *inter*-label coupling d for PGLa 6-10 (a-d) and PGLa 6-13 (e-h) were found with a grid research. The best-fits of D_1, D_2 are found by comparing the simulated and experimental spectra (b and f) by an rmsd (minima are marked with '+' and '×' in a and e).

The minima always occur in pairs with identical spectra, with the knowledge of the signs of the couplings from geometric considerations, the correct solution could be found, they are D_1 = + 380 Hz, D_2 = -1920 Hz for PGLa 6-10 (a), and D_1 = - 1730 Hz, D_2 = - 2030 Hz for PGLa 6-13 (e). With fixed D_1 and D_2, the best rmsd between simulated (d, h) and experimental CPMG spectra were obtained with *d* of 120 Hz and 26 Hz (Fig. 4, h, j). The corresponding splittings are 3*d* = 360 Hz and 78 Hz for PGLa 6-10 (c) and PGLa 6-13 (g) respectively, which are in good agreement with those measured with mono-fluorinated PGLa. In gray the dipolar patterns of the 6-spin systems with reduced linebroadening and omitted mosaic spread are shown.

Disccussion

The aim of this part in this study was to assess and compare the capability of the monofluoro- and CF_3-reporter as ^{19}F-NMR labels for addressing orientational constraints and distance constraints for the structural analysis of membrane-active peptides. 4F-Phg (Fig. 5.1.1a) and CF_3-Phg (Fig. 5.1.1b) were chosen, which have identical side chains and differ only in fluorine-reporter. They were incorporated into the antimicrobial peptide PGLa along the peptide sequence in single or two positions, giving four single-labeled PGLa analogues (PGLa 6, PGLa 10, PGLa 13, PGLa 14) with 4F-Phg and four double-labeled analogues (PGLa 6-10, 6-13) with either 4F-Phg or CF_3-Phg.

With the four single ^{19}F-labeled PGLa analogues, the orientational constraints (τ, ρ) were searched by analysing the chemical shifts, taking the phenylring torsion angle χ_1 into account, as the CSA elements are strongly determined by the phenylring rotation. As a first step to evaluate the influence of the phenyl rotamer angle on the orientation analysis, we calculated the chemical shift as a function of χ_1 and compared it with the respective measured value. Assuming that this angle is identical for all labeled positions and taking the fluctuation of the side chain into consideration, the best-fits of keeping the orientational constraints fixed (τ = 119°, ρ = 113 ° for T-state; τ = 91°, ρ = 125 ° for S-state) [110] were found with χ_1 around 30 - 40 °, and the favourite fluctuation angle is difficult to be determined for S-state and ± 60 ° for the T-state. The value of χ_1 we found here is ~40 °, far away from the favourite 110 ° as reported [31], which was observed with an α-helix, however close to that obtained with model compound N-acetyl-N'-methylamide-4-fluoro-phenylglycine [102]. Furthermore the phenylring does not rotate freely but is limited (± 60 ° for S-state).

In a second approach, the best-fitting orientational constraints (τ, ρ) were searched, taking the phenylring torsion angle χ_1 into account. Here, no conclusive picture could be obtained. For example, the rmsd in the case of the S-state was rather unaffected by the rotamer angle. It is

likely that the torsion angle is not universal for all substitutions by this label and for different protein systems, since it may depend on the local steric environment and it could be different under different conditions (such as temperature) and any subtle deviations would lead to large changes of the best-fit analysis. As a result of the ambiguous phenylring torsion angle χ_1, monofluoro-Phg for orientational analysis has to be used with care. Certainly, this torsion also exists in CF_3-Phg, but the fast methyl rotation makes the CSA symmetric along the C_α-C_β axis, which means, the chemical shift of CF_3-reporter depends solely on the C_α-C_β axis orientation. With four CF_3-Phg labeled PGLa analogues, the chemical shifts of the triplet resulting from the CF_3-reporter can be used to determine if the side chain orientation θ is above or below the magic angle, and the orientational constraints (τ, ρ) can be accurately determined by the inter-CF_3 dipolar couplings [110].

For distance measurements, it is crucial to know whether monoF- or CF3-reporter is more beneficial to resolve weak dipolar couplings. With the aid of CPMG, the weak inter-label dipolar coupling 3*d* of about 80 Hz in PGLa 6-13 was obtained with 4F-Phg (Fig. 5.1.6d), but with CF_3-Phg it seemed unresolved (Fig. 5.1.6f). At first glance, the dipolar spectra of CF_3-labeled peptides (Fig. 5.1.6e, f) show as a superposition of two triplets arising from different intra-CF_3 dipolar couplings D_1 and D_2, with a further splitting in the middle line indicating the weak inter-label coupling. Unlike the mono-fluorinated peptides, it is essential to analyse the triplet-like dipolar spectra with further computer simulations, to reveal the complex multi-line pattern of the 6-spin system, which is broadened by mosaic spread. With the lineshape simulations and best-fit analysis, even the unresolved inter-CF_3 dipolar couplings (Fig. 5.1.7g, h) could be revealed. However, in the case of PGLa 6-13, couplings lower than the best-fitting d = 26 Hz would also have a low rmsd, and even the absence of a coupling cannot be excluded. The underlying dipolar pattern indicated with reduced linebroadening and omitted mosaic spread in Fig. 5.1.7, indicate that, although the CF_3-groups may enjoy the advantages of slower T_2 relaxation, the larger number of signal contributions due to the complex 6-spin system would reduce signal intensity and the resolution.

Conclusion

The performance of 4F-Phg and CF_3-Phg as ^{19}F-NMR labels for structural studies of membrane-active peptides were evaluated here in terms of orientational analysis and distance measurements. CF_3-Phg is more suitable to determine the peptide alignment in oriented membranes precisely on basis of orientation-dependent dipolar couplings, whereas with 4F-

Phg it is hampered by the ambiguous value of phenylring torsion. Otherwise, single ^{19}F-labelss are more beneficial for distance measurements, which could characterise the oligomeric assemblies in the membrane environment. We were able to observe a long distance ~11 Å within PGLa labeled with 4F-Phg in fluid membranes, while with the CF_3-reporter the small dipolar splitting is unresolved, and more effort and computer simulations are required for the data analysis. The two broadly used ^{19}F-labels were systematically analysed and compared in this study, this can be an important reference for further ^{19}F-labeling designs to study biomembranes.

5.2 TisB dimerization

Introduction

To directly proof the existence of TisB dimerization, two double-labeled TisB analogues were designed to go insight into the salt bridges, as shown in Fig. 5.2.1. All the labeled TisB analogues are summarized in Tab. 5.2.1. The labeled analogues are TisB D5-K26 labeled with U-^{13}C, ^{15}N-Asp in position 5 and $^{15}N_2$-Lys in position 26, and TisB K12-D22 labeled with $^{15}N_2$-Lys in position 12 and U-^{13}C, ^{15}N-Asp in position 22. The labels were designed such that the intramolecular dipolar couplings between Lys and Asp are too weak to be observed, however, the intermolecular dipolar couplings may be observed if the peptides are dimerized. Since the Asp were uniformly ^{15}N-, ^{13}C-labeled, a modified REDOR experiment, the so-called sel-REDOR, was developed to get rid of the impact from C_β, C_α of U-Asp and even from the natural abundance of lipids. Hence, the dipolar couplings between ^{15}N and ^{13}C=O only could be selected, and the coupling to other ^{13}C nuclei was suppressed. Furthermore, the central Gln19 was investigated with a novel ^{19}F-label, referred to as ^{19}F-Gln, which is structurally similar to Gln. CPMG experiments to gain the inter-^{19}F distances *r* were applied to TisB labelled with this amino acid.

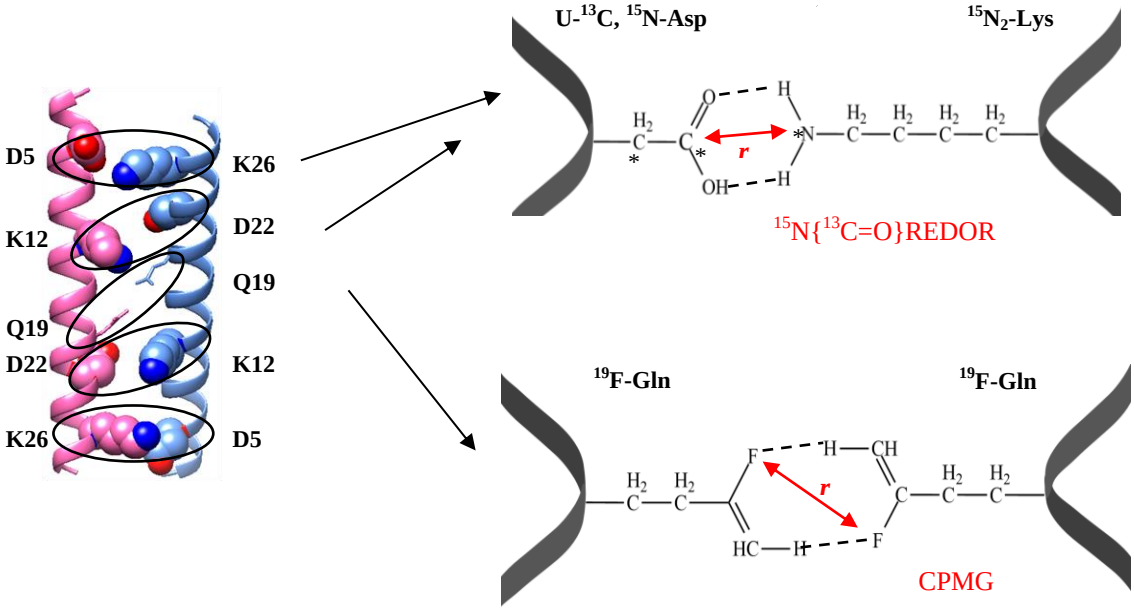

Fig. 5.2.1 Illustration of distance measurements of TisB dimers. TisB were double-labeled by U-^{13}C, ^{15}N-Asp (^{13}C, ^{15}N uniformly labeled) and U-$^{15}N_2$-Lys ($^{15}N_2$-labeled) to give TisB D5-K26 and TisB K12-D22 (Tab. 5.2.1). Sel-REDOR experiments were performed to measure the distances between ^{15}N and carbonyl-^{13}C. Besides, TisB

were ^{19}F-labeled with ^{19}F-Gln, to use the CPMG approach to measure the intermolecular distances. '*' denote labeled ^{15}N or ^{13}C.

Tab. 5.2.1 Synthesized TisB analogues with labels of ^{13}C, ^{15}N, ^{19}F.

Name	Sequence	Molar mass [g/mol]
TisB K12-D22	MNLVDIAILIL-**$^{15}N_2$-Lys**-LIVAALQLL-**U-Asp**-AVLKY LK	3229
TisB D5-K26	MNLV-**U-Asp**-IAILILKLIVAALQLLDAVL-**$^{15}N_2$-Lys**-Y LK	3229
TisB ^{15}N-L21$_a$	MNLVDIAILILKLIVAALQL-**^{15}N-Leu**-DAVLKYLK	3223
TisB Q19	MNLVDIAILILKLIVAAL-**^{19}F-Gln**-LLDAVLKYLK	3223
TisB Q19-A16	MNLVDIAILILKLIV-**^{15}N-Ala**-AL-**^{19}F-Gln**-LLDAVLKY LK	3224

'U-Asp' : ^{15}N, ^{13}C uniformly labeled Asparagine

'$^{15}N_2$-Lys': ^{15}N uniformly labeled Lysine

^{19}F-Gln: ^{19}F-labeled Gln analogue

'a': only for tests before the REDOR distance measurements

REDOR curve simulation

The general CODEX curve can be given as follows [115]:

$$\frac{S_0 - S}{S_0} = 1 - \frac{1}{2\pi}\int_0^{\pi}\int_0^{\pi} \cos(\emptyset)\sin\beta d\alpha d\beta \tag{5.4}$$

where α, β denote the internuclear orientation, which are summed over (0 ~ π) for powder samples, and ϕ describes the net dipolar dephasing angle after the trains of dephasing pulses and can be calculated by:

$$\emptyset = \frac{NT_r D}{\pi}\sqrt{2}\sin 2\beta \sin\alpha \tag{5.5}$$

with the dephasing time NT_r and the dipolar coupling D. T_r indicates the rotor period. N describes the number of rotor cycles on the dephasing channel. D can be calculated according to eq. 1.3.

The simulations of REDOR curves in this study were achieved according to eq. 5.4 and eq. 5.5 with the aid of the software MATLAB.

Test substances

Before all the measurements, the REDOR experiments were tested using the following test substances, as shown in Fig. 5.2.2: (a) 10% diluted N-acetyl-2-$^{13}C_\alpha$, ^{15}N-glycine (NAG), (b) tripeptide ^{15}N-Gly-1-^{13}C-Ala-Leu (GAL), (c) uniformly labeled glycine (U-glycine). The NAG, which gives a short distance of 1.44 Å [141], was firstly applied to verify the REDOR NMR-equipment and methods. After the REDOR approach was established, the tripeptide GAL (b) with a rather long distance of 5.35 Å [142] was measured to confirm that the REDOR approach was able to detect weak dipolar couplings. Furthermore, a modified pulse sequence, so-called sel-REODR, was developed to extract only those distances involving carbonyl-^{13}C, which was of interest in our TisB project. The U-glycine (c) was then used to verify the sel-REDOR. The test substance NAG was obtained from Dr. Marco Klein, and the tripeptides GAL from Parvesh Wadhawani, U-glycine from Sigma-Aldrich GmbH. They were mixed with unlabeled material (labeled : unlebeled = 1 : 9) and recrystallized to give homogeneous 10 % diluted samples.

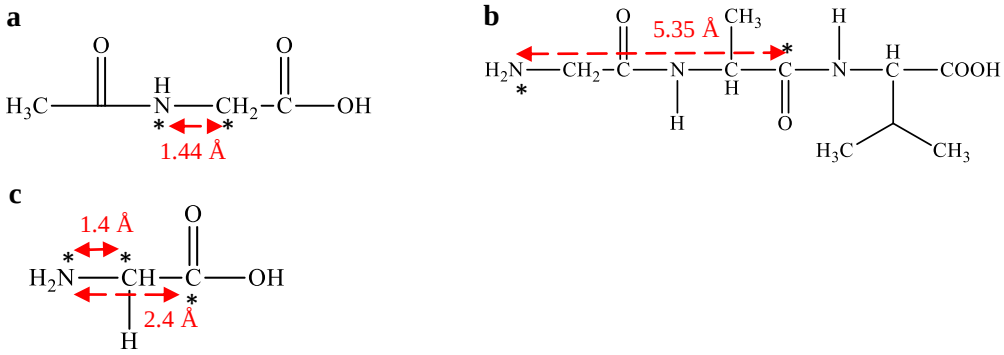

Fig. 5.2.2 Test substances for REDOR experiments. (a) N-acetyl-2-$^{13}C_\alpha$, ^{15}N-glycine, (b) tripeptide ^{15}N-Gly-1-^{13}C-Ala-Leu, (c) uniformly labeled glycine. '*' denote labeled ^{15}N or ^{13}C.

Results and discussion

- **^{15}N{^{13}C}REDOR tests with NAG**

The test measurements were performed with N-acetyl-2-$^{13}C_{\alpha}$, ^{15}N-glycine using different MAS spinning speed, composite pulses or different dephasing sequences (Fig. 5.2.3):

(a) Different MAS spinning speed

Different MAS spinning speed had no any effect on the REDOR experiments. Thus, 8 kHz was chosen for further measurements.

(b) Different composite pulses on the dephasing channel (^{13}C)

Compared to novel composite pulse $90_{-y}225_{x}315_{-y}$ [118], the estabilished pulse $90_{-y}180_{x}90_{-y}$ [143] performed better. Thus, $90_{-y}180_{x}90_{-y}$ was kept in use for the further REDOR experiments.

(c) Single or composite pulses on the dephasing channel (^{13}C)

With composite pulses the REDOR curve seemed stable, mprobably because the composite pulses suppressed the errors which arised from the imperfection of π-pulses.

(d) Single or composite pulses on the observing channel (^{15}N)

The composite pulse on ^{15}N did not enhance the dephasing efficiency. Thus a normal π-pulse was adopted for the further measurements.

(e) SFAM or REDOR

The simultaneous SFAM pulse sequence has been reported to perform better in extracting weak dipolar couplings [144-146]. The important parameters used for SFAM are the depth of the frequency modulation of 40 kHz and the maximum of the RF amplitude of 32 kHz. In the case of NAG with short internuclear distance, SFAM yields higher recoupling efficiency (> 90 %). Thus, SFAM is a good candidate for the REDOR experiments of biological samples.

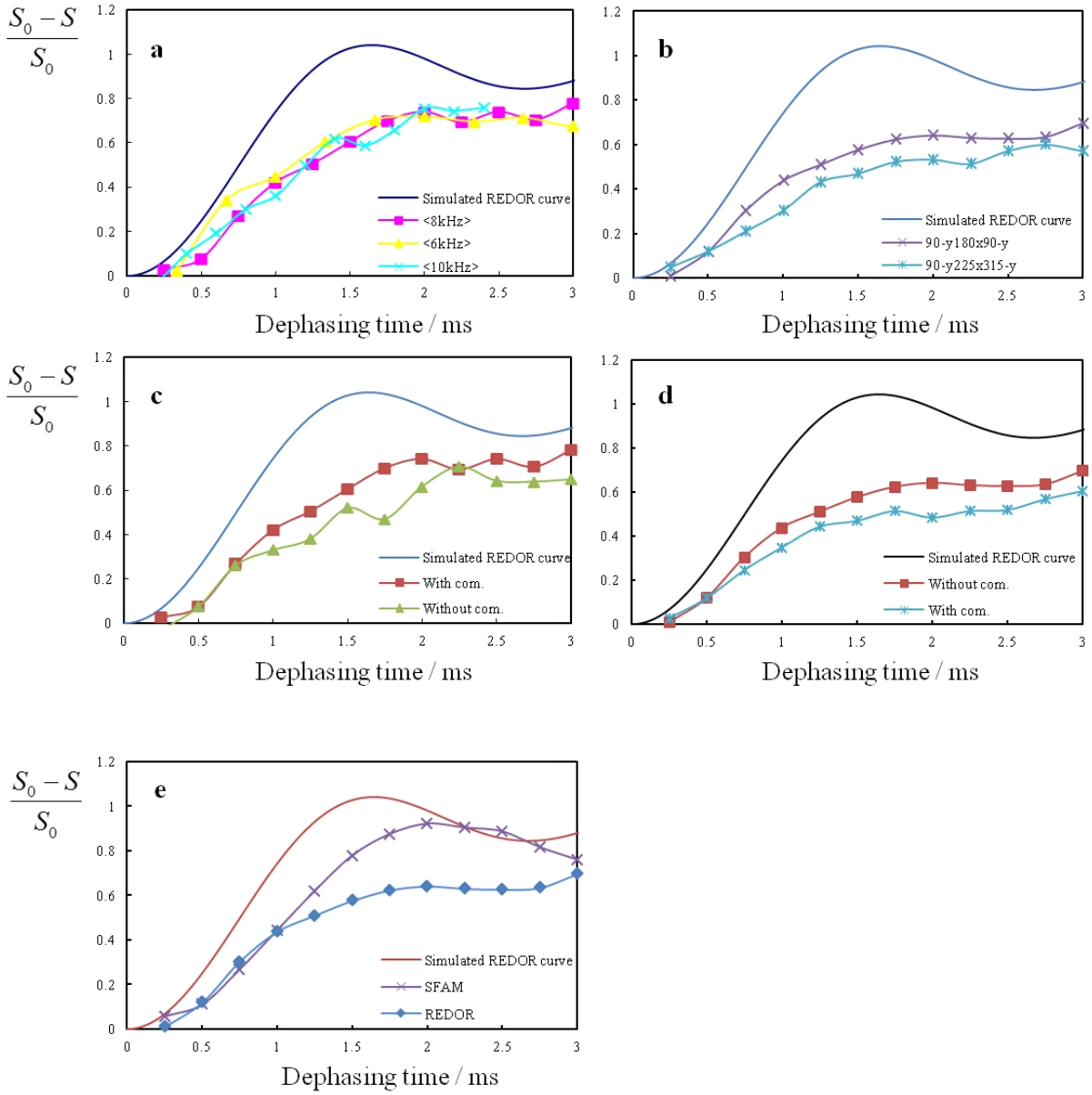

Fig. 5.2.3 REDOR tests with NAG using (a) different MAS spinning speed, (b) Different composite pulses on the dephasing channel (^{13}C), (c) single or composite pulses on the dephasing channel (^{13}C), (d) single or composite pulses on the observing channel (^{15}N), (e) SFAM or REDOR. Each experimental point was obtained with 32 scans and recycle delay of 20 s.

The experimental data obtained with MAS spinning speed of 8 kHz, and $90_{-y}180_{x}90_{-y}$ composite pulses on the dephasing channel show the best performance (see Fig. 5.2.3e). To find the best-fit distances, rmsd-plots were drawn comparing the simulated spectra and experimental data. The observed ^{15}N-^{13}C distances in NAG were found to be 2.0 ± 0.4 Å with REDOR dephasing pulses (Fig. 5.2.4A), and 1.6 ± 0.2 Å with SFAM (Fig. 5.2.4B). Compared to reported distance of 1.44 Å in crystals [141], SFAM showed a good agreement (within 12 %), probably due to its higher tolerance for the rf field inhomogeneties and MAS

instability, since the measurements of dipolar couplings are strongly dependent on an exact setting of experimental parameters and rotor synchronization.

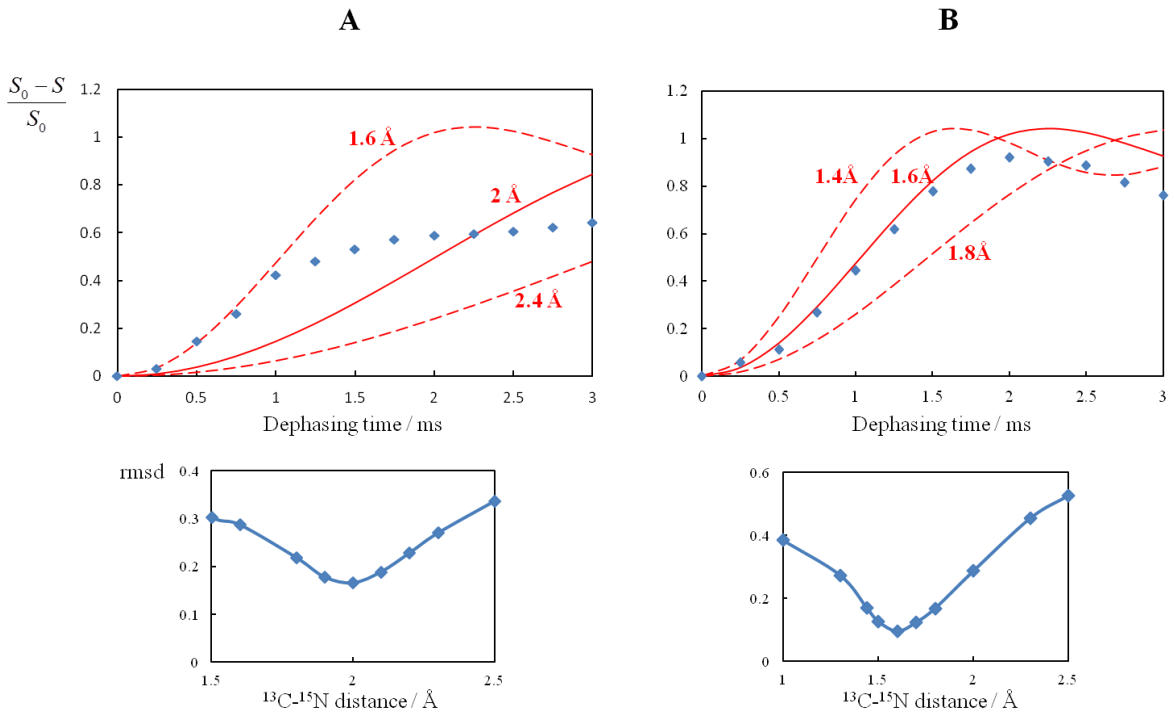

Fig. 5.2.4 Data analysis of REDOR experiments on N-acetyl-$^{13}C_\alpha$/^{15}N--glycine measured with REDOR (A) and SFAM (B) dephasing pulse chain. The rmsd-plots underneath the REDOR curves demonstrate the best-fits of the ^{13}C-^{15}N distances between experimental data and simulated curves. The best-fit distances were found with minimum rmsd value. The errors calculated from S/N ratio are too small to be visible.

- **^{15}N{^{13}C}REDOR tests with tripeptide GAL**

The tripeptide ^{15}N-Gly-1-^{13}C-Ala-Leu, which possesses a weak ^{15}N-^{13}C dipolar coupling, was then measured with both the REDOR and SFAM sequences to check the applicability of the approach for further measurements of biological samples. As shown in Fig. 5.2.5, the REDOR dephasing sequence leads to an internuclear distance of 5.7 ± 0.3 Å between the ^{13}C-^{15}N labels, and SFAM to 5.0 ± 0.5 Å, both agree well with the theoretical distance of 5.35 Å [142]. However, as seen in Fig. 5.2.5, the SFAM dephasing curve stays below that of the REDOR experiment and the values vary more. As illustrated above, SFAM is capable to reach a higher recoupling efficiency (90 %) compared to REDOR (70 %), which means the dephasing curve with the SFAM sequence is approaching the oscillatory maximum of 1 after several ms dephasing time. However, with the long-range distance, measurements with longer dephasing time to achieve such 90 % recoupling efficiency are impossible due to the short relaxation time, and REDOR seems to be able to cope with long dephasing times better. Thus, for long-

range distance measurements, SFAM is no longer competitive. Considering a further selective pulse designed on observed channel, the REODR sequence appeared more suitable and was therefore chosen also for the sel-REODR development.

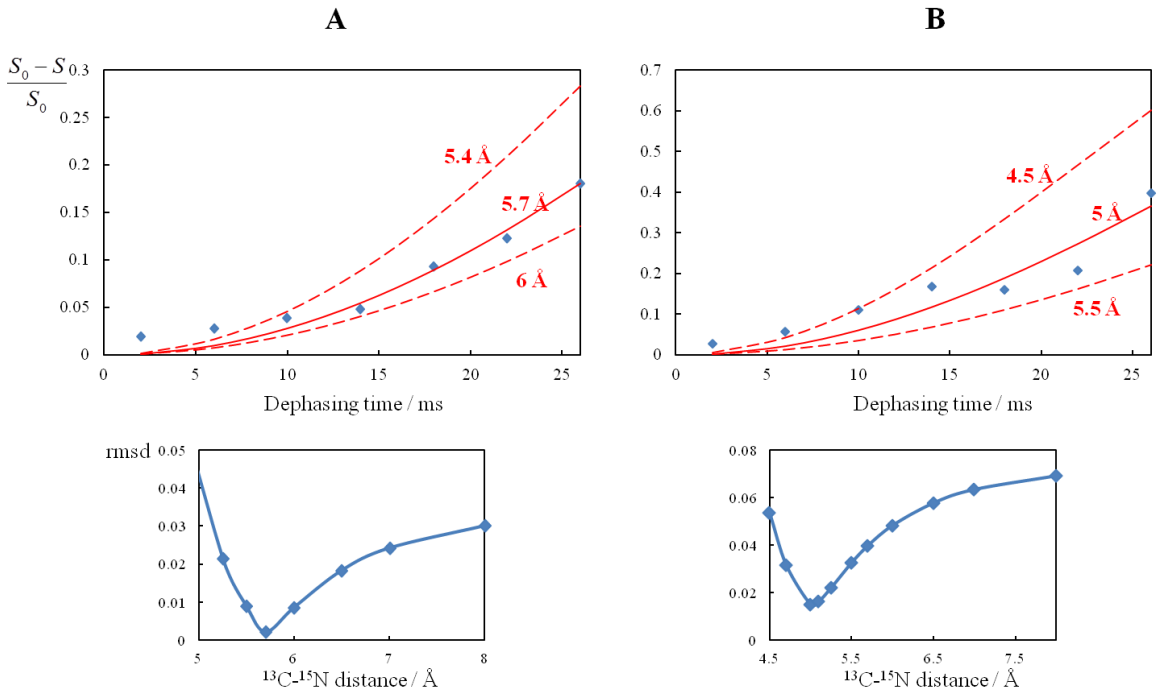

Fig. 5.2.5 Data analysis of REDOR experiments on tripeptide GAL measured with REDOR (A) and SFAM (B) dephasing sequence.The rmsd-plots underneath the REDOR curves demonstrate the best-fits of the ^{13}C-^{15}N distances between experimental data and simulated curves. The best-fit distances were found with minimum rmsd value. The errors calculated from S/N ratio are too small to be visible. MAS = 8 kHz. Each experimental points were obtained with 100 scans and recycle delay = 20 s.

- **Sel-REDOR tests with U-glycine**

The sel-REDOR experiment was modified from normal REDOR (see Fig. 2.4.2.3), in that the central simple echo 180 °-pulse on the observed ^{15}N channel was replaced by a selective inversion 180 ° Gaussian pulse [147], placed in a delay D of an integer number of rotor periods T_r, as shown in Fig. 5.2.6A. The Gaussian pulse duration G is corresponds to the selective inversion region, here the region of ^{13}C=O, as shown in Fig. 5.2.6B. The selective inversion region is about 2 kHz, thus the Gaussian pulse length was 1 / (2 kHz) = 500 µs, and D was set to be 600 µs. With such a selective Gaussian pulse incorporated in a normal ^{13}C measurement, the ^{13}C = O signal is inverted phase and can be distinguished from other signals. This way, all the signals outside the selected region could be suppressed in sel-REDOR experiments.

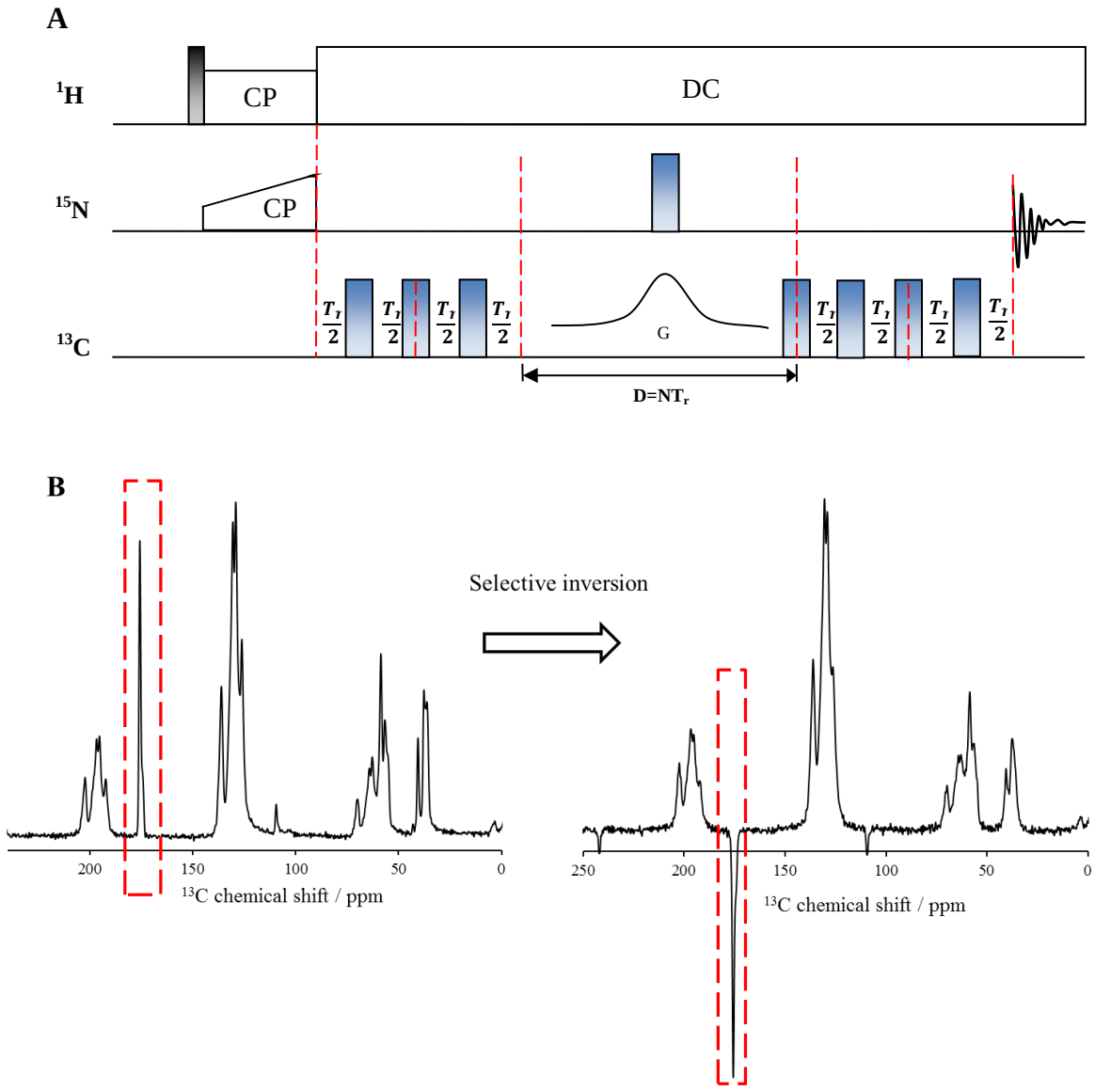

Fig. 5.2.6 Schematic illustration of sel-REDOR experiments (A) and the normal ^{13}C spectrum of selectively inverted ^{13}C=O in U-Phe (uniformly ^{13}C, ^{15}N-labeled Phenylalanine) (B). MAS = 10 kHz.

After the selective pulse was established and verified, the U-glycine was used to test the performance of sel-REDOR experiments. The ^{15}N of U-glycine possesses dipolar couplings to both $^{13}C_{\alpha}$ and ^{13}C=O, with internuclear distances of 1.4 Å (^{15}N - C_{α}) and 2.4 Å (^{15}N - ^{13}C=O) respectively [148]. A normal REDOR and a sel-REDOR selectively suppressing couplings to $^{13}C_{\alpha}$ were performed in turn. As shown in Fig.5.2.7, the normal REDOR experiment resulted in a distance mixture of 1.4 ~ 2.4 Å as expected, whereas the sel-REDOR successfully suppressed the coupling to $^{13}C_{\alpha}$, leaving only the internuclear dipolar coupling between ^{15}N - ^{13}C=O, which lead to experimental points along the simulated REDOR curve of 2.4 Å.

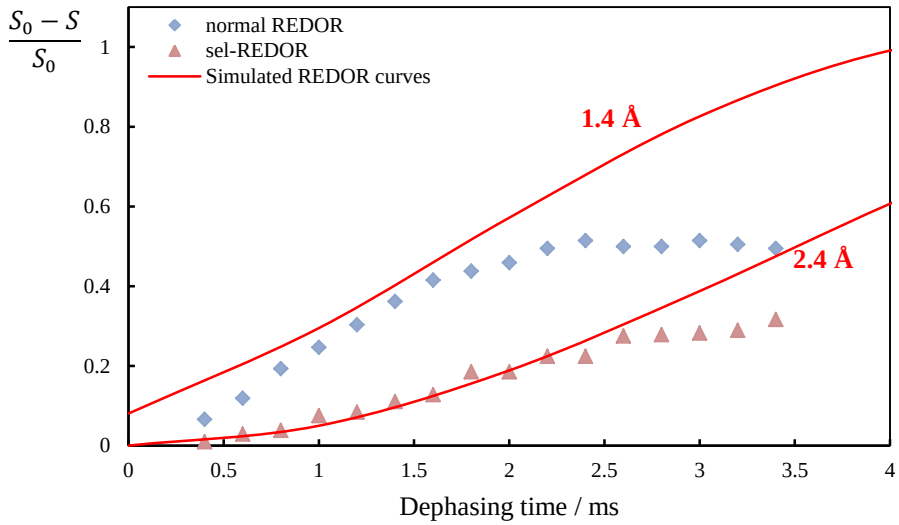

Fig. 5.2.7 Sel-REDOR experiment of U-glycine compared with normal REDOR measurements. The normal REDOR experimental spots show a mixture of distances between 1.4 ~ 2.4 Å, while the sel-REDOR successfully filtered the carbonyl-^{13}C and extract the internuclear distance between ^{15}N-^{13}C=O of 2.4 Å. MAS = 8 kHz. Each experimental points were obtained with 40scans and D1 = 6 s.

With these experiments, the sel-REDOR experiment is well established and suited for the distance measurements on the biological application of the TisB peptide.

- **Sel-REDOR experiments on TisB**

It is known that, the distance-range determined by ^{15}N{^{13}C}REDOR experiments is limited by the low gyromagnetic ratio of the ^{15}N and ^{13}C nuclei. In biological samples, it is even more difficult to detect the weak internuclear dipolar coupling, since the observed dipolar coupling would be further attenuated by the peptide motion around membrane normal. Thus, it is necessary to perform the distance measurements on frozen TisB samples (-20 ℃), where the lipids POPC (transition temp. -2 ℃) are in the gel phase and lock the peptides within the lipid membrane matrix. Before the REDOR measurements, two questions should be sorted out. Firstly, all the peptides purified by HPLC are acidic, and the free H^+ ions would hydrolyze the phospholipids to be lysolipids or even free fatty acid chains, and this way the lipid membrane would be broken down. Such problem is more significant for liposome samples compared to oriented lipid bilayers, and the TisB dimerization would be also destroyed. Thus it is very important that for REDOR experiments the peptides are neutralized by dialysis. The second question is, whether the TisB peptides maintain the transmembrane state, aggregate or aligns on the membrane surface when the bilayers are frozen. To answer these questions, the TisB ^{15}N-L21, which was neutralized by dialysis, was chosen to be measured for a test.

The membrane integrity was confirmed by ^{31}P-NMR spectra. To this aim, the sample was prepared in a 4 mm rotor but measured without MAS. Thus all the spectra possess a powder pattern-like shape resulting from the liposomes, as shown in Fig. 5.2.8, Before peptide dialysis, the peptide was acidic (HCl came from HPLC), thus the lipid POPC was hydrolyzed to phosphate headgroups as illustrated by the sharp peak around 0 ppm, and lyso-POPC giving rise to the small peak near the POPC at -15 ppm (Fig. 5.2.8A, upper spectrum). After the peptide was desalted, the ^{31}P-NMR spectrum showed a perfect powder shape without any components from hydration (Fig. 5.2.8A, lower spectrum), demonstrating that the small amount of acid introduced by the peptides did lead to destruction of lipids, and fortunately could be completely removed by dialysis. With the integrated liposome conformation, ^{15}N-spectra (Fig. 5.2.8B) were then acquired and shown that even under lower temperature, the peptides stand in transmembrane state (powder spectrum with the higher shoulder on the right), which means, the temperature doesn't influence the peptide alignment within the membranes.

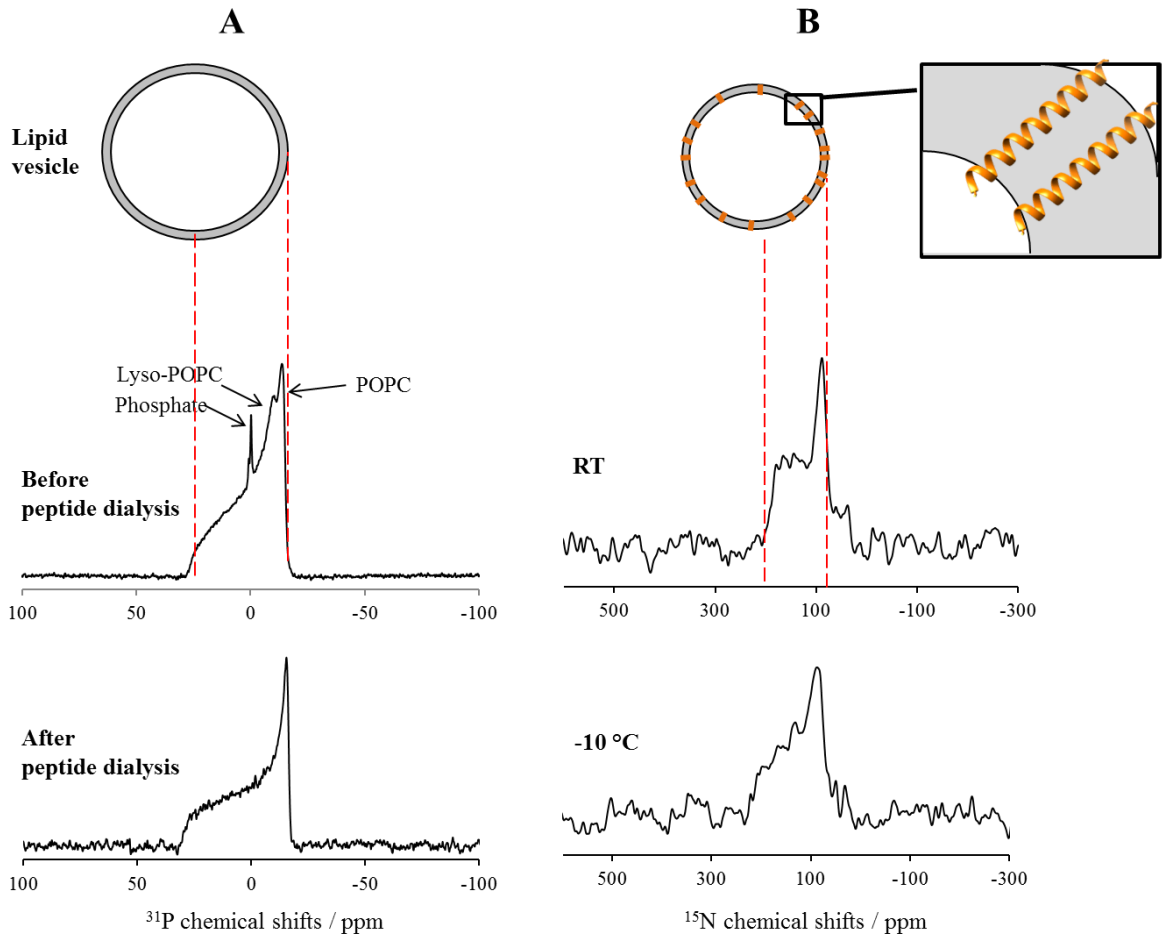

Fig. 5.2.8 ^{31}P-NMR spectra before and after peptide dialysis (A) and ^{15}N-NMR spectra at different temperatures (B) of TisB ^{15}N-L21. The samples with TisB embedded in POPC were filled in a 4 mm rotor but measured

statically. The ^{31}P-NMR spectra show a typical powder pattern-like shape attributing from the lipid liposome conformation. The transmembrane peptides TisB are shown as orange strips in B. The ^{31}P-NMR spectra were measured with 258 scans and ^{15}N-spectra with ca. 10000 scans (over 14 h).

Since the sel-REDOR approach and equipment were verified and the samples were checked for the effects of acidic proton ions and temperature, the samples with TisB D5-K26 and TisB K12-D22 embedded in POPC liposomes were prepared for the REDOR experiments. Firstly, ^{13}C-NMR spectra were obtained and clearly demonstrated that the ^{13}C-nucleus cannot be chosen as observed nucleus, as the signals from the peptides are broad and overlapped with the peaks arising from the natural abundance of lipids, as shown in following Fig. 5.2.9. The red spectrum was obtained with only POPC lipid and shows natural abundance ^{13}C-peaks after 800 transients. However, even with 20000 scans (more than 12 h) the carbonyl-^{13}C from uniformly labeled Asp in TisB (black spectrum) were not seen, and the C_α, C_β peaks around 58 ppm and 40 ppm, respectively, are also broad.

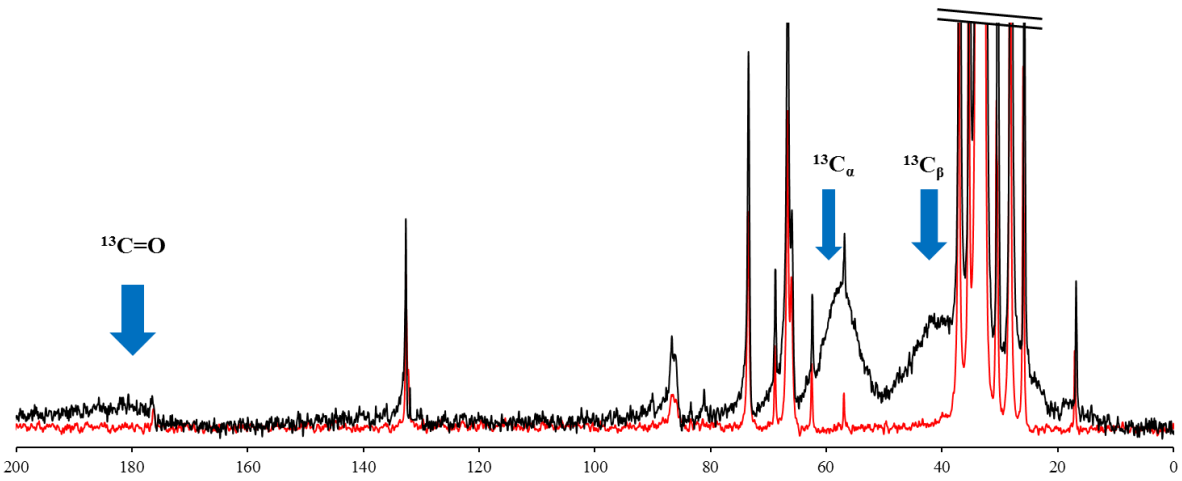

Fig. 5.2.9 ^{13}C-NMR spectra of TisB embedded in POPC (black) and only POPC (red) at -20 ℃. MAS = 8 kHz. The broad peaks marked by blue arrows result from carbonyl-^{13}C, $^{13}C_\alpha$ and $^{13}C_\beta$ of U-Asp in TisB, and natural abundance signal of the peptides. Contact time used for CP-ramp from ^{1}H to ^{13}C. Red spectrum was obtained with 800 scans, and black one with 20000 scans.

^{15}N-NMR spectra were then obtained as shown in Fig. 5.2.10. The right line at 33 ppm originates from the amine-^{15}N of Lys in TisB, and left line at 119 ppm from the amide-^{15}N in the TisB backbone. The line of amide-^{15}N is a little broader than that of amine-^{15}N, probably because the backbone amide-^{15}N is more rigid.

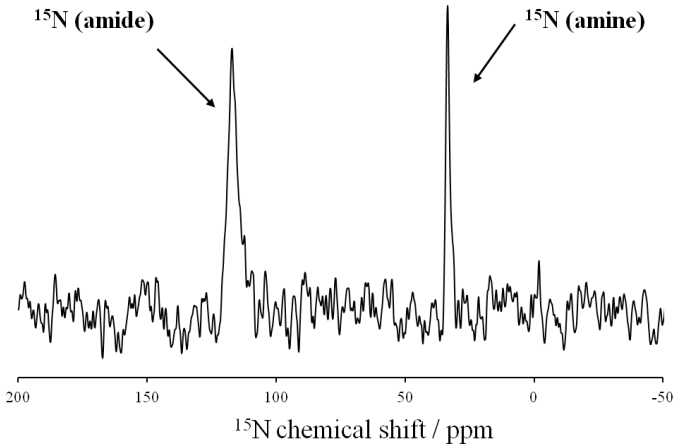

Fig. 5.2.10 ^{15}N-NMR spectrum of TisB D5-K26 embedded in POPC at -20 ℃. MAS = 8 kHz. The right line refers to amine-^{15}N of Lys in TisB, and left line to amide-^{15}N from TisB backbone. Spectrum was obtained with 2000 scans with contact time of 3 ms.

After that, the sel-REDOR experiments were performed with ^{15}N as observed and ^{13}C as dephasing channel. Five points of the REDOR dephasing curve (two spectra S_0, S) up to 40 ms dephasing time individually were obtained. The resulting spectra S_0 and S of TisB D5-K26 are summarized in Fig. 5.2.11. The amide-^{15}N signal disappeared after 5 ms dephasing time, probably due to a very short T_2 relaxation time. Nevertheless, the signal of amine-^{15}N was observable, but no dephasing was obtained in spectra S. Due to the limit in S/N and T_2 relaxation time, further measurements with longer dephasing time were not possible. The TisB K12-D22 showed the same results, which means that, the intermolecular distances between ^{15}N and ^{13}C in the TisB dimer are longer than 5 Å and beyond the ability of our REDOR measurements.

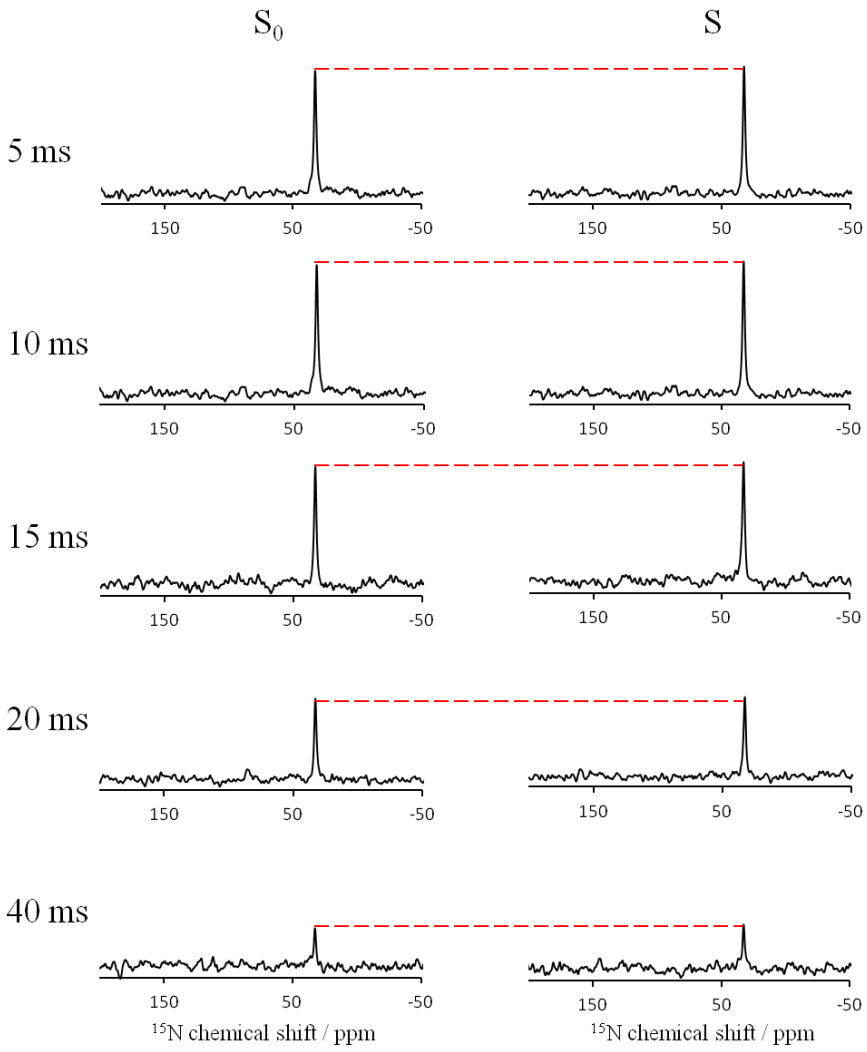

Fig. 5.2.11 Spectra S_0 and S acquired by sel-REDOR experiments with TisB D5-K26 at -20 ℃. MAS = 8 kHz. Five different dephasing times were applied, they were 5 ms, 10 ms, 15 ms, 20 ms, 40 ms. No dephasing in spectra S was obtained. From the above ^{13}C-NMR spectra (Fig. 5.2.9), the ^{13}C=O region was selected to be 5 kHz, thus the selective Gaussian pulse length was set to be 200 µs (1 / 5kHz). The transmitter frequency was set to the line of ^{13}C=O. During the REDOR pulse trains and the acquisition, ^{1}H-decoupling of 80 kHz was applied for higher resolution of the spectra. Each spectrum was obtained with 8000 scans with recycle delay of 6 s.

- **CPMG experiments on TisB (in corporation with Benjamin Zimpfer)**

The ^{19}F-labeled TisB Q19 was synthesized to address the long-range ^{19}F-^{19}F distance between the labels with the aid of CPMG experiments. ^{19}F-labeled Gln analogue (^{19}F-Gln) was used as ^{19}F-label (see section 4.1), since it is chemically and structurally similar to the original Gln in position 19.

Firstly, since the ^{19}F-Gln analogue is novel and the CSA was unknown, the ^{19}F-powder spectra with and without MAS were obtained. In addition, the static powder spectrum was also acquired of the labeled TisB Q19. The CSA values obtained from the ^{19}F-label alone and from TisB Q19 were very similar, as the respective ^{19}F-NMR powder spectra show almost the same CSA shapes, as shown in Fig. 5.2.12a (The black line denotes the powder spectra of the amino acid ^{19}F-Gln, and the red line refers to the peptide TisB Q19, both of them possessing a CSA region of about 120 ppm).

In addition, the ^{19}F-label was measured with MAS = 25 kHz (Fig. 5.2.12b), indicating that the isotropic position is at -93 ppm. With MAS = 10 kHz (c), several components were observable, which came from different crystal forms. Taking the broad line as the dominant component, a lineshape-fitting (Fig. 5.2.12d, red one) resulted in the following CSA tensor parameters:

σ_{iso} = -93ppm (isotropic chemical shift)
δ = 53 ppm (anisotropy parameter)
η = 0.55 (asymmetry)

The CSA parameters fit also perfectly to the powder spectrum without MAS (Fig. 5.2.12d, black one). Consequently, the CSA values were calculated (see section 1.5) to be:

σ_{11} = -154 ppm
σ_{22} = -105 ppm
σ_{33}= -40 ppm

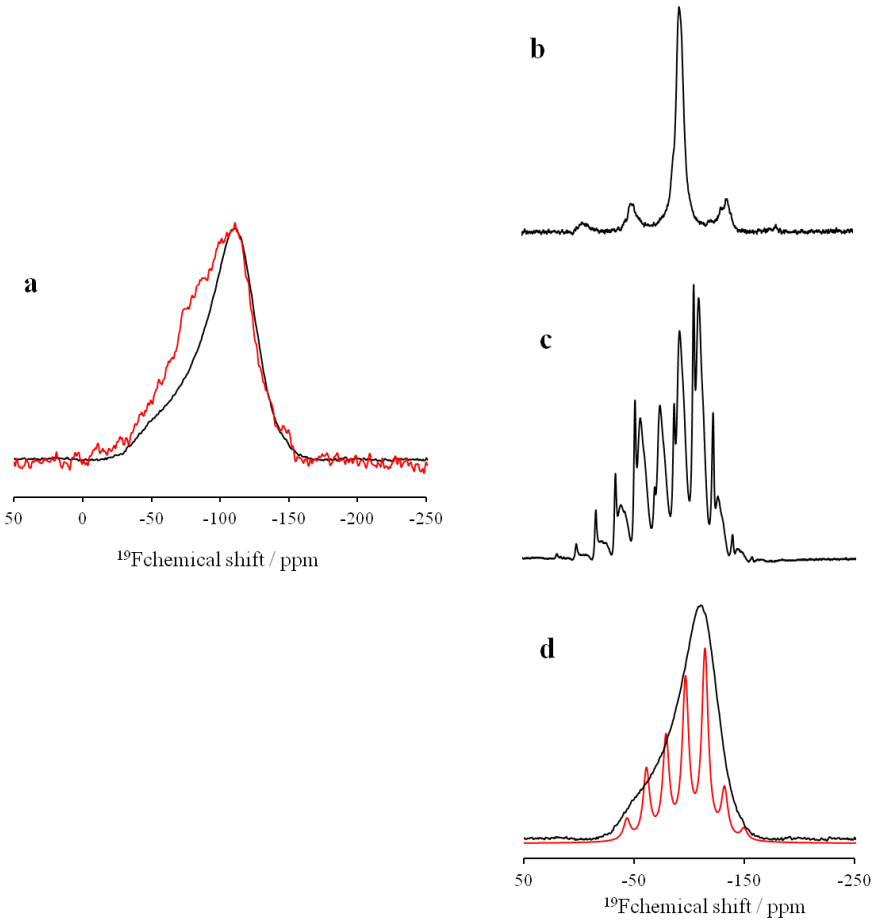

Fig. 5.2.12 ^{19}F-NMR powder spectra of the amino acid ^{19}F-Gln analogue and the peptide TisB Q19 at room temperature. (a) The powder spectra without MAS were compared between the ^{19}F-label (black) and the peptide TisB (red); (b) the MAS spectrum of ^{19}F-Gln analogue obtained with MAS spinning speed of 25 kHz; (c) the MAS spectrum of ^{19}F-Gln analogue obtained with spinning speed of 10 kHz. The ^{19}F-label measured was Fmoc-protected and unpurified; (d) the MAS spectrum obtained by lineshape-fitting (red) of spectrum (b) and (c) compared with the powder spectrum (a).

Now that the CSA values were available, oriented sample of TisB Q19 embedded in POPC (peptide = 1 mg) were prepared, as previously described (see section 4.4). CPMG spectra of TisB were obtained at 10 ℃ above the phase transition temperature of POPC, where the lipids are in the liquid-crystalline phase. As a sequence of the long CPMG sequence, the sample would get dried shortly. Therefore a peptide to lipid ratio of 1 : 100 was applied, as more lipids lead to more hydration, which helps the sample to stay longer hydrated. And at such lower peptide concentration, TisB also adopts a transmembrane orientation within POPC (Dissertation, Benjamin Zimpfer). 1-pulse ^{19}F-NMR spectra were firstly observed with 4000 transients at 10 ℃. 60 kHz ^{1}H decoupling was applied and the 90 ° rf pulse was set to be 2.5 µs at 7.5 dB. Interestingly, we observed two signals in the 1-pulse ^{19}F-NMR spectrum from singly monofluorated peptides. A racemization of ^{19}F-label could be excluded by liquid-state

NMR, where only one sharp peak was obtained. Thus these two peaks were attributed to two states in the membranes, namely monomers and dimers. In Fig. 5.2.13, the dotted red line denotes the isotropic position near -93 ppm. The peaks around this position, which did not move when orientation of the sample changed (Fig. 5.2.13a→b, c→d), indicate monomers freely rotating outside of the membrane. The left peaks, which are shifted to the right with the reorientation of the sample (Fig. 5.2.13a→b, c→d), were assigned to dimers. The small component on the left at ca. 75 ppm of spectrum b probably resulted from remaining TFA from HPLC, which is volatile and disappeared after two months as shown in spectra c and d.

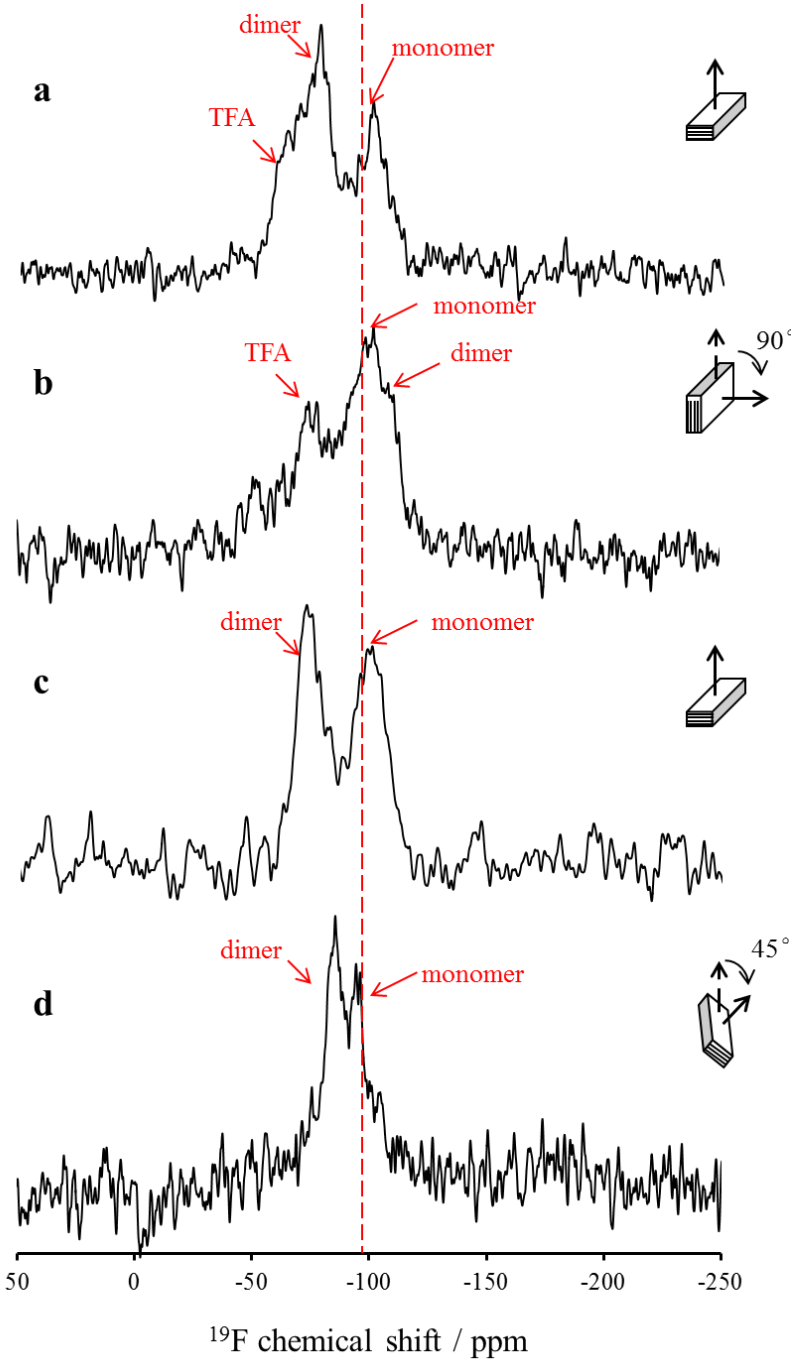

Fig. 5.2.13 ^{19}F-NMR spectra of TisB Q19 embedded in oriented POPC lipid bilayers at 10 ℃ acquired with 4000 scans. The sample was freshly prepared and measured with the membrane normal parallel (a, 0°) and perpendicular (b, 90°) to the magnetic field. After two months storage at -40 ℃, the sample was measured again with the membrane normal parallel (c, 0°) and tilted (d, 45°) to the magnetic field. The red dotted line denotes the isotropic position of ^{19}F.

As shown in Fig. 5.2.14, a dimer / monomer coexistence model of TisB was proposed. The peptides used for the CPMG experiments were not neutralized, since the desalted peptides were insoluble in organic solvent, and for sample preparation the peptide and lipid powders should be firstly dissolved in MeOH or CH_2Cl_2. Thus the remaining acids in the peptides may destroy the dimerization, the monomers emerge on the surface of the membranes or break away in water, where they are mobile and can rotate quickly, attributing to the isotropic peaks around -93 ppm (Fig. 5.2.14).

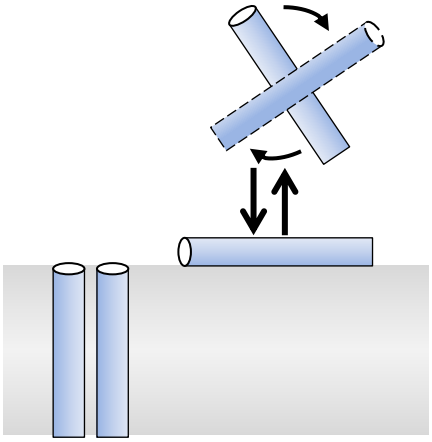

Fig. 5.2.14 Schematic illustration of dimer / monomer coexistence model of TisB in oriented POPC membranes.

To remove the monomer-component in the ^{19}F-NMR spectra, the CP-ramp experiment was applied. It is known that, the CP-ramp was mostly used for nuclei (^{15}N, ^{13}C) with lower gyromagnetic ratio to enhance the signals by transferring the magnetization from ^{1}H. And the efficiency of the transfer depends on the dipolar couplings between them (^{1}H-^{15}N or ^{1}H-^{13}C). In our case of TisB, the dipolar couplings between ^{1}H-^{19}F (TisB monomers) are weakened by the motions of the peptides, and this property can be utilized to remove the signals from monomers. As shown in Fig. 5.2.15, using CP-ramp experiment (red line), the right peak around -93 ppm, which denotes the component of TisB monomers, is totally removed. This experiment has further confirmed the dimer / monomer model of our TisB samples.

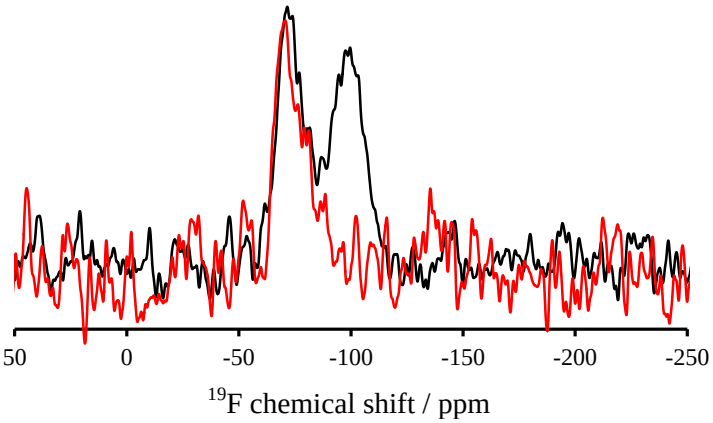

Fig. 5.2.15 ^{19}F-spectra obtained with TisB Q19 embedded in oriented POPC membranes at 10 ℃ by a normal one pulse (black) and CP-ramp (red) experiment. The contact time of CP-ramp experiment was set to 1 ms. The spectra were obtained with 4000 scans.

In view of the small amount of the peptide TisB, a second batch with ^{19}F-Gln analogue (in position 19) for distance measurements and ^{15}N-Ala (in position 16) for monitoring the peptide alignment were synthesized, giving TisB Q19-A16. The peptide / lipid mixture (P : L = 1 : 100) was dissolved in MeOH / H_2O and neutralized by dialysis to get rid of the HCl from HPLC, the suspension was directly spread on the glass plates without lyophilization. And as expected, only one peak was obtained from the single one pulse measurement, as shown in Fig. 5.2.16 (c), however, further components on the bottom of the spectrum were still visible, probably originating from powders or monomers, which were then suppressed by the CP-ramp experiment. The membrane alignment was monitored by the ^{31}P-spectra before (a) and after (b) the measurements, which showed well-oriented membranes (> 90%). The ^{15}N-NMR spectrum with one peak around 150 ppm indicates a tilted-state of TisB within the POPC membrane.

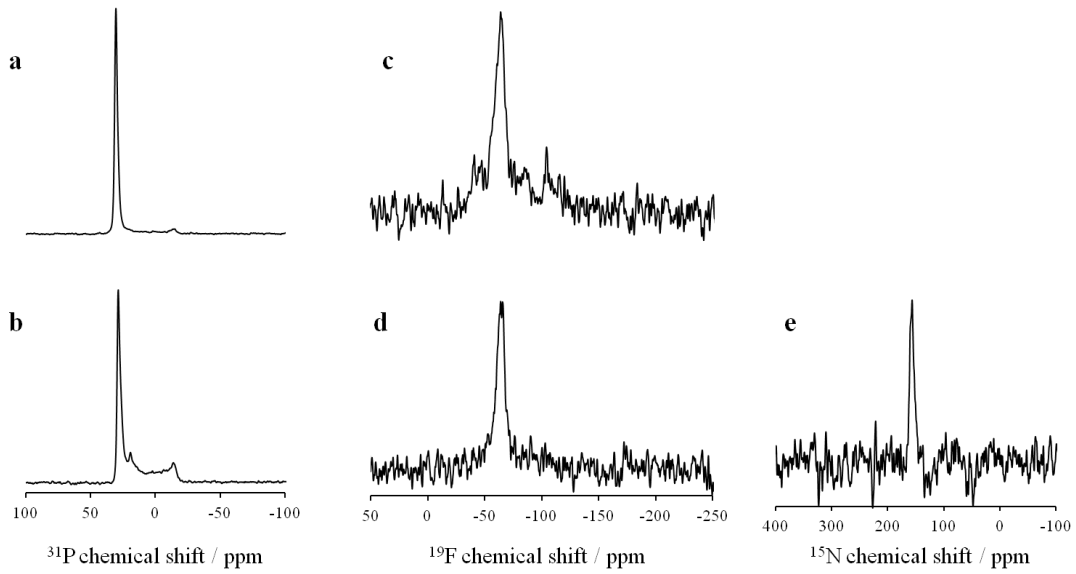

Fig. 5.2.16 ^{19}F-NMR spectra obtained with neutralized TisB Q19-A16 embedded in oriented POPC membranes at 10 ℃. ^{31}P-NMR spectra were obtained before (a) and after (b) all the other measurements with 248 transients. ^{19}F-NMR spectra were acquired with normal one pulse (c) and CP-ramp (d) with 4000 transients. The ^{15}N-spectrum (e) with more than 20000 transients was acquired to address the peptide orientation.

As illustrated above, no matter whether the TisB peptide was neutralized or not, components of monomers or powders were visible more or less in the 1-pulse ^{19}F-spectra, and they could be totally removed by CP-ramp experiments. Also, the CPMG acquired from the acidic or neutralized samples were unchanged. A modified CPMG sequence, combining with CP-ramp so-called CP-CPMG, was developed to eliminate the effects of unpaired TisB peptides. As shown in Fig. 5.2.17, the CPMG spectrum (a) was obtained with 15000 transients and the CP-CPMG spectrum (b) with twice more scans. Both of them were symmetrically processed to improve the quality of the observed doublet from CP-CPMG. Whereas the CPMG spectrum showed only one peak without splitting, the CP-CPMG experiment successfully removed the 0 kHz dipolar couplings from monomers and revealed a doublet resulting from dimers. After lineshape simulation (b, grey line), the intermolecular dipolar coupling between the ^{19}F labels can be directly read to be d_{obs} = 315 Hz. To translate the dipolar coupling into an internuclear distance, knowledge of the orientation of the internuclear vector is necessary. However, as the side chain conformation is uncertain, this orientation is not known. Hence, only a range of distances in agreement with the dipolar coupling can be specified. Taking the molecular order parameter S_{mol} as 1, the largest intermolecular distances r between the ^{19}F-labels of 10 Å could be obtained with an orientation θ of inter-^{19}F vector with respect to the external magnetic field B_0 of 0 °, as shown in 5.2.18 (c).

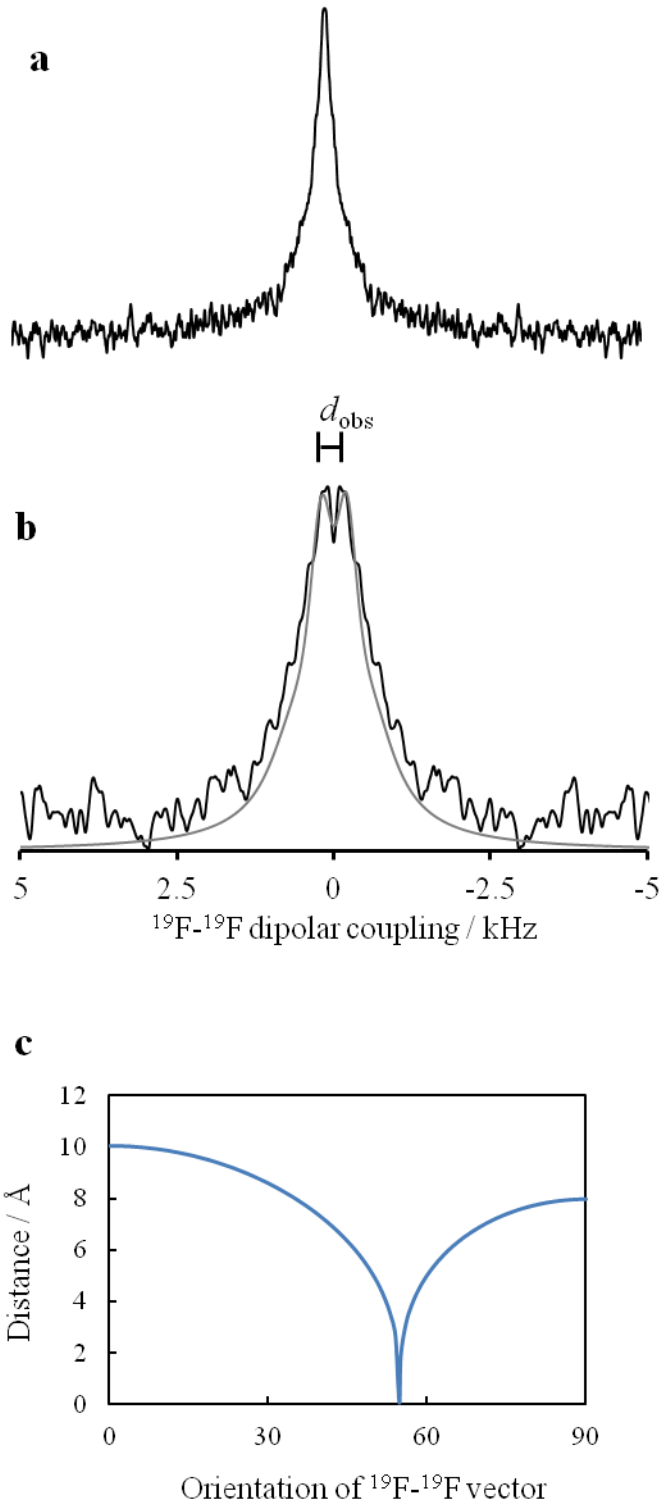

Fig. 5.2.18 CPMG (a) and CP-CPMG (b) spectra obtained with TisB Q19 embedded in oriented POPC membranes at 10 ℃. The CPMG spectrum was obtained with 15000 scans and the CP-CPMG spectrum with 30000 scans. The underlying spectrum in b drawn in gray shows the best simulation. (c) shows the relationship between obtained inter-^{19}F distance and the ^{19}F-^{19}F vector orientation.

Conclusion

The stress-response peptide TisB is supposed to form antiparallel dimers, and the dimerization is stabilized by four salt bridges between Asp5 - Lys26, Lys12 - Asp22, Lys26 - Asp5, Asp22 - Lys12 and hydrogen bonds between Gln19 - Gln19.

To investigate the dimer interactions, TisB were doubly labeled with U-Asp and $^{15}N_2$-Lys, giving TisB D5-K26 and TisB K12-D22. To measure the intermolecular distances between the amine-^{15}N of Lys and the side chain carbonyl-^{13}C of Asp, a modified sel-REDOR experiment was developed to extract only the dipolar coupling between ^{15}N and ^{13}C=O. For the REDOR experiments, frozen samples were required to eliminate the peptide motion which could weaken the observed dipolar coupling. However, no dephasing was observed from these two TisB analogues, indicating that these intermolecular distances of interests are most probably longer than 5 Å, which is beyond the capability of our REDOR experiments. Nevertheless, the sel-REDOR approach is well established and successfully tested with test substances, which is beneficial for other distance measurements in the future, since the amino acids purchased from the market are not always labeled in positions expected but mostly uniformly labeled, and the sel-REDOR is suited for filtering the dipolar interactions of interest. Besides, the intermolecular distances between these labeled positions (Asp5 - Lys26, Lys12 - Asp22) can be restricted to be > 5 Å.

To detect long-range intermolecular distances between TisB dimers, a ^{19}F-Gln-analogue was chosen to substitute the Gln in position 19, as the ^{19}F-label is structurally and chemically similar to the original Gln. The CPMG approach was applied to measure the distance dependent ^{19}F-^{19}F dipolar couplings. However, a significant problem for addressing such distances was demonstrated in one-pulse ^{19}F-NMR spectra. As shown in Fig. 5.2.13, more components were obtained, indicating a TisB dimer / monomer coexistence within the oriented POPC membrane. The most probable reason is that the HCl resulting from HPLC destroyed the salt bridges and thus the dimerization. Nevertheless, these monomer or powder parts cannot be totally removed even by neutralization using dialysis. Thus, the CP-ramp experiment, which is always employed for low-gamma nuclei, was applied here for ^{19}F-NMR spectra to successfully get rid of the signals from monomers, because the CP efficiency was lower for mobile monomer molecules. Then, a so-called CP-CPMG was developed to reveal the inter-^{19}F dipolar couplings only from dimers and a doublet could be detected. The dipolar coupling could be directly read from the splitting after lineshape simulation, which was d_0 =

315 Hz. According to formula 2.3, the distance obtained is strongly depended on the orientation θ of the ^{19}F-^{19}F vector with respect to the magnetic field, as shown 5.2.18 (c). And the largest inter-^{19}F distance obtained with $\theta = 0$ and $S_{mol} = 1$ is 10 Å, which means that, the intermolecular distance between the two Gln of TisB dimers is < 10 Å.

Although no precise intermolecular distances have been obtained within TisB dimers in this study, the four intermolecular salt bridges, which are supposed to initiate and stabilize the TisB antiparallel dimerization, could be constrained to be over 5 Å. And the middle hydrogen bound between Gln19 - Gln19 shows a maximum intermolecular distance of 10 Å. These distance constraints may provide important information for the TisB dimer modeling and peptide function.

5.3 Dimer interfaces of E5

Introduction

To determine the E5 protein oligomeric structure, it is essential to measure inter-molecular distances. In structural biology, NMR distance measurements play an important role, and they are mostly based on dipolar recoupling under magic-angle spinning (MAS), however, challenged by molecular motion. Carr-Purcell-Meiboom-Gill (CPMG) was successful in revealing a long-range distance of ~11 Å without MAS in fluid membranes. Thus the CPMG approach was used also to obtain inter-helical contacts of E5 dimers at ambient temperature. Another approach, the so called the centerband-only detection of exchange (CODEX), was also utilized, which is based on ^{1}H-driven ^{19}F-^{19}F spin diffusion and recoupling of the ^{19}F-CSA to enable not only spin counting but also extracting inter-molecular distances.

For the experiments, we chose 4F-Phg as NMR label, as it is beneficial for addressing long-range inter-nuclear distances (see section 5.1). In view of the large bulky side chain of the label, Phe was the favorite labeling target to minimize local structural changes, and Leu was left as a second choice. Thus, as shown in Fig.5.3.1, based on the proposed dimer model [58], positions Phe6 and Phe28 should be on the side of the dimer interfaces and were labeled to give potential inter-helical contacts. Remarkably is that, among the unusually hydrophobic sequence of E5, Gln17 is the only polar amino acid in the transmembrane region, which probably forces the E5 dimerization and simultaneously forms a hydrogen bond with Thr513 of the PDGFβ receptor. Thus, the Gln17 is of large interest for the investigation of E5 dimerization. Considering that Gln17 occurs in the dimer interface, a ^{19}F-labeled Gln analogue (^{19}F-Gln) instead of 4F-Phg was incorporated in this position, which is structurally similar to the original Gln. As a blank control, Phe9 and Leu7 were chosen, as they were expected to be located on the opposite side of the dimer interface. Overall, five single ^{19}F-labeled E5 analogues were chemically synthesized. The sequence of the E5 analogues was also truncated to 36 amino acids, lacking the two C-terminal Cys that are known to form disulfide bonds. This truncation is possible because the absence of the two Cys does not influence the α-helix structure and self-dimerization [69]. The synthesized sequences are summarized in Tab. 5.3.1.

With these five selectively ^{19}F-labeled E5 analogues, solid-state NMR CODEX and CPMG experiments were performed to detect the inter-molecular distance-dependent dipolar couplings between pairs of ^{19}F-labels within the dimers. Although with CPMG no direct distances were obtained, the dipolar coupling could be deduced from the line-broadening. A direct evidence of E5 dimerization and inter-molecular distance constraints were determined here for the first time using CODEX.

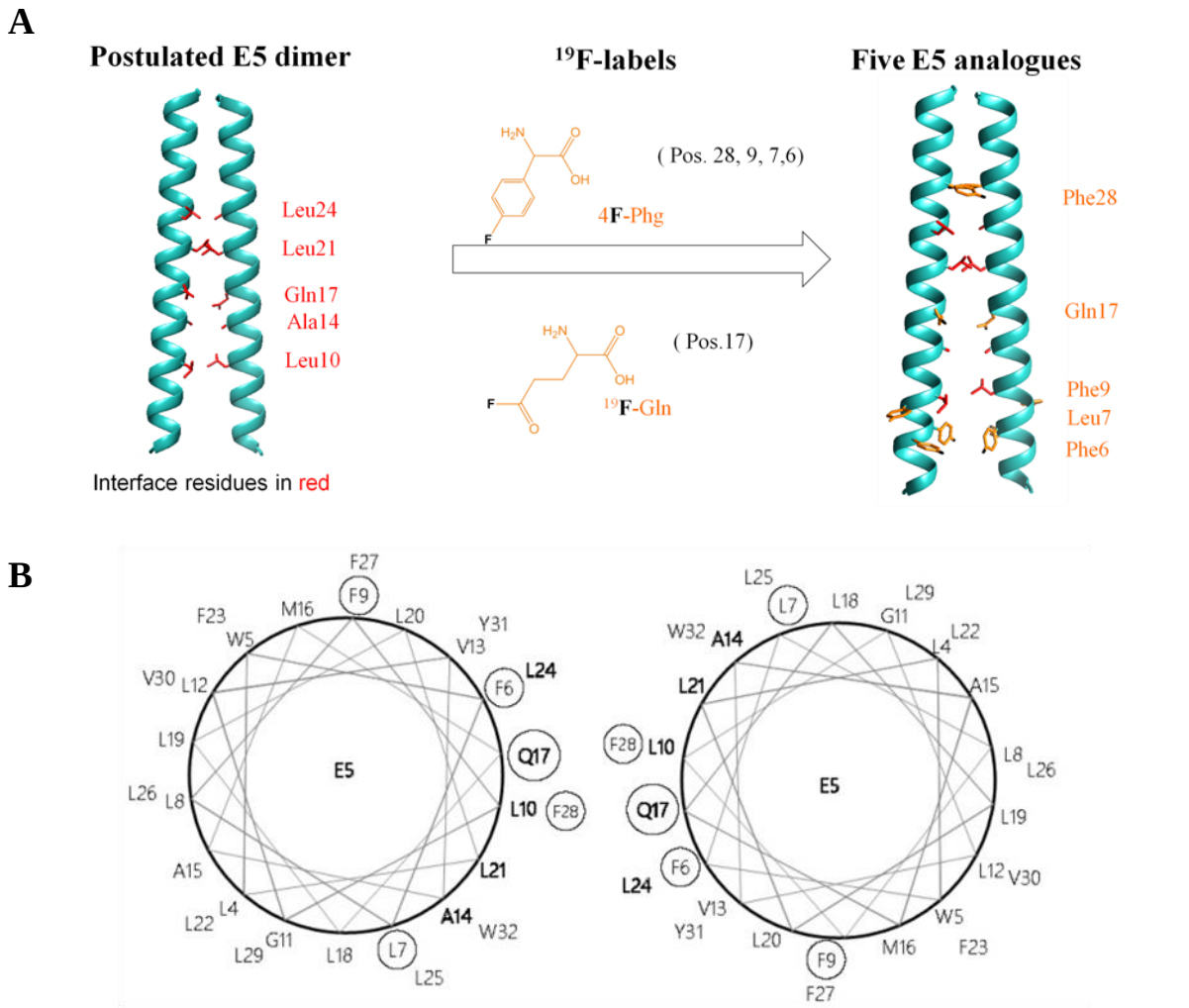

Fig. 5.3.1 Schematic Illustration of the E5 labeling strategy. (A) The labels were incorporated into E5 in positions 28, 17, 9, 7, 6 using appropriate ^{19}F-labels, which were expected to give distance-dependent inter-molecular dipolar couplings. (B) Helical wheel representation of E5 dimer with dimer interface amino acids (in solid) and labeling residues (in circles). Only transmembrane segments (TM, 4-32) are shown here, and helical turn of 100 °was applied.

Tab. 5.3.1 Synthesized labeled E5 analogues.

Name	Sequence	Molar mass [g/mol]

E5 F6	MPNLW-**4F-Phg**-LLFLGLVAAMQLLLLLFLLLFFLVY WDHFE	4405
E5 L7	MPNLWF-**4F-Phg**-LFLGLVAAMQLLLLLFLLLFFLVY WDHFE	4439
E5 F9	MPNLWFLL-**4F-Phg**-LGLVAAMQLLLLLFLLLFFLVY WDHFE	4405
E5 Q17	MPNLWFLLFLGLVAAM-**^{19}F-Gln**-LLLLLFLLLFFLVY WDHFE	4402
E5 U-Q17$_a$	MPNLWFLLFLGLVAAM-**U-Gln**-LLLLLFLLLFFLVY WDHFE	4405
E5 F28	MPNLWFLLFLGLVAAMQLLLLLFLLLF-**^{19}F-Gln**-LVY WDHFE	4405
E5 ^{15}N-L25$_b$	MPNLWFLLFLGLVAAMQLLLLLFL-**^{15}N-Leu**-LFFLVY WDHFE	4405

'a': this E5 analogue was uniformly ^{13}C, ^{15}N-labeled by Master student Violetta Schneider in our group.

'b': labeled by ^{15}N in position 25, purchased from W. Dirk in our group for orientation test before CODEX experiments

Results and discussion

o CPMG experiments

The five ^{19}F-labeled E5 analogues were reconstituted in oriented lipid membranes (DErPC, C22:1(Cis), transition temp. 13.2 °C) at two different peptide concentrations and measured at ambient temperature, where the lipids were in the liquid-crystalline state. Unfortunately, no dipolar splitting was obtained. Therefore, the CPMG spectra with the sample orientation perpendicular (90°) to the magnetic field were acquired as well, and by comparing the line broadening of the spectra, evidence for ^{19}F-^{19}F dipolar couplings could be revealed. As the fast rotation around the membrane normal after the 90° flip of the sample would attenuate the dipolar couplings by a factor of 1/2, a dipolar coupling would also be visible in a change in the linewidth, even if the dipolar splitting cannot be resolved. All the CPMG spectra are summarized in Fig. 5.3.2.

As shown in Fig. 5.3.2, except for E5 labeled in Leu7, all the CPMG spectra obtained at 90° sample orientation are narrower than those at 0°, indicating the existence of ^{19}F-^{19}F dipolar couplings between these positions, although their exact values are inaccessible. It has been reported that, even at lower peptide : lipid ratio of 1 / 200, the dimerization of E5 was observable [69]. Here, from CPMG spectra, an increasing number of dimers was observed with higher peptide : lipid ratio (1 / 50 compared to 1 / 100) for all positions except of Leu7, as the lines of them were broader at a peptide : lipid ratio of 1/50. This increase in dimerization with peptide : lipid ratio demonstrates the coexistent of dimers / monomers or higher order oligomers.

In the case of Leu7, the opposite was observed, and the CPMG spectra at 90° were broader than at 0° sample orientation, probably due to the specific relaxation time in this position. Furthermore, the linebroadening due to higher peptide concentration was also not observed in this position. Thus, it is probable that ^{19}F-labels in this position are located far away from each other (> 11 Å) within the E5 dimers, as the side chains are pointing away from the dimer interface, and the dipolar coupling between them is too weak to be detected by our CPMG experiments.

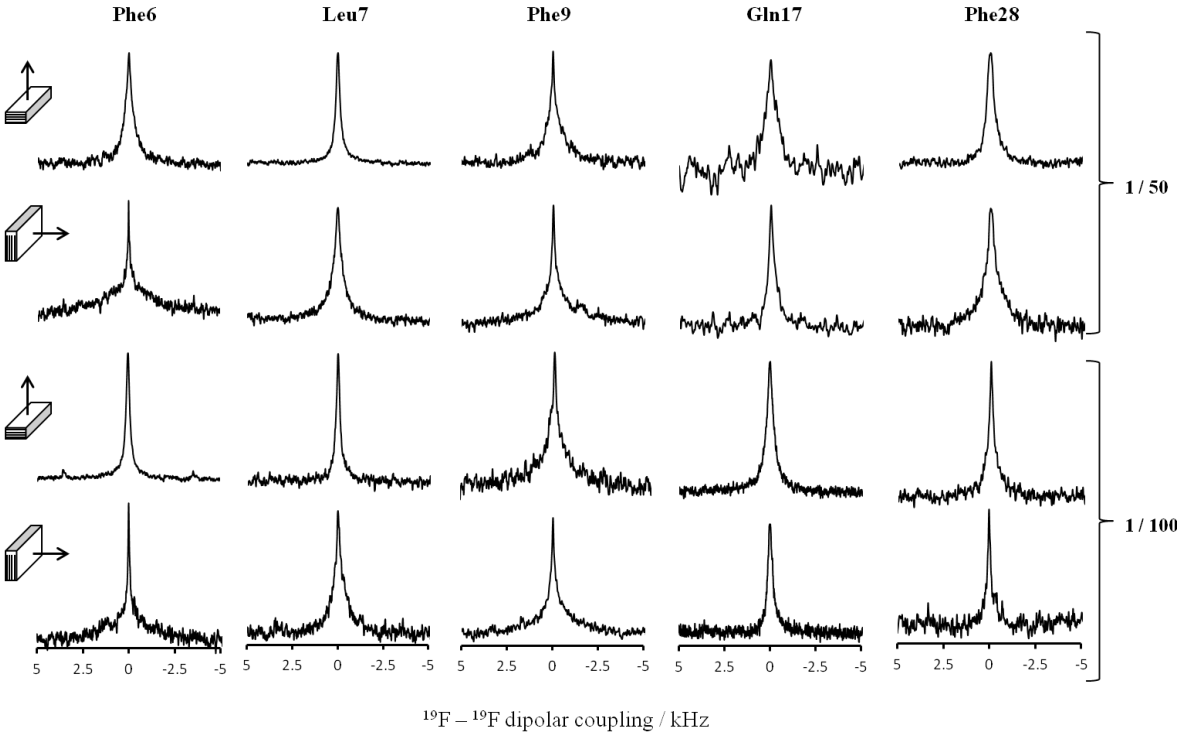

Fig. 5.3.2 CPMG spectra of five ^{19}F-labeled E5 analogues embedded in oriented DErPC membranes at room temperature (ca. 20 ℃). Peptide to lipid ratios of 1 : 50 and 1 : 100 were used, and for each ratio, the samples

were measured with membrane normal parallel (0 °) and perpendicular (90 °) to the magnetic field. All the CPMG spectra were acquired with more than 15000 transients (ca. 12 h).

Since the variation of peptide concentration indicated a E5 dimer / monomer mixture or existence of higher oligomers, the potential formation of large aggregates of the peptides was of large interest. One-pulse ^{19}F-NMR spectra were measured for this purpose and summarized in Fig. 5.3.3. The CSA tensor principal axis values of the 4F-Phg label are known to be σ_{11} = - 62 ppm, σ_{22} = - 125 ppm, σ_{33} = - 154 ppm, and σ_{iso} = - 113 ppm [99], and those of ^{19}F-Gln analogue are σ_{11} = -154 ppm, σ_{22} = -105 ppm, σ_{33}= -40 ppm and σ_{iso} = - 93 ppm (see section 5.2). The large chemical shift anisotropies (CSA, ca. 100 ppm) narrowed down to only 20 ppm, as can be deduced from the shifts of the NMR lines when the samples were turned by 90 °. This reduction in CSA indicates that the peptides undergo fast rotational diffusion around the lipid bilayer normal. Hence, the peptides seem to be properly reconstituted and not aggregated, as otherwise this motion would not be possible. It is interesting that, the ^{19}F chemical shifts from all the positions were around the isotropic chemical shifts (Phe6, Leu7, Phe9, Phe28 with 4F-Phg around -113 ppm, Gln17 with ^{19}F-Gln around -93 ppm), no matter what the peptide concentrations or the sample orientation was. The most probably cause is, the peptides are all penetrating the membrane (I-state), and this way the side chain orientations α = 53.2 ° [149] are near the magic angle (54.7 °), giving the chemical shifts around the isotropic position. These results confirm a transmembrane alignment of the peptides, and that the peptides could span the membrane without aggregating or emerging on the membrane surface, which is also supported by the highly hydrophobic character of the peptide E5.

In total, the CPMG experiments were able to provide some first evidence for E5 dimers, but only in a rather indirect way analyzing the response of the linewidth to sample tilt and to peptide : lipid ratio. The failure to obtain resolved splittings could be explained by the presence of monomers, which would give rise to a central signal in the CPMG spectra obscuring a potential splitting. Another reason could be that, the dipolar couplings are further weakened by the mobility rotation of the peptides. Thus another approach of distance measurements is necessary. It should firstly reduce the peptide mobility, and secondly could address the oligomeric states of the peptide, and the best candidate is the CODEX experiment.

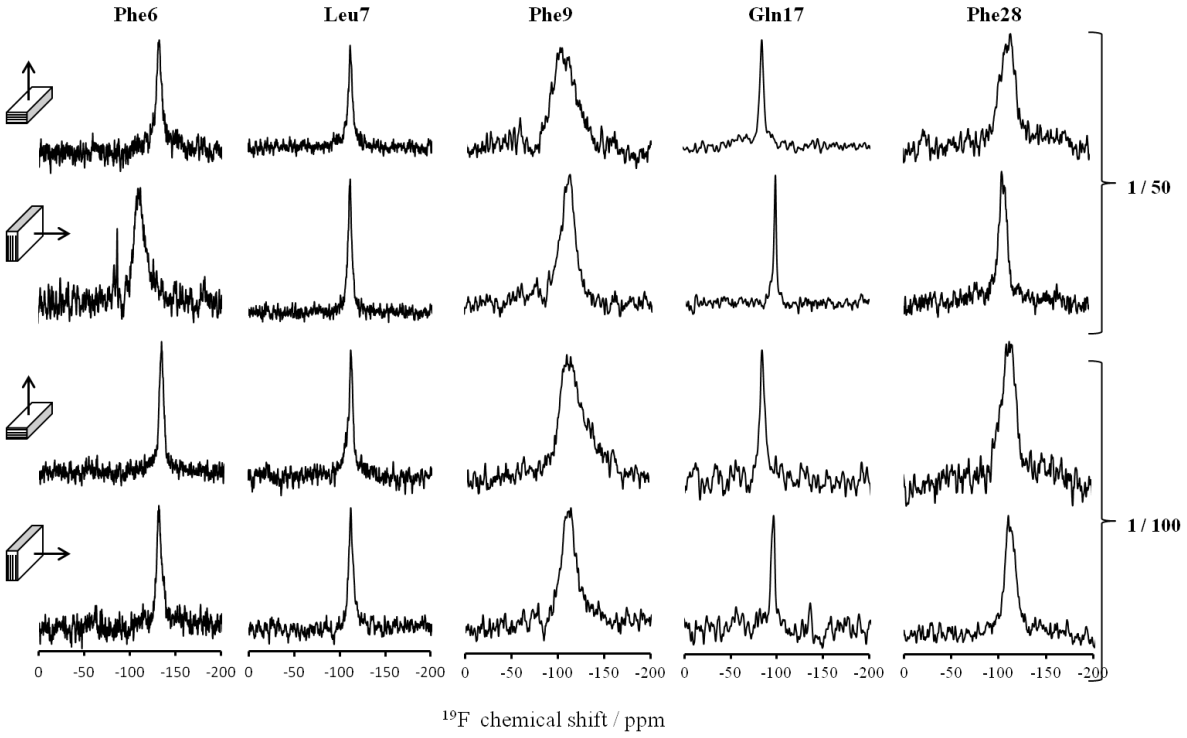

Fig. 5.3.4 1-pulse ^{19}F-spectra of five ^{19}F-labeled E5 analogues embedded in oriented DErPC membrane at room temperature (ca. 20 °C). The peptide to lipid ratios of 1 : 50 and 1 : 100 were used, and for each ratio, the samples were measured with membrane normal parallel (0°) and perpendicular (90°) to the magnetic field. All the CPMG spectra were acquired with 4000 scans (ca. 3 h).

- **CODEX experiments**

CODEX was applied to detect the oligomer state and extract distance constraints on the basis of spin diffusion, which has been firstly demonstrated by M. Hong [104]. For CODEX, frozen samples with E5 protein embedded in DErPC vesicles (P / L = 1 / 50) were employed to rule out all the molecular motions, leaving only ^{19}F-^{19}F dipolar coupling contributing to CODEX echo intensity dephasing. A spinning speed of MAS = 25 kHz was chosen to avoid any side bands, as small side bands are difficult to integrate. Also, faster MAS is beneficial for larger signal. At varied mixing times T_m, always two experiments (S: exchange experiment, S_0: reference experiment) were conducted.

Before the CODEX measurements, it should be confirmed that, the peptide E5 does not aggregate or change its orientation in the membrane by freezing. Thus the E5 labeled with ^{15}N in position 25 from Dr. Windisch (KIT), was tested for the effect of temperature. The sample was prepared as previously described for CPMG experiments and measured at 30 °C and -

20 °C respectively. As shown in Fig. 5.3.5, both give the chemical shifts around 200 ppm, demonstrating a perfect membrane-spanning orientation even when the sample is frozen.

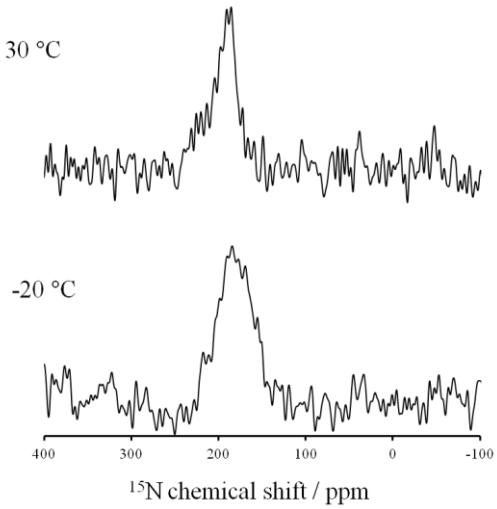

Fig. 5.3.5 ^{15}N-NMR spectra of E5 ^{15}N-L25 embedded in oriented DErPC membrane at 30 ℃ and -20 ℃. Each spectrum was obtained with 20000 transients (ca. 12 h),

After the five ^{19}F-labeled E5 analogues were measured using the by CODEX sequence, for each peptide, the S_0 / S ratios were obtained for more than five different mixing times T_m. This CODEX curve of S_0 / S as a function of T_m was fitted by an exponential decay function (Fig. 5.3.6). The relationship between the decay constant k and ^{19}F-^{19}F dipolar coupling D can be expressed as:

$$1/k = 0.5\pi D^2 F(0) \qquad (5.6)$$

where $F(0)$ denotes an overlap integral, which is influenced by the NMR properties of the ^{19}F-reporter groups (isotropic chemical shifts, chemical shift principal values) and of the ^{1}H-driven spin diffusion (which depends on MAS spin speed). M. Hong [104] gives the average value of $F(0)$ as 37 μs for ^{19}F-CODEX with MAS = 8kHz, which has been calibrated using model compounds with known inter-nuclear distances such as 5-^{19}F-Trp. We used the $F(0)$ value of 37 μs as well for this study for two reasons: (1) Since r depends on $F(0)$ as $(F(0))^{1/6}$ (eq. 2.2), small deviations of $F(0)$ have little effect on the observed distance r; (2) The two ^{19}F-labels we used were ^{19}F-Phg and ^{19}F-Gln, and the chemical shift anisotropies (CSA) of them are 64 ppm and 54 ppm respectively, which are similar to that of 5-^{19}F-Trp with 48 ppm. It is furthermore reported that the spin diffusion is strongly affected by the spinning rate. In the calibration with several test compounds at different MAS rates, the $F(0)$ value has been found to be approximately reversely proportional ($1/\nu_r$) to the MAS rate [104]. Thus with the

overlap integral value $F(0)$ of 37 µs at 8 kHz scaled by 8/25, we got $F(0)$ = 12 µs for our CODEX experiments at 25 kHz. This value of $F(0)$ was then verified using the test substance D/L-4F-Phe.

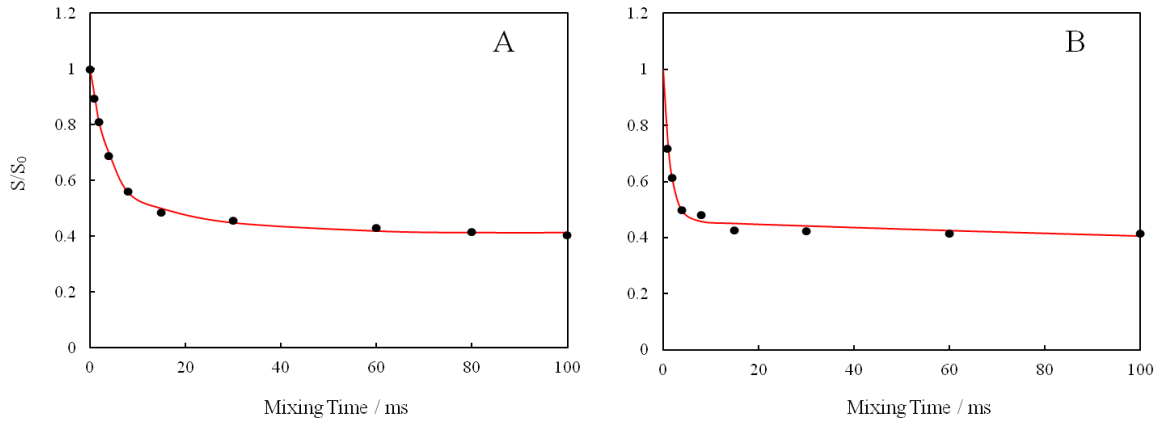

Fig. 5.3.6 ^{19}F CODEX of D/L-4F-Phe at 243 K and with MAS = 25 kHz (A) and MAS = 16 kHz (B). Recycling delays of 70 s and 248 scans were applied. The black spots denote the experimental points. The points are fitted by double exponential curves (red), and indicate tetramers. Each experimental point was obtained with more than 30000 transients (ca. 1 d).

As shown in Fig. 5.3.6, the CODEX of D/L-4F-Phe was measured with mixing times T_m up to 100 ms. A recycle delay time as long as 70 s was used because of the long relaxation time of D/L-4F-Phe [150], and the dependence of the $F(0)$ values on MAS was obtained at two different spinning speeds. The experimental points were then fitted by double exponential curves $y = a_1 \times e^{-t/k_1} + a_2 \times e^{-t/k_2} + a_3$ ($a_1 + a_2 + a_3 = 1$), where a_3 is the equilibrium value of the curve and indicates the oligomer number, and in our case it was 0.25. The two important parameters k_1, k_2 reflect the decay constants of a fast and slow decay, respectively. With MAS = 25 kHz, k_1 = 4.46 ms, k_2 = 246 ms with rmsd = 0.0007 (Fi.g 5.3.6A), while they are 1.5 ms, and 334 ms respectively with MAS = 16 kHz, rmsd = 0.0023 (Fig. 5.3.6B). The double exponential CODEX curves are the result of oligomers with mixed distances, and although the shorter distance distributions cannot be revealed, the shortest distance can be assigned to the faster decay constant k_1. Estimating the ^{19}F-^{19}F distance to be 4 ~ 6 Å, $F(0)$ of D/L-4F-Phe results to be in the range of 6 ~ 53 µs, which means that the $F(0)$ value of our test substance agrees within a factor of 2 with the values of the study of M. Hong, which is acceptable given the weak dependence of the distance of $F(0)$. As a consequence, we took the F(0) value of 12 µs for the further CODEX experiments according to M. Hong's calibration [104], as it was comprehensively analyzed with several compounds and different MAS spinning speeds.

Tab. 5.3.2 Experimental decay constant k1 for D/L-4F-Phe at two different MAS rates

Compound	25 kHz	16 kHz
	k_1 / ms	k_1 / ms
D/L-4F-Phe	4.46	1.5

After the parameter *F*(0) had been estimated using test compounds, it was now possible to evaluate the data of the E5 dimers. As shown in Fig. 5.3.7, the experimental data of the S / S_0 intensities of the ^{19}F-labeled E5 as a function of the mixing time T_m could be fitted by single-exponential curves ($y = 0.5*e^{-t/k}+0.5$). The curves were found to decay to an equilibrium values of 0.5, and this value denotes the oligomer numbers as 1 / 0.5 = 2, which means dimer formation. These CODEX curves yield decay constants *k* of 1.68 ms, 0.25 ms and 0.7 ms, and according to eq. 5.6, the corresponding intermolecular ^{19}F-^{19}F distances can be revealed as 3.8 Å, 2.8 Å, 3.3 Å for position Phe28, Gln17 and Phe6 respectively. As expected, we did not see any decay in the position Leu7 within 35 ms mixing time, which means no intermolecular contact occurs in this position.

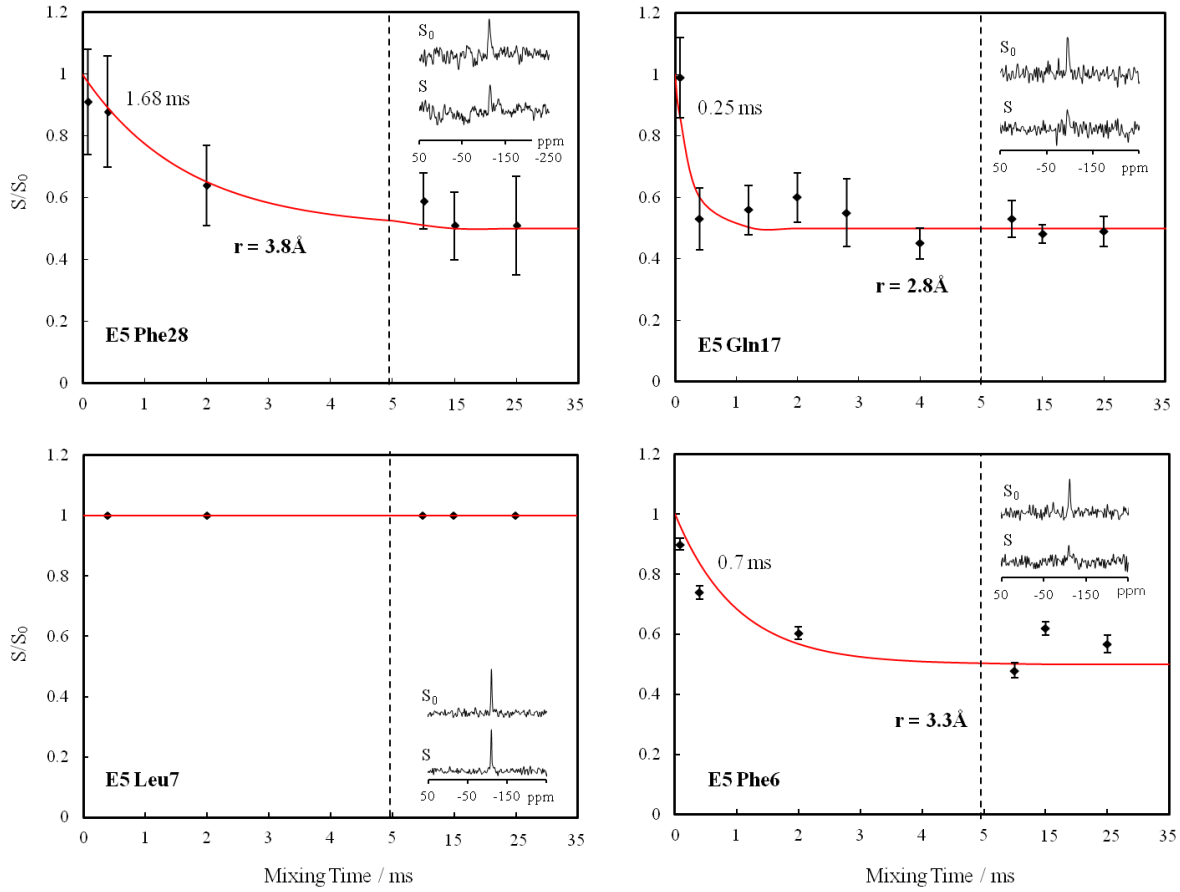

Fig. 5.3.7 ^{19}F CODEX of single labeled E5 analogues in DErPC liposome at 243K and with MAS = 25 kHz. Inserted are the spectrum of S_0 and S with mixing time of 2 ms. The positions Phe28, Gln17, Phe6 and Leu7 are shown here. The experimental points (dots) are best fitted to single exponential decay with time constants alongside in ms, and the inter-helical ^{19}F-^{19}F distances *r* written under the curves are addressed from the decay constants. Error bars were calculated from the signal-to-noise (S / N) ratio of the S and S_0 spectra.

Most interesting was the behavior of the CODEX curve of the E5 Phe9, shown in Fig. 5.3.8. The experimental points can be fitted by the bi-exponential curve S/S_0=0.33+0.43e$^{-t/1.08}$+0.24e$^{-t/18.05}$ (solid line, rmsd = 0.06) indicating a trimer, or S/S_0=0.25+0.44e$^{-t/1.1}$+0.31e$^{-t/30}$ (dotted line, rmsd = 0.059) as a tetramer, both of which decayed to values below 0.5 (Fig. 5.3.8A). Because of the shorter T_2-relaxation time of our ^{19}F-labeled E5 peptides, it is difficult to measure beyond 35 ms and to determine the exact value of S / S_0 for T_m → ∞. Nevertheless, combined with the results of the other E5 analogous, the unusual decay curve of position Phe9 indicates contacts to neighboring dimers rather than trimer or tetramer. As it is difficult to determine the distance distribution in the presence of multiple dipolar couplings, only the nearest inter-helical ^{19}F-^{19}F distance can be conservatively estimated to lie inbetween the fit of the experimental points of short T_m times and long T_m times, and it is 3.5 ~ 4.5Å (Fig. 5.3.8B).

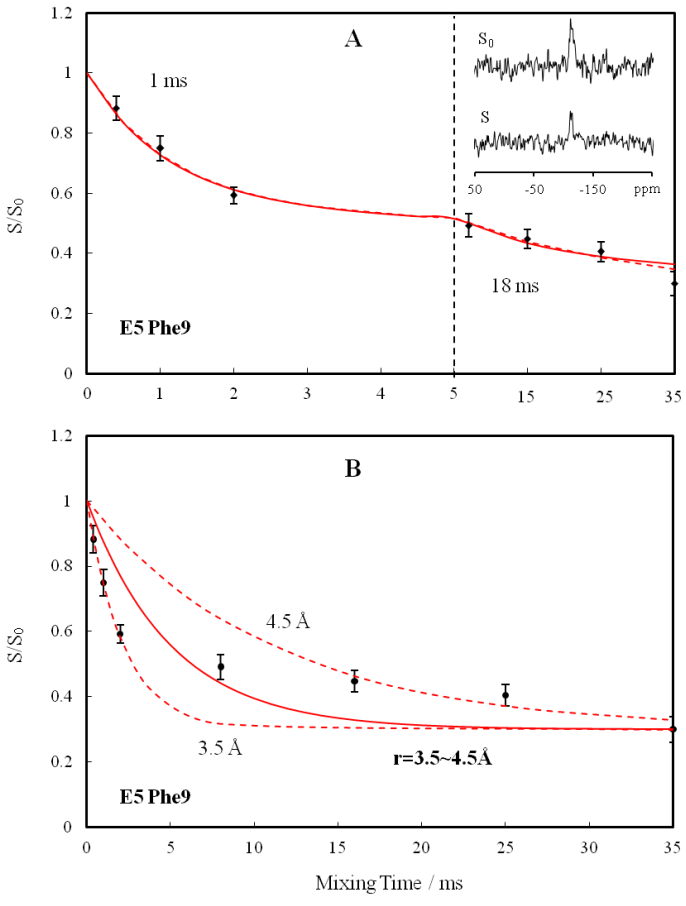

Fig. 5.3.9 ^{19}F CODEX of single ^{19}F-labeled E5 in position 9 embedded in DErPC vesicles measured at 243 K and with MAS = 25 kHz. (A) The best-fits of bi-exponential curves decaying to 0.33 (solid line) or 0.25 (dotted line) indicate a trimer or tetramer model. Inserted are the spectrum of S_0 and S with mixing time of 2ms. (B) The distance distribution in multispin system is difficult to deconvoluted, thus the nearest ^{19}F-^{19}F distance can be estimated in the range by fitting to the long and short time points (dotted lines).

Conclusion

The highly hydrophobic peptide E5 was investigated using ^{19}F-Phg for intermolecular distance measurements, as it is supposed to span the membrane and self-associate as parallel homodimers. The ^{19}F-label was incorporated into E5 in positions Phe28, Phe6, which are outside the region of the proposed dimer interfaces, to avoid any interference but still be close enough to give intermolecular contacts. Phe9 and Leu7 were also labeled to serve as controls. Furthermore, Gln17 was studied with ^{19}F-labled Gln analogues. With these five ^{19}F-labeled E5 analogous, CPMG and CODEX experiments were performed to evaluate possible intermolecular contacts.

Although CPMG experiments did not reveal direct dipolar splittings, indirect evidence for dipolar coupling was found through line broadening analysis. It is meaningful to compare the CODEX results with those of CMPG, since for CODEX frozen samples were applied, which might lead to different behavior of the peptides. As shown in Tab. 5.3.3, a good agreement was found with Phe6, Phe9, Gln17 and Phe28, where the intermolecular contacts could be directly proven. Position Leu7 showed an ambiguous result in the CPMG experiments probably due to relaxation issue, while it exhibited no intermolecular contacts in the CODEX experiments. Most interesting is that, Phe9 showed contacts from neighboring dimers in the CODEX measurements, and the extraordinary broad lines in the 1-pulse ^{19}F-NMR spectra obtained with Phe9 can be explained this way as well by an oligomer complex, because a restricted motion in this position leads to broader lines.

Tab. 5.3.3 Schematic summary of CPMG and CODEX results

	Phe6	Leu7	Phe9	Gln17	Phe28
CPMG	Y	-	Y	Y	Y
CODEX	Y	N	Y	Y	Y

Y: ‘yes’, dipolar coupling obtained

N: ‘no’, no dipolar coupling obtained

Investigations have demonstrated that E5 adopts a left-handed coiled coil dimer with a tilt angle of 15° in DErPC membranes, and the direction of the tilt vector is determined by Ala14 (data from Dirk Windisch not published yet). With this data, E5 dimers within the lipid bilayer were proposed as shown in Fig. 5.3.8. Phe28, Gln17, Phe6 shown intermolecular contacts within dimers, and the distances measured by CODEX are approximated to be 3.8 Å, 2.8 Å, 3.3 Å respectively. Leu7 are far apart by pointing in opposite directions and thus showed no dipolar couplings. Phe9 lies on the opposite side of the dimer interface and may be close to neighboring dimers. The precise distances and distance distributions cannot be determined, however, the shortest intermolecular distance between position Phe9 can be determined to be 3.5 Å ~ 4.5 Å. These distance constraints help establishing an E5 dimer model and understanding the interaction mechanism of E5 and PDGFβR.

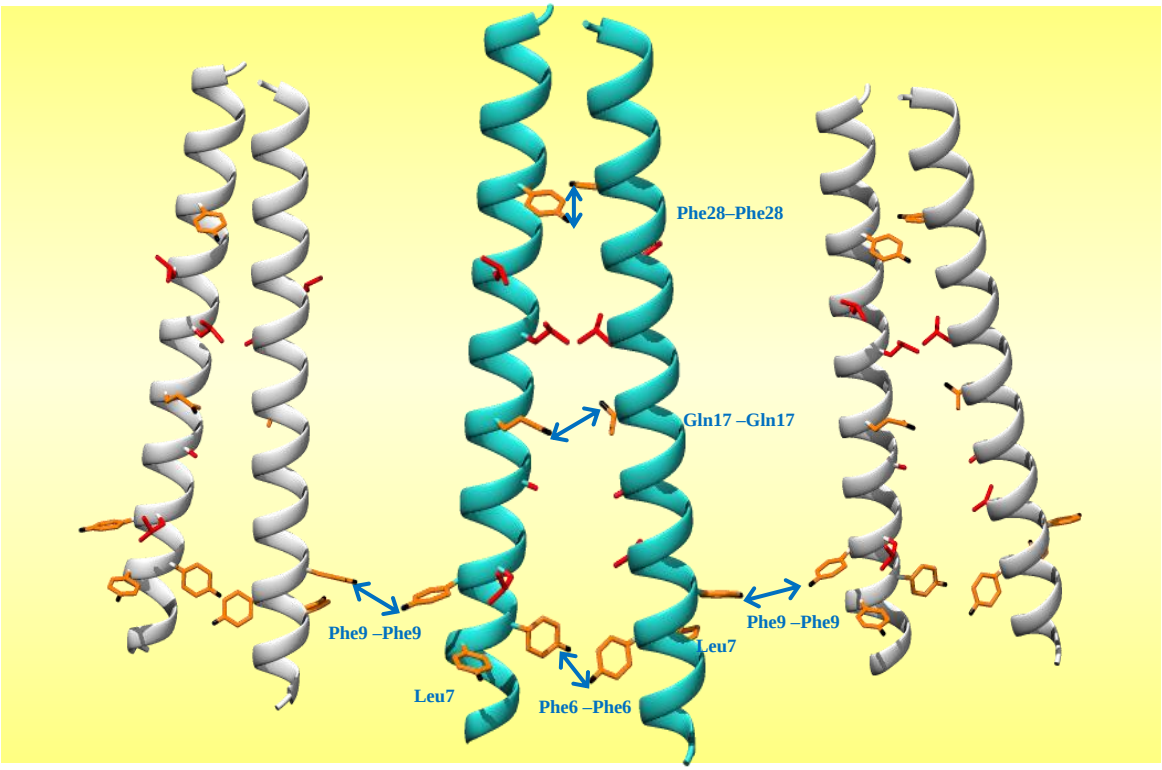

Fig. 5.3.8 Proposed E5 dimers with dimer interface amino acids in red and labeled residues in orange denote positions Phe28, Gln17, Phe6, respectively and show intermolecular contacts within the E5 dimer. Phe9 shows contacts from neighboring dimers, and Leu7 showed no dipolar coupling.

The collaboration partners Prerna Sudera and Prof. Wolfgang Wenzel then developed a Gō-Model of the E5 dimer using the helix tilt τ angle and the Gln17 - Gln17 interaction as constraints (Fig. 5.3.9 shows snapshot of the simulation), leaving a conventional force field as the sole driving force for the protein folding. From the simulation, the inter-residual distances

were averaged and summarized in Tab. 5.3.4, which shows qualitative agreement with our experimental data measured by solid-state NMR. The interesting case of position Phe9, which indicates a contact not only within but also between dimers using the CODEX experiments (Fig. 5.3.8), also agrees well with the results of the Gō-Model that showed a similar interhelical distance as Phe6 (Fig. 5.3.9), as the dynamic interaction between dimers is difficult to be captured unless the sample is frozen and the Gō-Model simulation employs only an isolated dimer.

Tab. 5.3.4 Average internuclear distances determined by Gō-model and compared with the experimental data measured by solid-state NMR

	Phe6-Phe6	Leu7-Leu7	Phe9-Phe9	Gln17-Gln17	Phe28-Phe28
Gō-model	2.6-6.9 Å	11-14.8 Å	4.9-9.9 Å	2.3-2.5 Å	2.7-7.7 Å
NMR	3.3 Å	N	>3.5 Å	2.8 Å	3.8 Å

N: ‘no’, no contact obtained

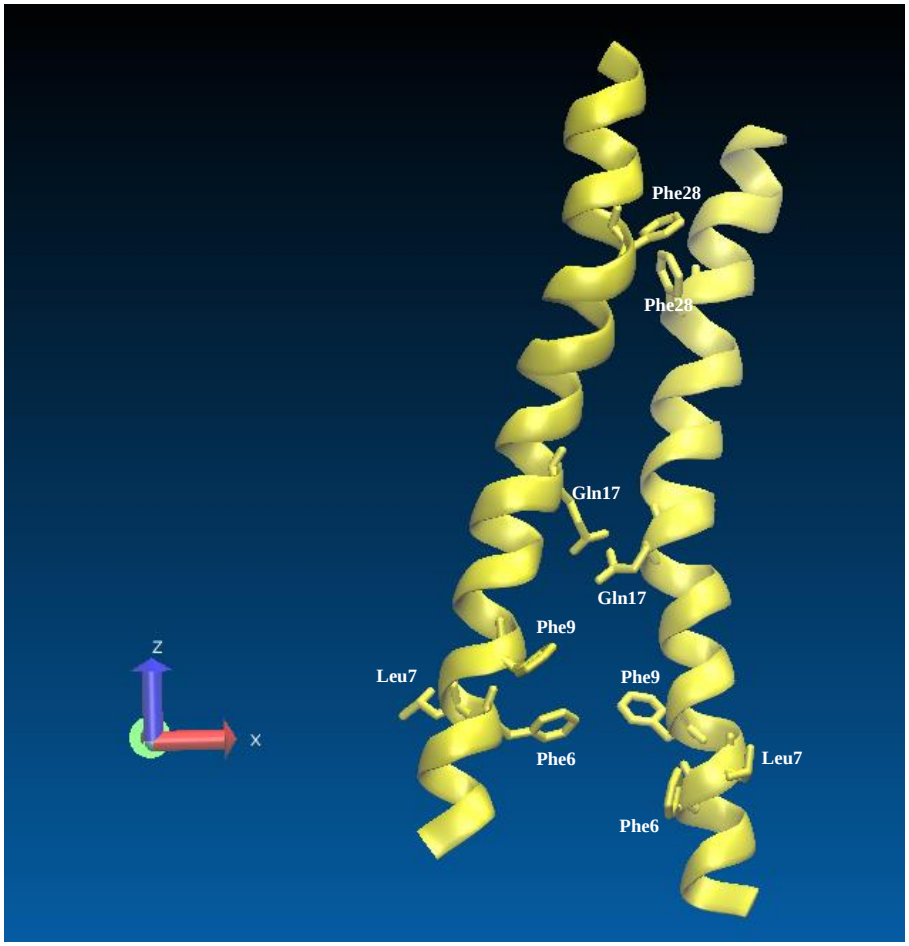

Fig. 5.3.9 A snapshot of the Gō-model of the E5 dimer. Constraints are τ angle of 10 ∼ 15 °and the Gln17 - Gln17 interaction.

5.4 Interaction of E5 and PDGFβR

Introduction

The platelet-derived growth factor receptor (PDGFR) protein located in the cell membrane consists of two subunits α, β and is responsible for multiple cellular processes. The oncogenic peptide E5 is encoded by bovine papillomavirus and can self-dimerize in the membrane and bind to the transmembrane segment of the PDGFβR protein with high affinity, inducing the cellular signaling in a ligand-free manner.

The E5 / PDGFβR complex is stabilized by the electrostatic interactions between Thr513 in PDGFβR and Gln17 in E5, as well as Lys499 in PDGFβR and Asp33 in E5 [71], as shown in Fig. 4.5.1. In order to investigate these interactions, we substituted Thr513 of PDGFβR with a novel ^{19}F-label, referred to as so-called CF_3-Thr analogue (see section 4.1) and Lys499 with $^{15}N_2$-Lys. E5 was labeled with U-^{13}C, ^{15}N-Gln in position 17 or U-^{13}C, ^{15}N-Asp in position 33. With these labeled E5 and PDGFβR (summarized in Tab. 5.4.1), ^{15}N{^{13}C}REDOR experiments were performed to determine the intermolecular distance between PDGFβR Lys499 and E5 Asp33. ^{13}C{^{19}F}REDOR and ^{15}N{^{19}F}REDOR were applied for distance measurements between PDGFβR Thr513 and E5 Gln17.

As illustrated in section 5.3, Gln17 plays an important role in the E5 dimerization, but might turn away from its interaction partner within the E5 dimer in the presence of PDGFβR to interact with Thr513 of PDGFβR. Thus, a CODEX experiment was performed with E5 Gln17 mixed with unlabelled PDGFβR, when compared with the CODEX results of only E5 Gln17, interactions between E5 and PDGFβR could be revealed.

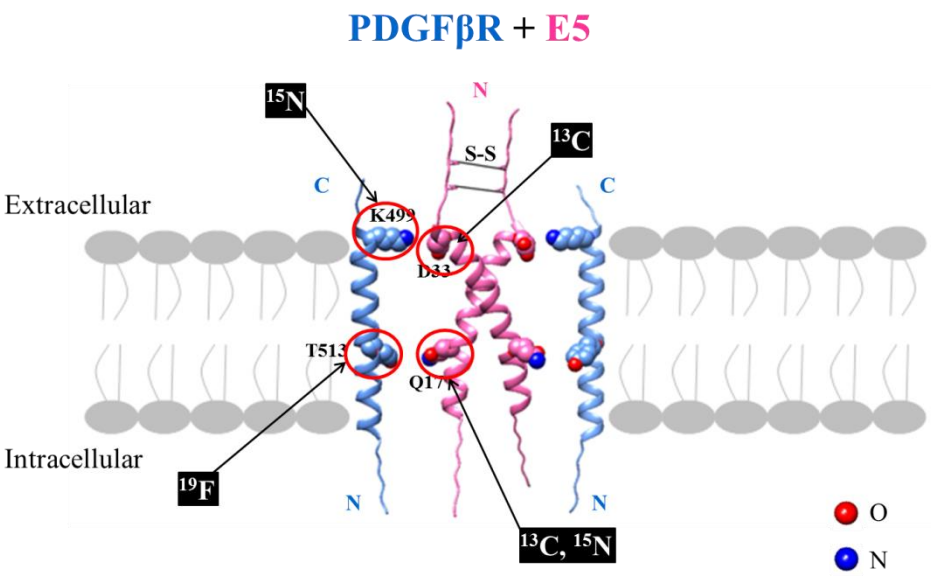

Fig. 5.4.1 Illustration of oncogenic peptide E5 and PDGFβR complex. The two postulated interactions between them are the electrostatic interaction between PDGFβR Lys499 and E5 Asp33, and hydrogen bound between PDGFβR Thr513 and E5 Gln17.

Tab. 5.4.1 Synthesized PDGFβR analogues.

Name	**Sequence**	**Molar mass [g/mol]**
E5 U-Q17$_a$	MPNLWFLLFLGLVAAM-U-**Gln**-LLLLLFLLLFFLVYWDHFE	4408
E5 U-D33	MPNLWFLLFLGLVAAMQLLLLLFLLLFFLVYW-U-**Asp**-HFE	4405
PDGFβR T513-CF_3	GHSLPFKVVVISAILALVVL-**CF_3-Thr**-IISLIILIMLWQKKPRYE	4496
PDGFβR K499	GHSLPF-**$^{15}N_2$-Lys**-VVVISAILALVVLTIISLIILIMLWQKKPRYE	4403
PDGFβR ^{15}N-L520$_b$	GHSLPFKVVVISAILALVVLTIISLII-**^{15}N-Leu**-IMLWQKKPRYE	4397

'U-': ^{15}N, ^{13}C uniformly labeled

'a': purchased from master student Violette Schneider

'b': purchased from Dirk W. in our group, for peptide orientation test before REDOR experiments

Results and discussion

o Peptide orientation within the membrane

Like E5 (see Fig. 5.3.5), the peptide orientation of PDGFβR within the membrane was also checked for the effect of temperature, since the REDOR experiments should be performed at -10 ℃ to reduce the peptide mobility. The peptide PDGFβR with a ^{15}N-label in position 520 was obtained from Dirk Windisch in our group; it was then embedded in oriented DErPC bilayers and measured at 30 ° and -20 °. As shown in Fig. 5.4.2, the peptide stayed in a transmembrane orientation (around 200 ppm) after the sample was frozen, which means, the peptide is tolerant to lower temperature and can be analyzed using REDOR experiments on frozen samples.

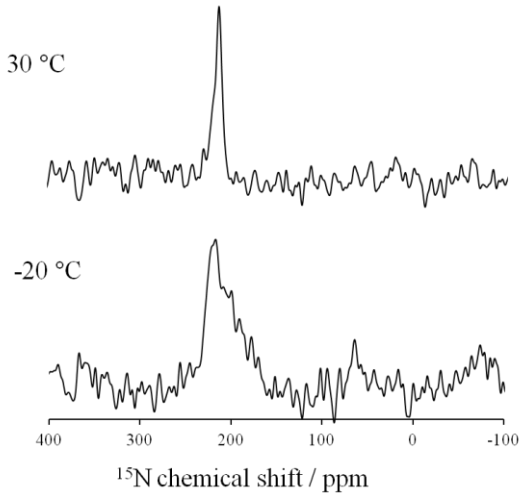

Fig. 5.4.2 ^{15}N-NMR spectra of PDGFβR ^{15}N-L520 embedded in oriented DErPC membrane at 30 ℃ and -20 ℃. Each spectrum was obtained with 12 h (over 15000 scans).

o ^{15}N{^{13}C}-REDOR experiments

As shown in Fig. 5.4.3, the Asp33 in E5 was uniformly labeled with ^{15}N and ^{13}C, and the Lys499 in PDGFβR was labeled with two ^{15}N, just like in the case of the stress-response peptide TisB (section 5.2). Hence, the sel-REDOR with a 180 ° Gaussian pulse as filter was applied to selectively determine the intermolecular distance of ^{15}N - ^{13}C=O between E5 and PDGFβR. ^{15}N was chosen as observed nucleus for the reason that the ^{13}C=O signal was too broad and may probably be overlapped by the high natural abundance signal of the lipids.

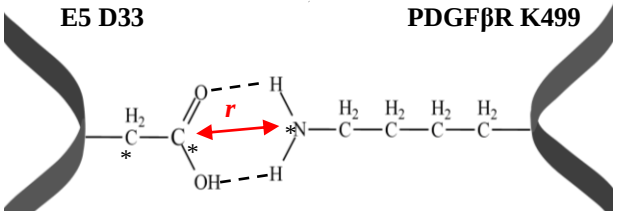

Fig. 5.4.3 Schematic illustration of ^{15}N-^{13}C intermolecular distance measurements between E5 D33 and PDGFβR K499. '*' indicates isotropic labeling.

The normal ^{15}N-spectrum (Fig. 5.4.4A) was firstly obtained. The right line denotes the amine-^{15}N from the side chain of Lys499, and the left one from the backbone amide. The sel-REDOR experiments were performed with two dephasing time, namely 10 ms, 20 ms. Measurements with longer dephasing times were impossible due to the limit imposed by the T_2-relaxation time. As shown in Fig. 5.4.4B, after 20 ms dephasing time, no obvious dephasing could be obtained in spectrum S, which means that the intermolecular distance of interest here is too long (> 6 Å) and exceeds the ability of the REDOR experiment.

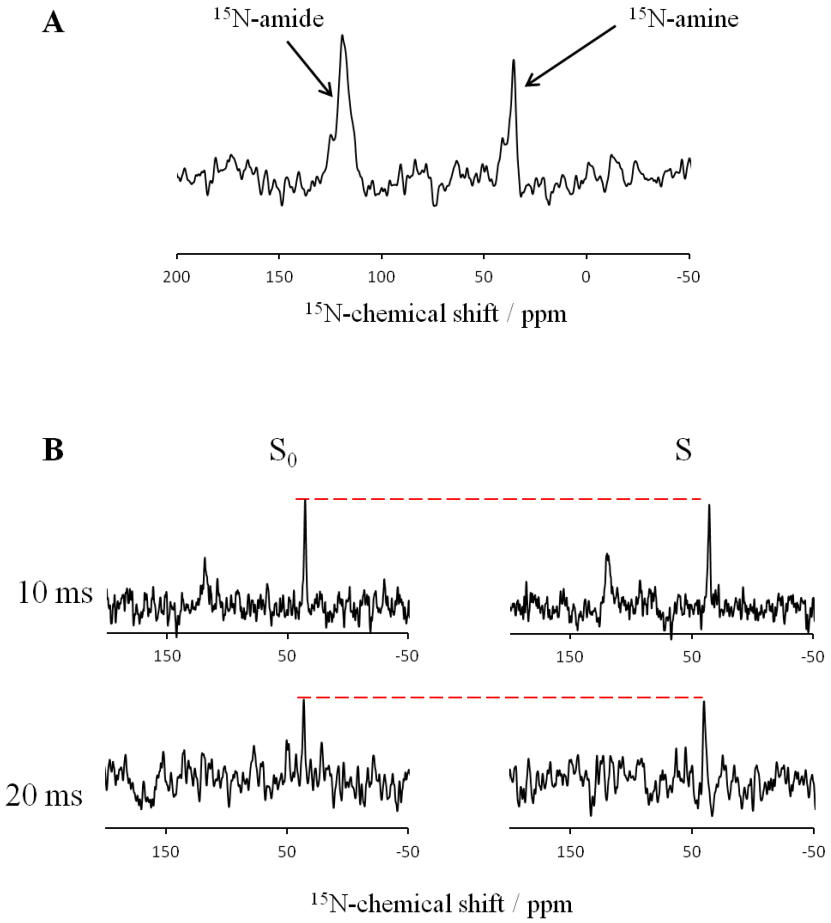

Fig. 5.4.4 Illustration of sel-REDOR experiments with E5 D33 and PDGFβR K499 in DErPC at -10 ℃, MAS = 8 kHz. (A) Normal ^{15}N-NMR spectrum with a contact time of 2ms, and 2000 transients. (B) Spectra S_0 and S

acquired by sel-REDOR experiments each with 7000 transients (12 h). Two different dephasing times, 10 ms and 20 ms, were applied. No dephasing in S spectra was obtained. 50 kHz ^{1}H-decoupling was applied. The transmitter of ^{15}N was then set to near the amine-^{15}N peak, and that of ^{13}C on the ^{13}C=O line around 170 ppm.

- **^{13}C{^{19}F}-REDOR experiments**

The second contact of E5 and PDGFβR is thought to be formed by the hydrogen bond between E5 Gln17 and PDGFβR Thr523. The novel ^{19}F-label was utilized in position Gln17 of E5, as ^{19}F is beneficial to obtain long-range distances because of its high-gama, however is limited by a short T_2-relaxation time.^{13}Cwas therefore chosen as the observed nucleus for the REDOR experiments. As shown in Fig. 5.4.5A, Gln was uniformly labeled with ^{13}C and ^{15}N, and ^{13}C signals are gut resolved, except for ^{13}C=O (Fig. 5.4.5B). Thus the intermolecular distance between C_γ and ^{19}F of the CF_3-Thr analogue label is of large interest for our ^{13}C{^{19}F}-REDOR experiments.

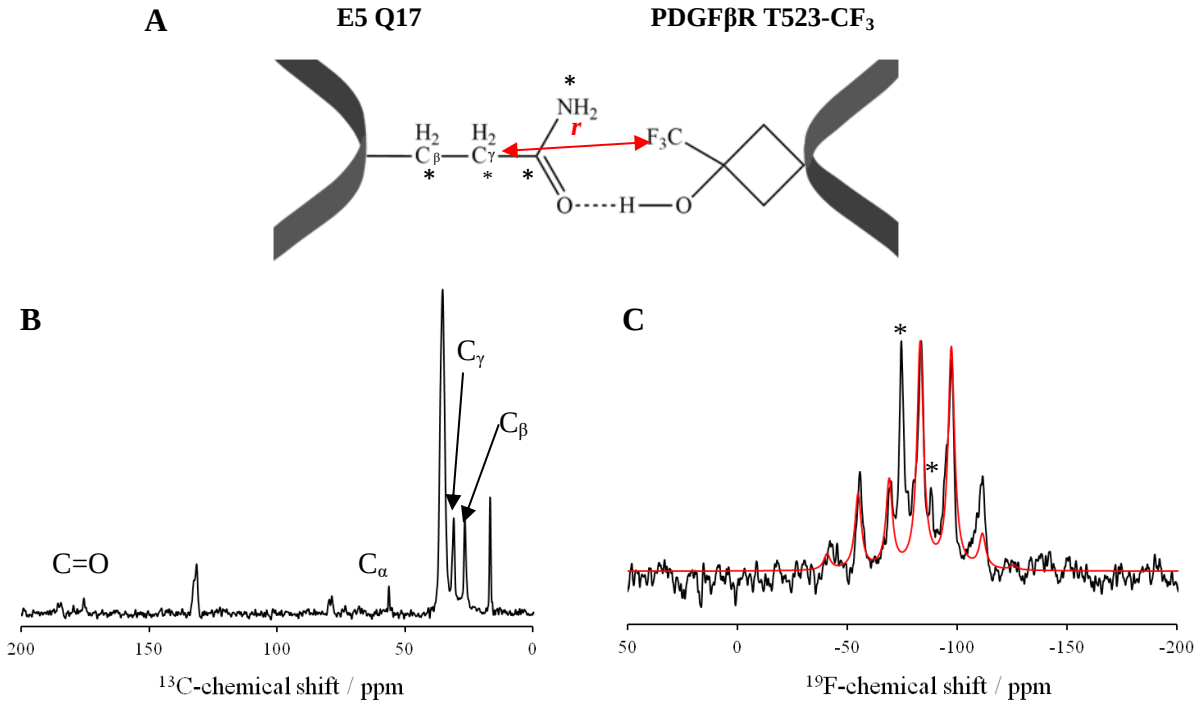

Fig. 5.4.5 (A) Schematic illustration of the ^{13}C-^{19}F intermolecular distance measurements between E5 Gln17 and PDGFβR Thr523; (B) Normal ^{13}C-NMR spectrum obtained by CP-ramp with contact time 200 μs at -20 ℃, MAS = 8 kHz; (C) 1-pulse ^{19}F-NMR spectrum (black) obtained at -20 ℃ with MAS = 8 kHz. The two peaks indicated by '*' refer to an impurity of TFA. The lineshape simulation (red) was done without TFA component.

The normal ^{13}C-NMR spectrum (Fig. 5.4.5B) obtained using CP-ramp with a contact time 200 μs and the one-pulse ^{19}F-NMR spectrum (Fig. 5.4.5C) were measured at -20 ℃ with MAS =

8 kHz. The chemical shifts of ^{13}C from Gln could be identified with the help of the BMRB database [151], they are $^{13}C_\alpha$ = 56 ppm, $^{13}C_\beta$ = 29 ppm, $^{13}C_\gamma$ = 33 ppm, ^{13}C=O = 176 ppm. In the ^{19}F-NMR spectrum, two components were observed, and one of them around -76 ppm is probably TFA, which is indicated by '*'. The lineshape simulation was then conducted ignoring the two peaks of TFA and is shown in red in Fig. 5.4.5. The CSA tensor elements obtained from the simulation are:

σ_{11} = -44.5 ppm

σ_{22} = -101 ppm

σ_{33} = -105 ppm

σ_{iso} = -83.5 ppm

The REDOR experiments were then performed. As shown in Fig. 5.4.6, the spectra S_0 and S were acquired with dephasing times of 15 ms, 20 ms and 25 ms. A dephasing (ca. 20%) of the $^{13}C_\gamma$ signal was observable in spectrum S with 25 ms dephasing time, indicating a close contact in these positions between E5 and PDGFβR. However, due to the limit imposed by a short T_2-relaxation time, further measurements were not possible. The intermolecular distance between E5 Q17 and PDGFβR T513 can be estimated to be in the range of 11 ~ 13.5 Å (Fig. 5.4.6B).

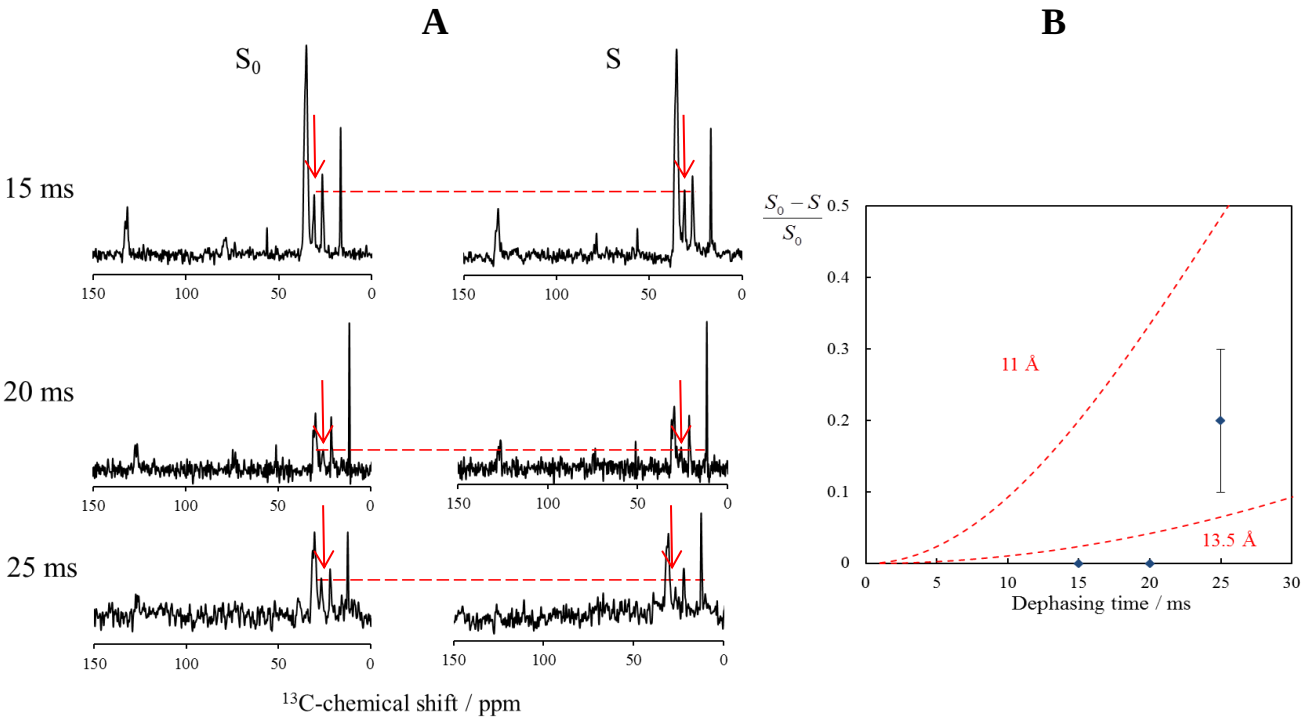

Fig. 5.4.6 (A) Spectra S_0 and S acquired by $^{13}C\{^{19}F\}$-REDOR experiments with E5 Q17 and PDGFβR T513 reconstructed in DErPC vesicles at -20 ℃. MAS = 8 kHz. Each spectrum was obtained with 7000 transients (12 h). Three different dephasing times, 15 ms, 20 ms and 25 ms, were applied. The ^{13}C transmitter was set near 33 ppm and ^{15}N at 83 ppm. (B) Data analysis of REDOR experiments, the inter-residual distance between E5 Q17 and PDGFRβR T513 is in the range of 11 ～ 13.5 Å.

○ $^{15}N\{^{19}F\}$-REDOR experiments

The REDOR experiments with ^{15}N as observed channel faced an important problem, which is shown in the normal ^{15}N-NMR spectrum in Fig. 5.4.7. The two ^{15}N signals resulting from the side chain amine and the backbone amide cannot be separated. The amine-^{15}N was expected to be much sharper than the amide-^{15}N as shown in Fig. 5.2.11 in the case of TisB, however, according the chemical shifts provided by the BMRB database [151], the sharper peak on the left (-119 ppm) corresponds to the amide-^{15}N, and the right peak (-111 ppm) is the amine-^{15}N. Thus, which signal was the amine-^{15}N of interest was uncertain.

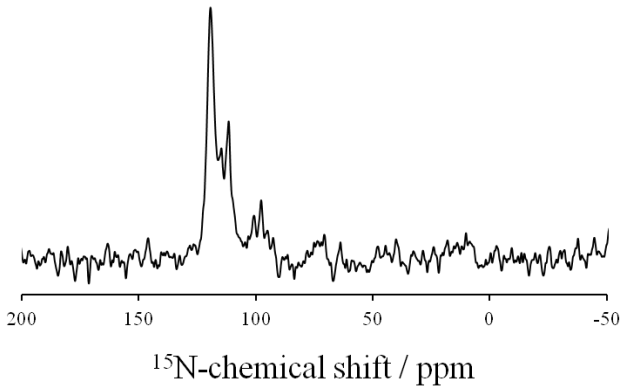

Fig. 5.4.7 ^{15}N-NMR spectrum of E5 Q17 and PDGFβR T513 reconstructed in DErPC vesicles at -20 ℃ with MAS = 8 kHz.

Since the backbone-^{15}N probably has a shorter relaxation time due to the rigidity of the backbone, the peak of amide-^{15}N would disappear soon after several ms dephasing time. Nonetheless, the $^{15}N\{^{19}F\}$-REDOR experiments were anyhow performed with dephasing times of 5 ms and 10 ms. As shown in Fig. 5.4.8, after 5 ms dephasing time, the right peak (-111 ppm) disappeared, indicating that the left sharp peak (-119 ppm) is most probably the amine-^{15}N of interest. However, after 10 ms, the signals were too weak to be distinguished from the noises, and no dephasing could be obtained. Further measurements with long dephasing times were impossible.

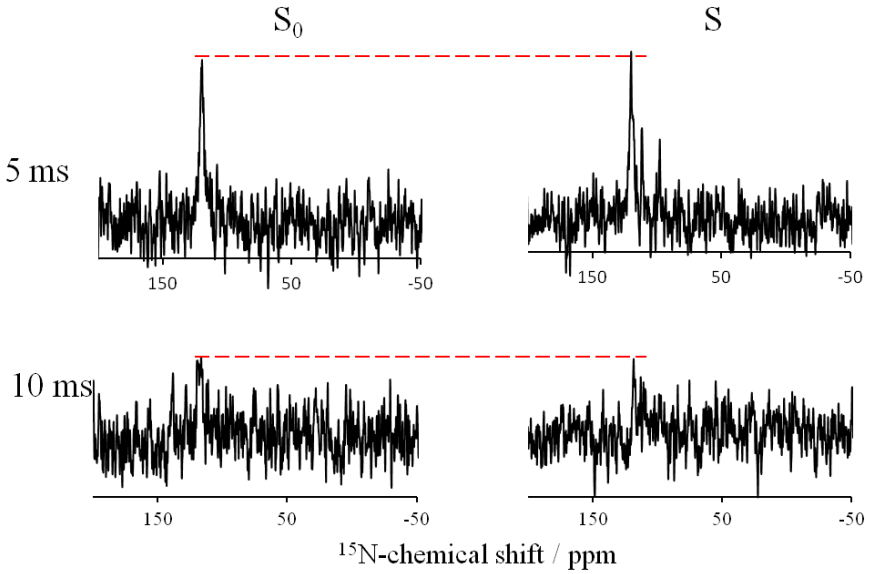

Fig. 5.4.8 Spectra S_0 and S acquired by $^{15}N\{^{19}F\}$-REDOR experiments with E5 Q17 and PDGFβR T513 reconstituted in DErPC vesicles at -20 ℃. MAS = 8 kHz. Two different dephasing times were applied, they are 5 ms, 10 ms. No dephasing in spectra S was obtained. Each spectrum was obtained with 9000 scans.

- **CODEX experiments**

A CODEX experiment with single ^{19}F-labeled E5 Q17 (Tab. 5.3.1) and unlabeled PDGFβR was performed under the same conditions as described in section 5.3. As shown in Fig. 5.4.9, the CODEX curve of only E5 Q17 shows a decay, indicating an inter-helical contact in this position, whereas in the presence of PDGFβR, no signal reduction was observed, demonstrating an interaction between E5 and PDGFβR. Hence, the interaction of PDGFβR Thr513 and E5 Gln17 drives Gln17 far away from each other, so that the Gln17 – Gln17 dipolar coupling decreases.

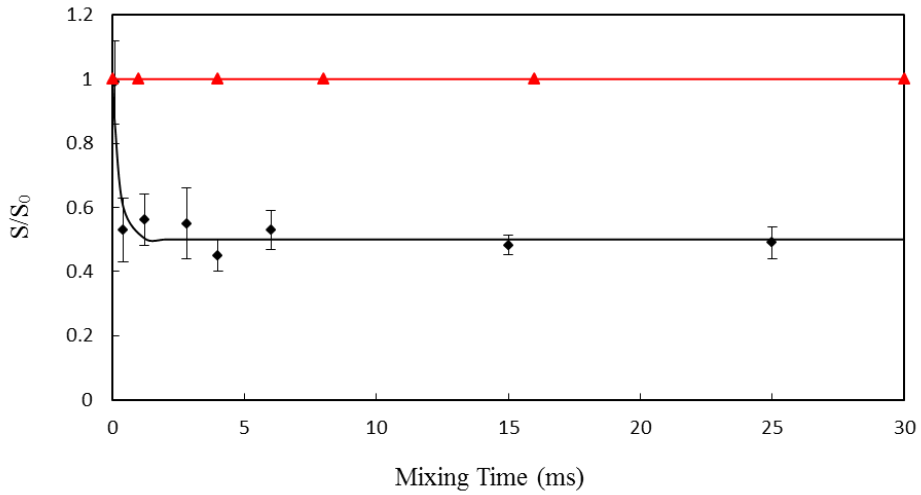

Fig. 5.4.9 ^{19}F CODEX of E5 Q17 (black) and E5 Q17 / wt PDGFβR (red) mixture embedded in DErPC vesicles measured at 243 K and with MAS = 25 kHz.

Conclusion

A complex of the oncogenic peptide E5 and membrane receptor protein PDGFβR was proposed to be initiated by two interactions with high affinity. Asp33 of E5 was suggested to interact with Lys499 of PDGFβR, and Gln17 of E5 with Thr513 of PDGFβR. These positions were investigated here with ^{13}C, ^{15}N, ^{19}F labels using a MAS approach consisting of the REDOR experiment, which is able to reveal the internuclear distances. Because of the limiting relaxation time, ^{19}F was usually employed as the dephasing channel. The E5 and PDGFβR mixtures were embedded in DErPC vesicles and measured at -20 ℃, where the peptides were frozen within the lipid matrix and molecular mobility leading to weakening of the observed dipolar coupling could be eliminated. After all the REDOR distance measurements between ^{15}N-^{13}C (PDGFβR Lys499 - E5 Asp33), ^{15}N-^{19}F (E5 Gln17 - PDGFβR Thr513), ^{13}C-^{19}F (E5 Gln17 - PDGFβR Thr513), a dephasing of about 20% was observable after 25 ms dephasing time between ^{13}C-^{19}F (Fig. 5.4.6). Though, measurements with longer dephasing times were not possible due to the limiting relaxation time, and a precise distance was not detectable, these experiments constitute the first direct evidence of a E5 – PDGFβR interaction by solid-state NMR distance measurements. According to Fig. 5.4.6B, the distance between E5 Gln17 - PDGFβR Thr513 can be estimated in the range of 11 ～ 13.5 Å. Moreover, this interaction between E5 Q17 and PDGFβR T513 could be further confirmed by a CODEX experiment (Fig. 5.4.9).

6. Conclusion

Strengths and weaknesses of the used methods for distance measurements

6.1 Why using solid-state NMR to study proteins?

There are plenty of powerful instrumental techniques to study proteins. Circular dichroism (CD) is valuable for the rapid determination of the protein secondary structure, however, suffers from lack of structural details [152, 153]. An alternative to study the peptide secondary structure is Fourier-Transform Infrared (FTIR) spectroscopy, which can excite characteristic resonances (such as amide, $-NH_2$ of Lys, His-ring and so on) by infrared light [154]. Fluorescence spectroscopy is capable to detect the protein conformational changes by tracing its natural fluorophores (such as tyrosine, tryptophan residues) or external fluorophores on specific sites [155]. The 3D structure of proteins at atomic level can be fully solved by X-ray crystallography, for which high quality crystals are required, and some systems of interest such as membrane proteins may present a great challenge, as these proteins assemble to specific conformations only upon binding to membranes [156]. Thus NMR technologies become an indispensable tool for structural studies of proteins in all kinds of environments such as fluid, soft and solid. Solution NMR is able to determine the dynamic structure of membrane proteins in solutions with the help of micelles and detergents, however, it is always limited by the size of the proteins [157-161].

Solid-state NMR is therefore an outstanding tool to study such system of membrane proteins by not only determining the complete structure of small proteins [162] but also addressing the local structural details in large proteins, such as precise measurements of distances within 15 Å between selectively labeled native sites, which can help addressing subtle conformational changes induced by specific protein-protein or protein-ligand interactions within membranes and thus to provide answers to their functions or disease-related factors [163].

6.2 Distance measurement methods

There are three broadly used technologies for distance measurements in protein studies; they are FRET, EPR and solid-state NMR. Fluorescence Resonance Energy Transfer (FRET) describes a process, by which the proteins are fused to donors and acceptors separately, and energy transfers in a non-radiative way from the excited donor fluorophore to the acceptor. Due to its sensitivity to donor-acceptor distances, FRET has been used to study protein-protein or protein-ligand interactions by measuring the intermolecular distances on nanometer scales or distance changes [164]. However, the introduction of a bulky fluorophore leads to conformational changes which should not be neglected. Electron paramagnetic resonance (EPR) spectroscopy, whose basic concept is similar to NMR (instead of the spin of nuclei, electron spin is excited), is excellent to measure 10 ～80 Å distances in large protein complexes using site-specific spin labels, although the labeling position is usually limited to be cysteine [165]. Solid-state NMR, which is studied in this work, provides a versatile tool to gain distance constraints on angstrom scales employing isotope labels (e.g., ^{2}H, ^{15}N, ^{13}C, ^{19}F) without compromising the structure and biological functions, and get insight into protein oligomerisation interactions.

A large variety of methods for distance measurements employing solid-state NMR has been developed in the last decades. These methods can be divided into two groups according to their basic concept:

(1) Utilizing homo-or hetero dipolar couplings, which are distance-dependent $\sim 1/r^3$ (see eq. 2.2), such as CPMG (Car-Purcell-Meiboom-Gill) [102, 103, 108-110], REDOR (Rotational-Echo DOuble-Resonance) [107, 114-118, 166, 167], SFAM (Simultaneous Frequency and Amplitude Modulation) [144-146], TEDOR (Transferred-Echo DOouble-Resonance) [168, 169], REAPDOR (Rotational-Echo Adiabatic-Passage Double-Resonance), R^2 (Rotational Resonance) [170, 171]. Among these methods, only CPMG employs oriented samples. It consists of a train of 180 °-pulses, as shown in Fig. 2.7, after these pulses, all the interactions but homonuclear dipolar coupling will be suppressed. All the other approaches employ magic angle spinning (MAS), during which all the interactions will be averaged out, and ‘recoupling’ technologies are used to reintroduce the dipolar couplings. The capability of these methods to measure long-range distances depends on the gyromagnetic ratio of the isotopic labels involved, and the upper distance limits corresponding to a weak dipolar coupling of 30 Hz are listed in Tab. 6.1. The longest distance up to 17.5 Å can be obtained by ^{19}F, just after ^{1}H. Note that such 30 Hz coupling is challenging to be detected, the actual longest measurable distances may probably not reach these values, as practically several

factors should be taken into consideration, such as the signal to noise (S/N) ratio, or the T_2-relaxation time.

Tab. 6.1 Measurable distances (Å) depending on dipolar couplings

	Proton (^{1}H)	Fluorine (^{19}F)	Carbon (^{13}C)	Deuterium (^{2}H)	Nitrogen (^{15}N)
Proton (^{1}H)	18.1	17.8	11.4	9.7	8.6
Fluorine (^{19}F)		17.5	11.3	9.5	8.3
Carbon (^{13}C)			7.2	6.16	5.4
Deuterium (^{2}H)				5.2	4.6
Nitrogen (^{15}N)					4

Interatomic distances listed are corresponding to a weak dipolar coupling of 30 Hz. Such weak dipolar couplings are difficult to be obtained, depending on several factors, including signal to noise ratio and the relaxation time T_2.

(2) Utilizing spin diffusion, which can demonstrate the oligomer states and also the interatomic distances, such as PDSD (Proton-Driven Spin Diffusion) [172, 173], CRDSD (Cross-Relaxation-Driven Spin Diffusion) [174], DARR (Dipolar Assisted Rotational Resonance) [175, 176], PMPT (Proton-Mediated Proton Transfer) [177], CODEX (Centerband-Only Detection of Exchange) [104]. The spin diffusion describes a process that the magnetisation exchanges between two chemically equivalent but orientationally inequivalent spins. The efficiency of this process is strongly depended on the dipolar coupling strength $D^2 \sim 1/r^6$, thus can be used for distance measurements.

6.3 Why do we use CPMG, REDOR and CODEX?

The membrane protein systems of interest in this thesis were antimicrobial peptide PGLa [30-46], the stress-response peptide TisB [52, 53, 59-62], the bovine papillomavirus E5 protein [63-71] and the membrane receptor protein PDGFβR [74-84], which are all supposed to dimerize to perform their specific functions or processes. Based on the reported structural information, distance measurements were performed to determine the distances between selective spins within these proteins, this way providing direct evidence for the dimerization and precise distance constraints for the further establishment of structural models.

The peptide PGLa has been broadly studied in terms of its biological function and structure, it therefore served as a test model in this study for the CPMG experiment and ^{19}F-labels. The CPMG experiment is of large interest, as it is a unique approach to study membrane-associated proteins in a quasi-native environment like a fluid-phase bilayer [102, 103, 108-110], and it is ideally suitable for homo-dimer studies with a simple label. Compared to other time consuming distance approaches, CPMG is time saving (several hours to two days for one qualified spectrum). The protein can be embedded in oriented lipid bilayers and measured statically above the lipid phase transition temperature, where the membrane mobility and peptide motion are maintained. We have revealed a long-range intramolecular distance of $\sim$ 11 Å in fluid membrane utilising the CPMG approach with ^{19}F-Phg labels [103]. Until now, it is the longest distance obtained in fluid membranes. Thus, for investigations of protein interactions within native membranes, CPMG presents an outstanding candidate. And in this study, the ability of monofluoro- and CF_3-reporters as NMR-labels to gain long-range distances were compared and evaluated.

The MAS technology has been widely used for protein studies, as it averages the chemical shift anisotropy (CSA) and all the dipolar couplings in a simple way by spinning the sample at the magic angle 54.7 °. Interesting for distance measurements is either the homo- or the heteronuclear dipolar coupling, which need to be reintroduced. With the R^2 approach, the dipolar coupling could be recovered when the MAS frequency (ω_r) and the difference of the isotropic chemical shifts ($\Delta\sigma_{iso}$) are fulfilling the relationship: $\Delta\sigma_{iso} = n\omega_r$ [170, 171], which is difficult for ^{19}F-lables. Thus, R^2 has been extensively used to measure distances $\sim$ 6 Å between two ^{13}C nuclei, since there are wide choses of ^{13}C-labels. Due to the small gyromagnetic ratio, there is barely a chance to detect distances between two ^{15}N nuclei (see Tab. 6.1). Consideration why we did not choose R^2 is: (1) it gives extremely weak signals as a result of the small number labels (simple ^{13}C-label pairs) within the big protein imbedded in membranes, and the protein used is always only 2 $\sim$ 4 mg; (2) it suffers from the natural abundance background of ^{13}C in the lipids, with which the ^{13}C signals of interest are probably covered or obscured; (3) for R^2 two chemically inequivalent ^{13}C-labels are acquired which a chemical shift difference of suitable size to match the spinning speed. In contrast to R^2, most other dipolar-based distance technologies restore heteronuclear dipolar couplings. The REDOR experiment, firstly introduced in 1989 [178], has been widely used for distance measurements between different spins, such as ^{15}N-^{13}C [114], ^{31}P-^{19}F [116], ^{2}H-^{19}F [117], ^{13}C-^{19}F [119], ^{15}N-^{19}F [121]. It involves a train of rotor-synchronized 180 ° pulses on the I-

spin (S/I system, S-spin to be monitored), which can prevent the heteronuclear dipolar coupling averaging by MAS. As an extension, TEDOR has been developed for systems, which involve more S-spins due to natural abundance but only one I-spin (S-spins are more isolated than coupled), as it applies a coherence transfer technology before detecting signals only from coupled S-spins. However, it is always limited by T_2 of both of S-and I-spin [168]. Similarly, SFAM, derived from REDOR with simultaneous frequency modulation on the I-spin, is reported to be more efficient for weak dipolar coupling detections at higher spinning speed [145]. Principally, REDOR is an excellent approach for measuring distances between two spins of 1/2, but if one quadrupolar nucleus is involved (such as ^{2}H-X), it becomes complicated due to the quadrupolar interaction. The REAPDOR has been developed especially for spin-1/2 and quadrupole spin pairs [170]. Nevertheless, REDOR has been successfully performed between spin pairs with ^{2}H as dephasing channel, such as ^{2}H-^{13}C [179], ^{2}H-^{19}F [117]. As discussed above, REDOR is a versatile experiment adaptable for measuring almost all the types of heteronuclear dipolar couplings. For the studied TisB model (with proposed four salt bridges between Asp - Lys and one hydrogen bond between the central Gln), E5/PDGFβR (with one salt bridge between Asp - Lys and one hydrogen bond between Thr - Gln), this versatility of the REDOR experiment found to be very useful with ^{13}C, ^{15}N and ^{19}F labels. Considering for example the used selective version of REDOR, SFAM was performed on test substances to verify its recoupling efficiency for weak dipolar coupling compared with REDOR. And we found that, SFAM showed higher recoupling efficiency with shorter distance (Fig. 5.2.4), whereas REDOR seems to be able to cope with weak dipolar coupling better (Fig. 5.2.5).

Based on the concept that spin diffusion is proportional to the square of the dipolar coupling, various methods for measuring cross correlations have been developed, such as PDSD [172, 173], CRDSD [174], DARR [175, 176], PMPT [177], which possess identical pulse sequence differing only in the mixing element for spin diffusion. These approaches are mostly applied for structural determination with uniformly or multiply ^{13}C- or ^{15}N-labeled proteins by detecting inter-residual cross peaks. The observable long-range distance limit for PDSD is about $\sim$ 7 Å for ^{13}C/^{13}C and $\sim$ 4 Å for ^{15}N/^{15}N, whereas CRDSD and PMPT are more efficient for spin diffusion across longer distances (e.g., > 6.5 Å for ^{15}N/^{15}N) [173]. The CODEX experiment is firstly introduced by Klaus Schmidt-Rohr as a 1-dimentional version of these 2-dimentional correlation experiments [111] . It has been adapted to measure the oligomeric state by M-Hong. Spin diffusion happens here between two chemically equivalent

but orientationally inequivalent ^{19}F-spins close in space. It can reveal not only the oligomer state but also the precise distances between two selectively labeled sites [104], and it is an idea method for studies of homo-dimers with the same type of label. The oncogenic protein E5 of interest in this study is a small protein consisting of 44 aa and proposed to dimerize by hydrophobic packing and salt bridges. The REDOR experiment was well suitable for such a system with a single ^{19}F-reporter to reveal oligomeric state and determine distances in the dimer interface.

6.4 Evaluation of distance approaches used in this study

Three distance approaches, CPMG, REDOR and CODEX, were utilized in this study. They are based on different physical principles, and therefore possess complementary advantages and weakness. CPMG reveals a spectrum of dipolar couplings, hence a doublet can be read from the spectrum and converted into a distance readily. It is compatible with oriented bilayers as it does not rely on magic angle spinning, and can be applied to fluid membranes, as immobilisation of the molecules is not required. REDOR is a robust technique employing MAS, and measures the dipolar coupling between unlike spins, which opens up the opportunity to combine different labels and renders this experiment very versatile. The CODEX experiment, finally, uses spin diffusion and allows to measure the oligomeric state. As it is based on a very different approach, it provides an alternative where other techniques might fail. It however, requires molecular motion to be immobilized, hence membranes cannot be studied in the fluid phase. Both CPMG and CODEX are homonuclear experiments, which even rely or benefit from chemically equivalent labels. Hence they are well suited for the study of homo-dimers with a single label in each monomer.

As a first step to get insight into the performance of the applied distance measurement methods, the ability of the CPMG experiment to detect long-range distances $\sim$ 11 Å within fluid membranes has been verified using 4F-Phg and CF_3-Phg. The monofluoro-label was found to perform better than the triad of the CF_3-group. Note, that the distances in the test models were are all intramolecular distances, and the inter-molecular distance measurements in the biological applications with the CPMG approach were challenged by two factors:

(1)If the proteins or peptides form a monomer/dimer mixture, there are isolated and coupled ^{19}F-labels coexisting, and the doublet of the CPMG spectrum resulting from the coupled ^{19}F-labels can be obscured or covered by the single line from isolated labels. As

shown in Fig. 5.2.18, the CPMG spectrum (Fig. 5.2.18a) of TisB labeled with ^{19}F-labeled Gln analogues showed a single peak without splitting, because monomer or powder components occurred (Fig. 5.2.15). However, after cross-polarisation (CP) had been incorporated into the CPMG sequence, which can filter the signal of flexible ^{19}F-labels in monomers, a small doublet emerged (Fig. 5.2.15b).

(2) If the formed dimers have inhomogeneous structures, or consist of a dimer-monomer equilibrium, the inter-helical distances of interest are not a single or an averaged value but distributed over a range which gives rise to broad lines consisting of a distribution of couplings in the CPMG spectrum. Such broadening has been observed in the case of the oncogenic protein E5 (Fig. 5.3.2).

Nevertheless, the CPMG experiment is an attractive distance approach, as it needs only a simple ^{19}F-label incorporated in peptides / proteins, and the ^{19}F-^{19}F homonuclear dipolar couplings could be recoupled by a train of $180°$ pulses without MAS technique or ^{1}H-decoupling, which means that, CPMG is technically much easier to apply and requires less measurement time compared to most other distance approaches. Furthermore, CPMG allows to obtain structural parameters in fluid membranes under physical conditions, as oriented sample is required and measured without freezing the sample, which is usually required for most MAS techniques. As shown in Fig. 5.1.6, a long-range distances $\sim$ 11 Å can be revealed with the CPMG experiments even in presence of high molecular mobility, which is always challenged with most other distance approaches. Thus, the CPMG experiment is a potential candidate for studies of interactions within native membranes, and the systems with homogeneous dimers and uniform inter-residue distances are particularly suitable.

The REDOR experiments have been performed in this study on the systems of TisB, and E5/PDGFβR, utilizing ^{13}C-, ^{15}N-, ^{19}F-labels. Thus, REDOR is a versatile experiment adaptable for measuring almost all types of heteronuclear dipolar couplings with wide choices of isotope labels. The advantages need to be balanced against the disadvantages according to the following considerations:

(1) The ^{13}C, ^{15}N-labeled amino acids available commercially are often not selectively labeled, but mostly uniformly labeled, and for the resulting multispin systems, the REDOR curves are much more complex [180]. Thus, it is beneficial to prepare an isolated 2-spin system. For this aim, ^{15}N of the side chain was chosen in this study as observed, and ^{13}C=O as dephasing nucleus using a selective REDOR sequence. There were three considerations: (a) ^{15}N occurs at most twice, in the backbone or sidechain, and the ^{15}N-^{15}N homonuclear dipolar

coupling is very weak and can be neglected. (b) ^{13}C is abundant everywhere, in the uniformly labeled side chain, and as natural abundance of the lipids and peptides, thus the ^{13}C peaks assignment and removal of 'rotational resonance' effects are difficult. (c) The ^{13}C nuclei, chosen as dephasing spins, can be selectively radiated by a Gaussian pulse in the middle of the ^{15}N channel, as shown in Fig. 5.2.6. In this study, ^{13}C=O of the side chain (Asp) was selected. The ^{13}C=O of the backbone is far away from the ^{15}N of the opposite helix, thus does not contribute to the dipolar coupling.

(2) Due to the small gyromagnetic ratio, ^{15}N-^{13}C REDOR has a distance limit of ca. 5 Å (see Tab. 6.1), and in practice, it could be even shorter. Thus, it is profitable to introduce a ^{19}F-label, as it can increase the distance range significantly to ∼ 11 Å (^{13}C-^{19}F) or ∼ 8 Å (^{15}N-^{19}F). As described in section 5.4 for E5/PDGFβR, three kinds of REDOR experiments were performed, they are $^{15}N\{^{13}C\}$, $^{15}N\{^{19}F\}$, $^{13}C\{^{19}F\}$, but only a small dephasing of 20% at 25 ms dephasing time could be observed with $^{13}C\{^{19}F\}$REDOR, indicating that the distance of interest is in the range of 11 ∼ 13.5 Å (Fig. 5.4.6). The increase of the distance range by ^{19}F hence proved to be crucial.

(3) The REDOR experiments are limited by the T_2-relaxation time of the observed nucleus. As described above (Fig. 5.4.6), a small dephasing was observed at 25 ms, and further measurements were impossible due to the limiting T_2 relaxation time of ^{15}N. Thus for long-range distances, REDOR is impractical and time consuming.

(4) The dipolar couplings of the intermolecular distances of interest are very weak and any peptide motion would weaken the coupling further. Thus, it is necessary to freeze or cool the sample, such that the lipid membrane is in the gel-state, and the peptides are may be immobilized in the lipid matrix. Note, that the peptides should not aggregate by upon freezing and the low temperature can lead to broader lines and a shorter T_2-relaxation time.

(5) Note, that the REDOR experiment is very sensitive to imperfections of the 180 °pulses, instability of the MAS rate and B_1-field inhomogeneities. SFAM has been reported to be more tolerant to these problems [144]. As described in section 5.2, SFAM was more efficient in recoupling the dipolar coupling, but at long dephasing times (weak dipolar couplings), there was no significant difference between SFAM and REDOR. Considering that we wanted to measure weak dipolar couplings in biological samples, and the continuous pulses on the I-channel of SFAM with a further sel-Gaussian pulse on the S-channel may probably impose a high stress on the hardware, REDOR was more suitable.

CODEX is a suitable approach to observe the oligomer state and also determine accurate intermolecular distances. For this experiment, the sample needs to be frozen to get rid of all the molecular motions leaving only spin diffusion contributing to the dephasing of the CODEX curves. In this study, the E5 system was checked with an extra ^{15}N-label before the CODEX measurements to assure that the peptide does not aggregate or change its alignment upon freezing. The ^{15}N-NMR spectra at 30 ℃ and -20 ℃ indicated that E5 maintained the transmembrane state even when it was frozen (as shown in Fig. 5.4.2). Generally, the CODEX experiment faces following technical challenges:

(1) The long pulse sequence including long mixing time leads to attenuated magnetisation, thus ^{19}F-labels are more recommended than other nuclei. However, ^{19}F has shorter T_2-relaxation times, and signal with long mixing times is difficult to be obtained.

(2) The calibration of the parameter $F(0)$ with a test substance is necessary, since $F(0)$ could be significantly different when the ^{19}F-reporter is attached to aromatic (Tryptophan, Phenylalanine) or aliphatic (Alanine, Glycine) amino acids.

(3) With lower MAS speed, more material can be utilized (for a lager rotor, e.g., 4 mm rotor, up to 4 mg protein can be filled, P / L = 1/50) to gain strong signals but only at the expense of spinning sidebands. With lower S/N ratio, the integration of the sidebands is difficult or even impossible. With higher MAS speed sidebands can be avoided, however, higher MAS speeds are challenged by the weak signals resulting from less materials (e.g., for 2.5 mm rotor, maximal 1 mg peptide, P / L = 1/50).

In general, the three typical distance approaches based on solid-state NMR were successfully used for different peptide / protein systems and their performance was evaluated. CPMG is proved to be an excellent static experiment for measuring ^{19}F-^{19}F homonuclear dipolar couplings within fluid membranes. Technically important is that no MAS or ^{1}H-decoupling is required. Note, that systems with homogeneous dimers are preferred for the CPMG experiments. REDOR is a representative of MAS techniques to recouple heteronuclear dipolar couplings, which can be adaptive for all types of peptide / protein systems with wide choices of isotope labels (e.g., ^{13}C, ^{15}N, ^{19}F, ^{2}H, ^{31}P), although it has a distance limit (Tab. 6.1) and is challenged by short T_2-relaxation times. Note, that a frozen sample is beneficial for REDOR experiments. CODEX is the first approach that can reveal not only the inter-helical distance but also the oligomeric state, even for systems, which consist of no universal dimers and where thus the CMPG experiment fails. Like REDOR, CODEX needs MAS and frozen

samples, however, with recommended ^{19}F-labels, CODEX can reveal longer distances than REDOR.

Altogether, the used experiments were offering complementary approaches for distance measurements, addressing different experimental issues of the biological applications. CPMG proved the only experiment to work for fluid membranes, but had difficulties in the case of the studied E5 and TisB dimers when a small amount of monomers obscured the dipolar coupling readout. In this case, CODEX was still able to reveal the oligomeric state and to yield distance estimates as shown for E5, as it is based on amplitude measurements rather than on a resolved splitting. The heteronuclear nature of the REDOR method proved very useful to address distances in the hetero-molecular mixture of E5 and PDGFβR. But also in homo-dimers REDOR became applicable using special labeling schemes and a selective experiment version. Hence, this thesis provides a toolbox for distance measurements of oligomeric assemblies in lipid bilayers, addressing the different requirements related studies of biomembranes.

References

1. Singer, S.J. and G.L. Nicolson, Fluid mosaic model of structure of cell-membranes, *Science*, **1972**, 175(4023): p. 720-731.
2. https://www.boundless.com/biology/textbooks/boundless-biology-textbook/biological-macromolecules-3/lipids-55/phospholipids-300-11433/
3. Sachs, J.N. and D.M. Engelman, Introduction to the membrane protein reviews: The interplay of structure, dynamics, and environment in membrane protein function, *Annual Review of Biochemistry*, **2006**, p. 707-712.
4. Engel, A. and H.E. Gaub, Structure and mechanics of membrane proteins, *Annual Review of Biochemistry*, **2008**, p. 127-148.
5. Cymer, F., G. von Heijne, and S.H. White, Mechanisms of integral membrane protein insertion and folding, *Journal of Molecular Biology*, **2015**, 427(5): p. 999-1022.
6. Hong, H., Role of Lipids in Folding, Misfolding and function of integral membrane proteins, *Lipids in Protein Misfolding*, **2015**, p. 1-31.
7. Ward, C.W. and M.C. Lawrence, Ligand-induced activation of the insulin receptor: a multi-step process involving structural changes in both the ligand and the receptor, *Bioessays*, **2009**, 31(4): p. 422-434.
8. Rydzak, J., A.M. Kmiecik, and E. Jaskiewicz, Human erythrocyte glycophorin C as the receptor for EBA-140 Plasmodium falciparum merozoite ligand, *Postepy Higieny I Medycyny Doswiadczalnej*, **2013**, 67: p. 1331-1339.
9. Hannibal, L., et al., Alternative conformations of cytochrome c: structure, function, and detection, *Biochemistry*, **2016**, 55(3): p. 407-428.
10. Overington, J.P., B. Al-Lazikani, and A.L. Hopkins, Opinion - How many drug targets are there? *Nature Reviews Drug Discovery*, **2006**, 5(12): p. 993-996.
11. Raman, P., Cherezov, V., Caffrey, M.,The Membrane Protein Data Bank, *Cell Mol. Life Sci*, **2006**, 63: 36-51
12. https://www.en.wikipedia.org/wiki/Membrane_protein
13. Goodsell, D.S. and A.J. Olson, Structural symmetry and protein function, *Annual Review of Biophysics and Biomolecular Structure*, **2000**, 29: p. 105-153.

14. Marianayagam, N.J., M. Sunde, and J.M. Matthews, The power of two: protein dimerization in biology, *Trends in Biochemical Sciences*, **2004**, 29(11): p. 618-625.

15. Cascio, M., Structure and function of the glycine receptor and related nicotinicoid receptors, *Journal of Biological Chemistry*, **2004**, 279(19): p. 19383-19386.

16. Gordon, Y.J., E.G. Romanowski, and A.M. McDermott, A review of antimicrobial peptides and their therapeutic potential as anti-infective drugs, *Current Eye Research*, **2005**, 30(7): p. 505-515.

17. Gilman, A.G., G-Poteins - Transducers of receptor-generated signals, *Annual Review of Biochemistry*, **1987**, 56: p. 615-649.

18. Ali, M.H. and B. Imperiali, Protein oligomerization: How and why, *Bioorganic & Medicinal Chemistry*, **2005**, 13(17): p. 5013-5020.

19. Hashimoto, K. and A.R. Panchenko, Mechanisms of protein oligomerization, the critical role of insertions and deletions in maintaining different oligomeric states, *Proceedings of the National Academy of Sciences of the United States of America*, **2010**, 107(47): p. 20352-20357.

20. Giovanni Gotte and Massimo Libonati (**2014**). Protein Oligomerization, Oligomerization of Chemical and Biological Compounds, Dr. Claire Lesieur (Ed.), ISBN: 978-953-51-1617-2, InTech, DOI: 10.5772/57489. Available from: http://www.intechopen.com/books/oligomerization-of-chemical-and-biological-compounds/protein-oligomerization

21. Jones, S. and J.M. Thornton, Principles of protein-protein interactions, *Proceedings of the National Academy of Sciences of the United States of America*, **1996**, 93(1): p. 13-20.

22. French, G.L., The continuing crisis in antibiotic resistance, *International Journal of Antimicrobial Agents*, **2010**, 36: p. S3-S7.

23. Hancock, R.E.W., *Peptide antibiotics. Lancet*, **1997**, 349(9049): p. 418-422.

24. Andreu, D. and L. Rivas, Animal antimicrobial peptides: An overview, *Biopolymers*, **1998**, 47(6): p. 415-433.

25. van 't Hof, W., et al., Antimicrobial peptides: Properties and applicability, *Biological Chemistry*, **2001**, 382(4): p. 597-619.

26. Zasloff, M., MAGAININS, A class of antimicrobial peptides from Xenopus skin - isolation, characterization of 2 active forms, and partial cdna Sequence of a precursor, *Proceedings of the National Academy of Sciences of the United States of America*, **1987**, 84(15): p. 5449-5453.

27. Conlon, J.M. and M. Mechkarska, Host-defense peptides with therapeutic potential from skin secretions of frogs from the family pipidae, *Pharmaceuticals (Basel, Switzerland)*, **2014**, 7(1): p. 58-77.

28. Maloy, W.L. and U.P. Kari, Structure-activity studies on magainins and other host-defense peptides, *Biopolymers*, **1995**, 37(2): p. 105-122.

29. Lohner, K. and F. Prossnigg, Biological activity and structural aspects of PGLa interaction with membrane mimetic systems, *Biochimica Et Biophysica Acta-Biomembranes*, **2009**, 1788(8): p. 1656-1666.

30. Bechinger, B., M. Zasloff, and S.J. Opella, Structure and dynamics of the antibiotic peptide PGLa in membranes by solution and solid-state nuclear magnetic resonance spectroscopy, *Biophysical Journal*, **1998**, 74(2): p. 981-987.

31. Glaser, R.W., et al., Orientation of the antimicrobial peptide PGLa in lipid membranes determined from ^{19}F-NMR dipolar couplings of 4-CF_3-phenylglycine labels, *Journal of Magnetic Resonance*, **2004**, 168(1): p. 153-163.

32. Glaser, R.W., et al., Concentration-dependent realignment of the antimicrobial peptide PGLa in lipid membranes observed by solid-state ^{19}F-NMR, *Biophysical Journal*, **2005**, 88(5): p. 3392-3397.

33. Strandberg, E., et al., Solid-state NMR analysis of the PGLa peptide orientation in DMPC bilayers: Structural fidelity of ^{2}H-labels versus high sensitivity of ^{19}F-NMR. *Biophysical Journal*, **2006**, 90(5): p. 1676-1686.

34. Strandberg, E., et al., Orientation and dynamics of peptides in membranes calculated from ^{2}H-NMR data, *Biophysical Journal*, **2009**, 96(8): p. 3223-3232.

35. Strandberg, E., et al., Influence of hydrophobic residues on the activity of the antimicrobial peptide magainin 2 and its synergy with PGLa, Journal of Peptide Science, **2015**, 21(5): p. 436-445.

36. Afonin, S., et al., Temperature-dependent transmembrane insertion of the amphiphilic peptide PGLa in lipid bilayers; observed by solid-state ^{19}F-NMR spectroscopy, *Journal of the American Chemical Society*, **2008**, 130(49): p. 16512-16514.

37. Huang, H.W., Action of antimicrobial peptides: Two-state model, *Biochemistry*, **2000**, 39(29): p. 8347-8352.

38. Shai, Y., Mechanism of the binding, insertion and destabilization of phospholipid bilayer membranes by alpha-helical antimicrobial and cell non-selective membrane-lytic peptides, *Biochimica Et Biophysica Acta-Biomembranes*, **1999**, 1462(1-2): p. 55-70.

39. Epand, R.M. and H.J. Vogel, Diversity of antimicrobial peptides and their mechanisms of action, *Biochimica Et Biophysica Acta-Biomembranes*, **1999**, 1462(1-2): p. 11-28.

40. Brogden, K.A., Antimicrobial peptides: Pore formers or metabolic inhibitors in bacteria? *Nature Reviews Microbiology*, **2005**, 3(3): p. 238-250.

41. Oren, Z. and Y. Shai, Mode of action of linear amphipathic alpha-helical antimicrobial peptides, *Biopolymers*, **1998**, 47(6): p. 451-463.

42. Berditsch, M., et al., Antimicrobial peptides can enhance the risk of persistent infections, *Frontiers in Immunology*, **2012**, 3.

43. Bigger, J.W., Treatment of staphylococcal infections with penicillin by intermittent sterilisation, *Lancet*, **1944**, 247(6320): p. 497-500.

44. Lewis, K., Persister cells, dormancy and infectious disease, *Nature Reviews Microbiology*, **2007**, 5(1): p. 48-56.

45. Dawson, C.C., C. Intapa, and M.A. Jabra-Rizk, "Persisters": Survival at the cellular level, *Plos Pathogens*, **2011**, 7(7).

46. Lewis, K., Persister Cells, *Annual Review of Microbiology*, **2010**, 64, p. 357-372.

47. Doerr, T., M. Vulic, and K. Lewis, Ciprofloxacin causes persister formation by inducing the TisB toxin in Escherichia coli, *Plos Biology*, **2010**, 8(2).

48. Unoson, C. and E.G.H. Wagner, A small SOS-induced toxin is targeted against the inner membrane in Escherichia coli, *Molecular Microbiology*, **2008**, 70(1): p. 258-270.

49. Fozo, E.M., M.R. Hemm, and G. Storz, Small toxic proteins and the antisense RNAs that repress them, *Microbiology and Molecular Biology Reviews*, **2008**, 72(4): p. 579-589.

50. Van Melderen, L. and M.S. De Bast, Bacterial toxin-antitoxin systems: more than selfish entities? *Plos Genetics*, **2009**, 5(3).

51. Blower, T.R., et al., A processed noncoding RNA regulates an altruistic bacterial antiviral system, *Nature Structural & Molecular Biology*, **2011**, 18(2): p. 185-U246.

52. Labrie, S.J., J.E. Samson, and S. Moineau, Bacteriophage resistance mechanisms, *Nature Reviews Microbiology*, **2010**, 8(5): p. 317-327.

53. Fernandez de Henestrosa, A.R., et al., Identification of additional genes belonging to the LexA regulon in Escherichia coli, *Molecular Microbiology*, **2000**, 35(6): p. 1560-1572.

54. Yamaguchi, Y., J.-H. Park, and M. Inouye, Toxin-antitoxin systems in bacteria and archaea, *Annual Review Genetics*, **2011**, 45, p. 61-79.

55. Wagner, E.G.H. and C. Unoson, The toxin-antitoxin system tisB-istR1 expression, regulation and biological role in persister phenotypes, *Rna Biology*, **2012**, 9(12): p. 1513-1519.

56. Vogel, J., et al., The small RNA IstR inhibits synthesis of an SOS-induced toxic peptide, *Current Biology*, **2004**, 14(24): p. 2271-2276.

57. Steinbrecher, T., et al., Peptide-lipid interactions of the stress-response peptide TisB that induces bacterial persistence, *Biophysical Journal*, **2012**, 103(7): p. 1460-1469.

58. Surti, T., et al., Structural models of the bovine papillomavirus E5 protein, *Proteins-Structure Function and Genetics*, **1998**, 33(4): p. 601-612.

59. Nasir, L. and M.S. Campo, Bovine papillomaviruses: their role in the aetiology of cutaneous tumours of bovids and equids, *Veterinary Dermatology*, **2008**, 19(5): p. 243-254.

60. Baker, C.C. and P.M. Howley, Differential promoter utilization by the bovine papillomavirus in transformed-cells and productively infected wart tissues, *Embo Journal*, **1987**, 6(4): p. 1027-1035.

61. Petti, L., L.A. Nilson, and D. Dimaio, Activation of the platelet-derived growth-factor receptor by the bovine papillomavirus-E5 transforming protein, *Embo Journal*, **1991**, 10(4): p. 845-855.

62. Schiller, J.T., et al., E5 open reading frame of bovine papillomavirus type-1 encodes a transforming gene, *Journal of Virology*, **1986**, 57(1): p. 1-6.

63. Burkhardt, A., D. Dimaio, and R. Schlegel, Genetic and biochemical definition of the Bovine Papillomavirus E5 transforming protein, *Embo Journal*, **1987**, 6(8): p. 2381-2385.

64. Settleman, J., et al., Genetic-Evidence That acute morphologic transformation, induction of cellular DNA-synthesis, and focus formation are mediated by a single activity of the bovine papillomavirus-E5 protein, *Molecular and Cellular Biology*, **1989**, 9(12): p. 5563-5572.

65. Nilson, L.A. and D. Dimaio, Platelet-derived growth-factor receptor can mediate tumorigenic transformation by the bovine papillomavirus E5 protein, *Molecular and Cellular Biology*, **1993**, 13(7): p. 4137-4145.

66. Petti, L. and D. Dimaio, Stable association between the bovine papillomavirus-E5 transforming protein and activated platelet-derived growth-factor receptor in transformed mouse cells, *Proceedings of the National Academy of Sciences of the United States of America*, **1992**, 89(15): p. 6736-6740.

67. Venuti, A., et al., Papillomavirus E5: the smallest oncoprotein with many functions, *Molecular Cancer*, **2011**, 10.

68. Burkhardt, A., et al., The E5-oncoprotein of bovine papillomavirus is oriented asymmetrically in golgi and plasma-membranes, *Virology*, **1989**, 170(1): p. 334-339.

69. Windisch, D., et al., Structural role of the conserved cysteines in the dimerization of the viral transmembrane oncoprotein E5, *Biophysical Journal*, **2010**, 99(6): p. 1764-1772.

70. DiMaio, D. and D. Mattoon, Mechanisms of cell transformation by papillomavirus E5 proteins, *Oncogene*, **2001**, 20(54): p. 7866-7873.

71. Oates, J., et al., In vitro dimerization of the bovine papillomavirus E5 protein transmembrane domain, *Biochemistry*, **2008**, 47(34): p. 8985-8992.

72. de Planque, M.R.R. and J.A. Killian, Protein-lipid interactions studied with designed transmembrane peptides: role of hydrophobic matching and interfacial anchoring (Review), *Molecular Membrane Biology*, **2003**, 20(4): p. 271-284.

73. Heldin, C.H. and B. Westermark, Mechanism of action and in vivo role of platelet-derived growth factor, *Physiological Reviews*, **1999**, 79(4): p. 1283-1316.

74. Betsholtz, C., et al., CDNA sequence and chromosomal localization of human platelet-derived growth-factor a-chain and its expression in tumor-cell lines, *Nature*, **1986**, 320(6064): p. 695-699.

75. LaRochelle, W.J., et al., PDGFD, a new protease-activated growth factor, *Nature Cell Biology*, **2001**, 3(5): p. 517-521.

76. Demoulin, J.-B. and A. Essaghir, PDGF receptor signaling networks in normal and cancer cells, *Cytokine & Growth Factor Reviews*, **2014**, 25(3): p. 273-283.

77. Heldin, C.H. and B. Westermark, Platelet-derived growth-factor - 3 isoforms and 2 receptor types, *Trends in Genetics*, **1989**, 5(4): p. 108-111.

78. Yarden, Y., et al., Structure of the receptor for platelet-derived growth-factor helps define a family of closely related growth-factor receptors, *Nature*, **1986**, 323(6085): p. 226-232.

79. Hubbard, S.R., Structural analysis of receptor tyrosine kinases, *Progress in Biophysics & Molecular Biology*, **1999**, 71(3-4): p. 343-358.

80. Muhle-Goll, C., et al., Hydrophobic matching controls the tilt and stability of the dimeric platelet-derived growth factor receptor (PDGFR) beta transmembrane segment, *Journal of Biological Chemistry*, **2012**, 287(31): p. 26178-26186.

81. Goldstein, D.J., et al., A glutamine residue in the membrane-associating domain of the bovine papillomavirus type-1 E5 oncoprotein mediates its binding to a transmembrane component of the vacuolar H^+-Atpase, *Journal of Virology*, 1992, 66(1): p. 405-413.

82. Klein, O., et al., Role of glutamine 17 of the bovine papillomavirus E5 protein in platelet-derived growth factor beta receptor activation and cell transformation, *Journal of Virology*, **1998**, 72(11): p. 8921-8932.

83. Smith, B.J., SDS Polyacrylamide gel electrophoresis of proteins, *Methods in molecular biology (Clifton, N.J.)*, **1984**, 1: p. 41-55.

84. Ilari, A. and C. Savino, Protein structure determination by x-ray crystallography, *Methods in Molecular Biology:Data, Sequence Analysis And Evolution*, **2008**, 1, p. 63-87.

85. Wuthrich, K., The way to NMR structures of proteins, *Nature Structural Biology*, **2001**, 8(11): p. 923-925.

86. Modesti, M., Fluorescent labeling of proteins, *Single Molecule Analysis: Methods and Protocols*, **2011**, p. 101-120.

87. Verardi, R., et al., Isotope labeling for solution and solid-state NMR spectroscopy of membrane proteins, *Isotope Labeling in Biomolecular NMR*, **2012**, p. 35-62.

88. Strandberg, E. and A.S. Ulrich, NMR methods for studying membrane-active antimicrobial peptides, *Concepts in Magnetic Resonance Part A*, **2004**, 23A(2): p. 89-120.

89. Chan, Y.-H.M. and S.G. Boxer, Model membrane systems and their applications, *Current Opinion in Chemical Biology*, **2007**, 11(6): p. 581-587.

90. Eeman, M. and M. Deleu, From biological membranes to biomimetic model membranes, *Biotechnologie Agronomie Societe Et Environnement*, **2010**, 14(4): p. 719-736.

91. https://www.en.wikipedia.org/wiki/Biological_membrane

92. Durr, U.H.N., L. Waskell, and A. Ramamoorthy, The cytochromes P450 and b(5) and their reductases - Promising targets for structural studies by advanced solid-state NMR spectroscopy, *Biochimica Et Biophysica Acta-Biomembranes*, **2007**, 1768(12): p. 3235-3259.

93. M. Levitt, Spin Dynamics: Basics of Nuclear Magnetic Resonance, *Wiley*, Chichester, **2001**.

94. Grage, S.L., et al., Solid-state ^{19}F-NMR Analysis of ^{19}F-Labeled Tryptophan in Gramicidin A in oriented membranes, *Biophysical Journal*, **2002**, 83(6): p. 3336-3350.

95. Tkachenko, A.N., et al., Design, synthesis, and application of a trifluoromethylated phenylalanine analogue as a label to Study peptides by solid-state ^{19}F-NMR Spectroscopy, *Angewandte Chemie-International Edition*, **2013**, 52(25): p. 6504-6507.

96. Tkachenko, A.N., et al., A ^{19}F-NMR label to substitute polar amino acids in peptides: a CF_3-substituted analogue of Serine and Threonine, *Angewandte Chemie-International Edition*, **2013**, 52(5): p. 1486-1489.

97. Mykhailiuk, P.K., et al., Synthesis of trifluoromethyl-substituted proline analogues as ^{19}F NMR labels for peptides in the polyproline II conformation, *Angewandte Chemie-International Edition*, **2008**, 47(31): p. 5765-5767.

98. Mikhailiuk, P.K., et al., Conformationally rigid trifluoromethyl-substituted alpha-amino acid designed for peptide structure analysis by solid-state ^{19}F-NMR spectroscopy, *Angewandte Chemie-International Edition*, **2006**, 45(34): p. 5659-5661.

99. Afonin, S., et al., 4-Fluorophenylglycine as a label for ^{19}F-NMR structure analysis of membrane-associated peptides, *Chembiochem*, **2003**, 4(11): p. 1151-1163.

100. Grage, S.L., et al., Solid-state ^{19}F-NMR analysis of ^{19}F-labeled tryptophan in gramicidin A in oriented membranes, *Biophysical Journal*, **2002**, 83(6): p. 3336-3350.

101. http://www.ibg.kit.edu/nmr/26.php

102. Salgado, J., et al., Membrane-bound structure and alignment of the antimicrobial beta-sheet peptide gramicidin S derived from angular and distance constraints by solid state ^{19}F-NMR, *Journal of Biomolecular NMR*, **2001**, 21(3): p. 191-208.

103. Grage, S.L., et al., ^{19}F-labeling of peptides revealing long-range NMR distances in fluid membranes, *Journal of Physical Chemistry Letters*, **2014**, 5(24): p. 4256-4259.

104. Luo, W. and M. Hong, Determination of the oligomeric number and intermolecular distances of membrane protein assemblies by anisotropic ^{1}H-driven spin diffusion NMR spectroscopy, *Journal of the American Chemical Society*, **2006**, 128(22): p. 7242-7251.

105. Naito, A., et al., Intermolecular and intramolecular contributions of neighboring dipolar pairs to the precise determination of interatomic distances in a simple C^{13},N^{15} -Peptide By C^{13},N^{15}-REDOR NMR-Spectroscopy, *Chemical Physics Letter*s, **1994**, 229(4-5): p. 506-511.

106. Studelska, D.R., et al., Long-range distance measurements of protein binding sites by rotational-echo double-resonance NMR, *Journal of the American Chemical Society*, **1996**, 118(23): p. 5476-5477.

107. Louie, E.A., et al., Using solid-state $^{31}P\{^{19}F\}$ REDOR NMR to measure distances between a trifluoromethyl group and a phosphodiester in nucleic acids, *Journal of Magnetic Resonance*, **2006**, 178(1): p. 11-24.

108. Meiboom, S. and D. Gill, Modified Spin-Echo Method For Measuring Nuclear Relaxation Times, *Review of Scientific Instruments*, **1958**, 29(8): p. 688-691.

109. Grage, S.L. and A.S. Ulrich, Structural parameters from ^{19}F homonuclear dipolar couplings, obtained by multipulse solid-state NMR on static and oriented systems, *Journal of Magnetic Resonance*, **1999**, 138(1): p. 98-106.

110. Grage, S.L., et al., Solid state NMR analysis of the dipolar couplings within and between distant CF_3-groups in a membrane-bound peptide, *Journal of Magnetic Resonance*, **2006**, 183(1): p. 77-86.

111. deAzevedo, E.R., et al., Centerband-only detection of exchange: Efficient analysis of dynamics in solids by NMR, *Journal of the American Chemical Society*, **1999**, 121(36): p. 8411-8412.

112. Buffy, J.J., A.J. Waring, and M. Hong, Determination of peptide oligomerization in lipid bilayers using ^{19}F spin diffusion NMR, *Journal of the American Chemical Society*, **2005**, 127(12): p. 4477-4483.

113. Pan, Y., T. Gullion, and J. Schaefer, Determination of C-N Internuclear Distances By Rotational-Echo Double-Resonance NMR of solids, *Journal of Magnetic Resonance*, **1990**, 90(2): p. 330-340.

114. Naito, A., et al., Determination of the three-dimensional structure of a new crystalline form of N-acetyl-Pro-Gly-Phe as revealed by ^{13}C REDOR, X-ray diffraction, and molecular dynamics calculation, *Journal of Physical Chemistry*, **1996**, 100(36): p. 14995-15004.

115. Gullion, T., Introduction to rotational-echo, double-resonance NMR, *Concepts in Magnetic Resonance*, **1998**, 10(5): p. 277-289.

116. Merritt, M.E., S.T. Sigurdsson, and G.P. Drobny, Long-range distance measurements to the phosphodiester backbone of solid nucleic acids using ^{31}P-^{19}F REDOR NMR, *Journal of the American Chemical Society*, **1999**, 121(25): p. 6070-6071.

117. Grage, S.L., J.A. Watts, and A. Watts, $^{2}H\{^{19}F\}$ REDOR for distance measurements in biological solids using a double resonance spectrometer, *Journal of Magnetic Resonance*, **2004**, 166(1): p. 1-10.

118. Wi, S., N. Sinha, and M. Hong, Long-range ^{1}H-^{19}F distance measurement in peptides by solid-state NMR, *Journal of the American Chemical Society*, **2004**, 126(40): p. 12754-12755.

119. Antonioli, G. and P. Hodgkinson, Resolution of ^{13}C-^{19}F interactions in the ^{13}C NMR of spinning solids and liquid crystals, *Journal of Magnetic Resonance*, **2004**, 168(1): p. 124-131.

120. Mani, R., et al., Membrane-bound dimer structure of a beta-hairpin antimicrobial peptide from rotational-echo double-resonance solid-state NMR, *Biochemistry*, **2006**, 45(27): p. 8341-8349.

121. Kim, S.J., et al., Structures of Staphylococcus aureus cell-wall complexes with vancomycin, eremomycin, and chloroeremomycin derivatives by $^{13}C\{^{19}F\}$ and $^{15}N\{^{19}F\}$ rotational-echo double resonance, *Biochemistry*, **2006**, 45(16): p. 5235-5250.

122. Carpino, L.A. and G.Y. Han, 9-Fluorenylmethoxycarbonyl amino-protecting group, *Journal of Organic Chemistry*, **1972**, 37(22): p. 3404-&.

123. Luebke, M., M. Jung, and G. Haufe, New histone deacetylase inhibitors based on 4-fluoro-2-amino acid esters: Synthesis and activity, *Journal of Fluorine Chemistry*, **2013**, 152: p. 144-156.

124. Merrifield, R.B., Solid Phase Peptide Synthesis 1. Synthesis of a tetrapeptide, *Journal of the American Chemical Society*, **1963**, 85(14): p. 2149-2154.

125. Kates S. A., Albericio F.(ed.), Solid-Phase Synthesis, a practical guide, Marcel Dekker, Inc., **2000** (86/VK 5500 K19)

126. Hackenberger, C.P.R., The reduction of oxidized methionine residues in peptide thioesters with NH4I-Me2S, *Organic & Biomolecular Chemistry*, **2006**, 4(11): p. 2291-2295.

127. Benjamin Zimpfer, dissertation, Structur-und funktionsanalyse des membraneaktiven bakterientoxischen peptides TisB aus Escherichia coli, **2016**.

128. Drechsler, A. and F. Separovic, Solid-state NMR structure determination, *Iubmb Life*, **2003**, 55(9): p. 515-523.

129. Creuzet, F., et al., Determination Of Membrane-protein structure by rotational resonance NMR - Bacteriorhodopsin, *Science*, **1991**, 251(4995): p. 783-786.

130. Ulrich, A.S. and A. Watts, ^{2}H NMR lineshapes of immobilized uniaxially oriented membrane-proteins, *Solid State Nuclear Magnetic Resonance*, **1993**, 2(1-2): p. 21-36.

131. Glaser, R.W., et al., Structure analysis of a fusogenic peptide sequence from the sea urchin fertilization protein bindin, *Biochemistry*, **1999**, 38(8): p. 2560-2569.

132. Afonin, S., et al., 'Boomerang'-like insertion of a fusogenic peptide in a lipid membrane revealed by solid-state ^{19}F NMR, *Magnetic Resonance in Chemistry*, **2004**, 42(2): p. 195-203.

133. Ulrich, A.S., High Resolution Solid State NMR, ^{1}H, ^{19}F A2 - Lindon, John C, *Encyclopedia of Spectroscopy and Spectrometry*, **1999**, Elsevier: Oxford. p. 813-825.

134. Mykhailiuk, P.K., et al., An optimized protocol for the multigram synthesis of 3-(trifluoromethyl)bicyclo 1.1.1 pent-1-ylglycine (CF_3-Bpg), *Journal of Fluorine Chemistry*, **2010**, 131(2): p. 217-220.

135. Tkachenko, A.N., et al., Design and synthesis of a monofluoro-substituted aromatic amino acid as a conformationally restricted ^{19}F-NMR label for membrane-bound peptides, *European Journal of Organic Chemistry*, **2014**, 2014(17): p. 3584-3591.

136. Mikhailiuk, P.K., et al., Conformationally rigid trifluoromethyl-substituted α-amino acid designed for peptide structure analysis by solid-State ^{19}F-NMR spectroscopy, *Angewandte Chemie International Edition*, **2006**, 45(34): p. 5659-5661.

137. Tremouilhac, P., et al., Conditions affecting the re-alignment of the antimicrobial peptide PGLa in membranes as monitored by solid state ^{2}H-NMR, *Biochimica Et Biophysica Acta-Biomembranes*, **2006**, 1758(9): p. 1330-1342.

138. Salnikov, E.S. and B. Bechinger, Lipid-controlled peptide topology and interactions in bilayers: Structural insights into the synergistic enhancement of the antimicrobial activities of PGLa and Magainin 2, *Biophysical Journal*, **2011**, 100(6): p. 1473-1480.

139. Gangl, S., et al., Perturbation of membrane organization by the antimicrobial peptide PGLa, *Biophysical Journal*, **2000**, 78(1): p. 180A-180A.

140. Wieprecht, T., et al., Membrane binding and pore formation of the antibacterial peptide PGLa: Thermodynamic and mechanistic aspects, *Biochemistry*, **2000**, 39(2): p. 442-452.

141. Saronjini, B.K., et al., Redetermination of the crystal structure of N-acetyl glycine (2-acetamidoacetic acid), $C_4H_7NO_3$, *Zeitschrift Fur Kristallographie-New Crystal Structures*, **2013**, 228(2): p. 245-246.

142. Chaturvedi, S., K. Go, and R. Parthasarathy, A sequence preference for nucleation of alpha-Helix - crystal-structure of Gly-L-Ala-L-Val And Gly-L-Ala-L-Leu - Some comments on the geometry of Leucine zippers, *Biopolymers*, **1991**, 31(4): p. 397-407.

143. Levitt, M.H. and R. Freeman, Compensation for pulse imperfections in NMR spin-echo experiments, *Journal of Magnetic Resonance*, **1981**, 43(1): p. 65-80.

144. Nishimura, K., R.Q. Fu, and T.A. Cross, The effect of RF inhomogeneity on heteronuclear dipolar recoupling in solid state NMR: Practical performance of SFAM and REDOR, *Journal of Magnetic Resonance*, **2001**, 152(2): p. 227-233.

145. Fu, R.Q., S.A. Smith, and G. Bodenhausen, Recoupling of heteronuclear dipolar interactions in solid state magic-angle spinning NMR by simultaneous frequency and amplitude modulation, *Chemical Physics Letters*, **1997**, 272(5-6): p. 361-369.

146. Fu, R.Q., M. Cotten, and T.A. Cross, Inter- and intramolecular distance measurements by solid-state MAS NMR: Determination of gramicidin A channel dimer structure in hydrated phospholipid bilayers, *Journal of Biomolecular NMR*, **2000**, 16(3): p. 261-268.

147. Veshtort, M. and R.G. Griffin, High-performance selective excitation pulses for solid- and liquid-state NMR spectroscopy, *Chemphyschem*, **2004**, 5(6): p. 834-850.

148. Marsh, R.E., A Refinement Of The Crystal Structure Of Glycine, *Acta Crystallographica*, **1958**, 11(9): p. 654-663.

149. Strandberg, E., et al., Solid-state NMR analysis comparing the designer-made antibiotic MSI-103 with its parent peptide PGLa in lipid bilayers, *Biochemistry*, **2008**, 47(8): p. 2601-2616.

150. Duerr, U.H.N., et al., Solid state ^{19}F NMR parameters of fluorine-labeled amino acids. Part I: Aromatic substituents, *Journal of Magnetic Resonance*, **2008**, 191(1): p. 7-15.

151. http://www.bmrb.wisc.edu/

152. Greenfield, N.J., Using circular dichroism spectra to estimate protein secondary structure, *Nature Protocols*, **2006**, 1(6): p. 2876-2890.

153. Kelly, S.M., T.J. Jess, and N.C. Price, How to study proteins by circular dichroism, *Biochimica Et Biophysica Acta-Proteins and Proteomics*, **200**5, 1751(2): p. 119-139.

154. Barth, A., Infrared spectroscopy of proteins. *Biochimica Et Biophysica Acta-Bioenergetics*, **2007**, 1767(9): p. 1073-1101.

155. Munishkina, L.A. and A.L. Fink, Fluorescence as a method to reveal structures and membrane-interactions of amyloidogenic proteins, *Biochimica Et Biophysica Acta-Biomembranes*, **2007**, 1768(8): p. 1862-1885.

156. Smyth, M.S. and J.H.J. Martin, X-Ray crystallography, *Journal of Clinical Pathology-Molecular Pathology*, **2000**, 53(1): p. 8-14.

157. Wuethrich, K., Protein structure determination in solution by NMR spectroscopy, *Science (Washington D C)*, **1989**, 243(4887): p. 45-50.

158. Liang, B. and L.K. Tamm, Structure of outer membrane protein G by solution NMR spectroscopy, *Proceedings of the National Academy of Sciences of the United States of America*, **2007**, 104(41): p. 16140-16145.

159. Arora, A., Solution NMR spectroscopy for the determination of structures of membrane proteins in a lipid environment, *Methods in molecular biology (Clifton, N.J.)*, **2013**, 974: p. 389-413.

160. Jaishree, T.N., et al., Solution structure of ribosomal protein S17 by high resolution NMR spectroscopy, *Journal of Cellular Biochemistry Supplement*, **1995**, 0(21B): p. 59-59.

161. Lee, Y.C., et al., Three-dimensional solution structure of apo-S100P protein determined by NMR spectroscopy, *Biophysical Journal*, **2003**, 84(2): p. 174A-174A.

162. McDermott, A.E., Structural and dynamic studies of proteins by solid-state NMR spectroscopy: rapid movement forward, *Current Opinion in Structural Biology*, **2004**, 14(5): p. 554-561.

163. Thompson, L.K., Solid-state NMR studies of the structure and mechanisms of proteins, *Current Opinion in Structural Biology*, **2002**, 12(5): p. 661-669.

164. Wang, J.J., X.C. Chen, and D. Xing, Fluorescence resonance energy transfer assay: Applications in the study of protein-protein interaction, *Progress in Biochemistry and Biophysics*, **2003**, 30(6): p. 980-984.

165. Klug, C.S. and J.B. Feix, Methods and applications of site-directed spin Labeling EPR Spectroscopy, *Biophysical Tools for Biologists*, **2008**, 1, p. 617-658.

166. Karp, E.S., et al., The structural properties of the transmembrane segment of the integral membrane protein phospholamban utilizing ^{13}C CPMAS, ^{2}H, and REDOR solid-state NMR spectroscopy, *Biochimica Et Biophysica Acta-Biomembranes*, **2006**, 1758(6): p. 772-780.

167. Grage, S.L. and A. Watts, Applications of REDOR for distance measurements in biological solids, *Annual Reports on NMR Spectroscopy*, **2007**, 60, p. 191-228.

168. Fyfe, C.A., A.R. Lewis, and J.M. Chezeau, A comparison of NMR distance determinations in the solid state by cross polarization, REDOR, and TEDOR techniques, *Canadian Journal of Chemistry-Revue Canadienne De Chimie*, **1999**, 77(11): p. 1984-1993.

169. Jaroniec, C.P., C. Filip, and R.G. Griffin, 3D TEDOR NMR experiments for the simultaneous measurement of multiple carbon-nitrogen distances in uniformly ^{13}C, ^{15}N-labeled solids, *Journal of the American Chemical Society*, **2002**, 124(36): p. 10728-10742.

170. Peersen, O.B., et al., Analysis of rotational resonance magnetization exchange curves from crystalline peptides, *Journal of the American Chemical Society*, **1995**, 117(27): p. 7228-7237.

171. Smith, S.O., et al., Structure of the transmembrane dimer interface of glycophorin A in membrane bilayers, *Biochemistry*, **2001**, 40(22): p. 6553-6558.

172. Castellani, F., et al., Structure of a protein determined by solid-state magic-angle-spinning NMR spectroscopy, *Nature*, **2002**, 420(6911): p. 98-102.

173. Traaseth, N.J., T. Gopinath, and G. Veglia, On the performance of spin diffusion NMR techniques in oriented solids: prospects for resonance assignments and distance measurements from separated local field experiments, *Journal of Physical Chemistry B*, **2010**, 114(43): p. 13872-13880.

174. Xu, J., J. Struppe, and A. Ramamoorthy, Two-dimensional homonuclear chemical shift correlation established by the cross-relaxation driven spin diffusion in solids, *Journal of Chemical Physics*, **2008**, 128(5).

175. Ohashi, R. and K. Takegoshi, Asymmetric ^{13}C-^{13}C polarization transfer under dipolar-assisted rotational resonance in magic-angle spinning NMR, *Journal of Chemical Physics*, **2006**, 125(21).

176. Takegoshi, K., S. Nakamura, and T. Terao, ^{13}C-^{1}H dipolar-driven ^{13}C-^{13}C recoupling without ^{13}C rf irradiation in nuclear magnetic resonance of rotating solids, *Journal of Chemical Physics*, **2003**, 118(5): p. 2325-2341.

177. Nevzorov, A.A., Mismatched Hartmann-Hahn conditions cause proton-mediated intermolecular magnetization transfer between dilute low-spin nuclei in NMR of static solids, *Journal of the American Chemical Society*, **2008**, 130(34): p. 11282-11283.

178. Gullion, T. and J. Schaefer, Rotational-Echo Double-Resonance NMR, *Journal of Magnetic Resonance*, **1989**, 81(1): p. 196-200.

179. Hughes, E., et al., Internuclear distance determination of S=1, I=1/2 spin pairs using REAPDOR NMR, *Journal of Magnetic Resonance*, **2002**, 156(2): p. 230-241.

180. Goetz, J.M. and J. Schaefer, REDOR dephasing by multiple spins in the presence of molecular motion, *Journal of Magnetic Resonance*, **1997**, 127(2): p. 147-154.

Appendices

A. Chemicals

Name	Source
^{19}F-Gln analogue	Prof. Dr. G. Haufe, University Muenster, Germany
L-4F-Phg	Acivate Scientific GmbH, Prien, Germany
Acetonitril	Fisher Scientific GmbH, Schwerte, Germany
Ammoniumiodid	Sigma-Aldrich, Steinheim, Germany
Chloroform	Merk KcaA, Darmstadt, Germany
CF_3-Thr analogue	Sergiy Anfonin, Karlsruhe Institute of Technology, Germany
Diethylether	Merk KcaA, Darmstadt, Germany
DMF	Biosolve, Valkenswaard, Niederlande
DCM	Biosolve, Valkenswaard, Niederlande
DIC	Iris Biotech GmbH, Marktredwitz, Deutschland
DIPEA	Iris Biotech GmbH, Marktredwitz, Deutschland
Dichlormethan	Biosolve, Valkenswaard, Niederlande
D/L-CF_3-Phg	ABCR GmbH (Karlsruhe, Germany)
DErPC	Avanti Polar Lipids, Alabaster, USA
DMPC	Avanti Polar Lipids, Alabaster, USA
Fmoc-protected amino acids	Merck Schuchardt, Hohenbrunn, Germany
Fmoc-Cl	Novabiochem ®, Merck KgaA, Darmstadt, Germany
Fmoc-$^{13}C_4$, ^{15}N-*L*-Asp (OtBu)-OH	Cortecnet, iosins Bretonneux, French
Fmoc-$^{15}N_2$-*L*-Lys(Boc)-OH	Cortecnet, iosins Bretonneux, French
Fmoc-$^{13}C_5$, $^{15}N_2$-*L*-Gln(trt)-OH	Iris Biotech GmbH, Marktredwitz, Deutschland
HBTU	Biosolve, Valkenswaard, Niederlande
HOBt	Biosolve, Valkenswaard, Niederlande

HCl (1 M)	Carl Roth GmbH, Karlsruhe, Germany
K_2SO_4	VWR International, West Chester, USA
Lipids	Avanti Polar Lipids, Alabama, USA
Me_2S	Merck Schuchardt, Hohenbrunn, Germany
MeOH (Spectroscopy)	Merck, Darmstadt, Germany
NH_4I	Sigma Aldrich Chemistry GmbH, Steinheim, Germany
NMP	Biosolve, Valkenswaard, Niederlande
Piperidin	Biosolve, Valkenswaard, Niederlande
Phenol (99%)	Sigma Aldrich Chemistry GmbH, Steinheim, Germany
POPC	NOF Corporation, White Plains, NY, US
TFA	Biosolve, Valkenswaard, Niederlande
TA (99%)	Biosolve, Valkenswaard, Niederlande
TIS (99%)	Merck Schuchardt, Hohenbrunn, Germany
Rink amide MBHA resin	Novabiochem ®, Merck KgaA, Darmstadt, Germany
Wang-Resin Fmoc-*L*-Lys(Boc)-OH	Novabiochem ®, Merck KgaA, Darmstadt, Germany
Wang-Resin Fmoc-*LL*-Glu (otBu)	Novabiochem ®, Merck KgaA, Darmstadt, Germany
Water (Milli-Q)	Millipore, Billerica, USA

B. Devices

Name	Modell	Producer
Analyse libra	BP 301 S BP 211D	Sartorius, Goettingen, Germany
Column (HPLC)	RP Protein C4, CAT 214TP1010 RP Protein C18, CA T218TP52 RP Protein C18, CAT 218TP1010	W.R. Grace & Co., USA
Freezer (-80 ℃)	HFC 286 Basic Heraeus	Kendro GmbH, Hanau, Germany
HPLC	Pump: PU-2087 Plus High-pressure mixer: 2080-DHD Column thermostat: Jetstream Plus Control box: LC-Net II/ACC UV-Detector: MD-2010 Plus Software: CHrompass	Jasco International Co., Ltd., Tokyo, Japan
LC-MS	LC-System: Agilent 1100 Series Software: Hystar	Bruker Daltonics, Bremen, Germany
Lyophilizer	Alpha 1-4 LSC Alpha 2-4 LD	Chris GmbH, Osterode, Germany
NMR-spectrometer	Avance II WB, 500 MHz Avance II WB, 600 MHz Software: Topspin V2.1 / V3.2	Bruker, Rheinstetten, Germany
4mm MAS HXY probe	600 MHz	Bruker, Rheinstetten, Germany

2.5mm MAS H/F/X probe	500 MHz	Bruker, Rheinstetten, Germany
MALDI-TOF		Bruker Daltonics, Bremen, Germany
Oven	Heraeus	Kendro GmbH, Hanau, Germany
Peptid synthesizer (Synthesis automat)	Liberty 431A Software: Pepdriver V2.5.4	CEM, Kamp-Lintfort, Germany
Peptid synthesizer (Microwave)	Discover	CEM, Kamp-Lintfort, Germany
Rotary evaporator	Labarata 4003-control	Heidolph instruments, Schwabach, Germany
Shaker (Schüttler)	KM2	Edmund Buehker GmbH, Tuebingen, Germany
Ultrasonic bath	UTR200	Hielscher Ultrasonics GmbH, Teltow, Germany
Vortex	Vortex Genius 3 Reax Top Genie 2 T TopMix FB 15024	Heidolph Instruments, Schwabach, Germany
Centrifuge	Minispin 3-18K	Eppendorf AG, Hamburg, Germany Sigma Centrifugen GmbH, Osterode, Germany

C. Publications

Hao Wang, Zesheng Zhang, Liya Liang, Shengping Wen, Chunyan Liu, **Xiaojun Xu**.A comparative study of high-performance liquid chromatography and colorimetric method for inulin determination. *European Food Research and Technology*, 2010. 230:701-706.

Stephan L. Grage, **Xiaojun Xu**, Markus Schmitt, Parvesh Wadhwani, Anne S. Ulrich. ^{19}F-labeling of peptides revealing long-range NMR distances in fluid membranes. *J. Phys. Chem. Lett.*, 2014, 5 (24), pp 4256–4259

Xiaojun Xu, Stephan L. Grage, Markus Schmitt, Parvesh Wadhwani, Anne S. Ulrich. Systematically Analysis of monoF-and CF_3 as NMR labels in biochemical structural studies. Manuscript.

Xiaojun Xu, Stephan L. Grage, Markus Schmitt, Parvesh Wadhwani, Anne S. Ulrich. E5 dimer interfaces revealed by ^{19}F-solid state NMR. Manuscript.

D. Conference contributions

36th FGMR discussion meeting, 29 September - 02October, 2014, Berlin, Germany

Poster: Distance measurements in membrane-active peptides in liquid-crystalline bilayers using solid-state ^{19}F-NMR

3rd workshop structural biology in the Helmholtz association, 5-6 November, 2015, Berlin, Germany

Poster: Solid-state 19F-NMR analysis reveals helix-helix contacts at the dimer interface of the viral oncoprotein E5 in membranes

Biophysics of Protein-Membrane Interactions: From Model Systems to Cells, 11-14 April 2016, Bad Herrenalb, Germany

Poster: Solid-state ^{19}F-NMR analysis of the viral oncoprotein E5 assembly in membranes